

**MODELLING AND INVESTIGATION OF DIFFERENT
MICRO TEXTURES ON CUTTING INSERTS FOR
MACHINING OF TITANIUM GR2**

A Thesis

Submitted in partial fulfillment of the requirements for the
award of the degree of

DOCTOR OF PHILOSOPHY

in

MECHANICAL ENGINEERING

By

**Rahul Sharma
41800527**

Supervised By

Dr. Swastik Pradhan



**LOVELY PROFESSIONAL UNIVERSITY
PUNJAB
2021**

Declaration

I hereby certify that the work which is being presented in the dissertation entitled, “Modelling and Investigation of Different Micro Textures on Cutting Inserts for Machining of Titanium Gr2”, by Rahul Sharma (Uni. Roll No. 41800527) in partial fulfillment of requirement for the award of the degree of Ph.D. (Mechanical Engineering) submitted in Lovely Professional University, Phagwara, Punjab (India) is an authentic record of my own work carried out during a period from July 2018 to August 2021 under the supervision of Dr. Swastik Pradhan, Assistant Professor, Mechanical Engineering Department. The matter presented in this thesis has not been submitted by me to any other University / Institute in India or abroad for the award of any degree or diploma.

(Rahul Sharma)

Signature of the Student

This is to certify that the above statement made by the candidate is correct to the best of my/our knowledge

(Dr. Swastik Pradhan)

Signature of the Supervisor

Certificate

Uni. Reg. Number: 41800527

Name: Rahul Sharma

Title of Dissertation: Modelling and Investigation of Different Micro Textures on
Cutting Inserts for Machining of Titanium Gr2

We the below signed, after checking the dissertation mentioned above and the official record book (s) of the student, hereby state our approval of the dissertation submitted in partial fulfillment of the requirement of the degree of Doctor of Philosophy in Mechanical Engineering at Lovely Professional University, Phagwara, Punjab (India). We are satisfied with the volume, quality, correctness, and originality of the work.

Dr. Swastik Pradhan
Principal Supervisor

Signature of Examiner

Abstract

Manufacturing industries are having a great requirement of the development of new practices concerning advanced materials, their machining, and the use of lubricating additives. In machining, the machinability of the cutting tool plays a significant role in proclaiming the manufacturing process appropriate for the fabrication of a product with desired properties. Machinability of a cutting tool merely depends on cutting temperature, surface finish and tool life, etc. Titanium Grade 2 has replaced various metals due to its countless properties and applications but it devours higher machining costs. Lower cutting insert life is the main reason behind that. Quality of machined surface, tool wear, and chip morphology need to be studied to improve the machinability of cutting insert. Massive work on the machinability improvement of difficult-to-cut materials has been done. Micro-surface grooving is a modern method in this arena. The micro design patterns grooved on the rake or flank face of cutting inserts decrease the coefficient of friction, cutting temperature which results in the reduction of cutting forces. The solid lubricant applied in the gaps of the grooved pattern makes a pool that results in improvement of output parameters and tool life. Fabrication of textured inserts is still a challenge. To improve the machinability of a textured cutting insert the most effective factors are the area covered, design pattern, and orientation of micro-texture. For the coated cutting inserts, the fabrication of micro-grooves must not remove the coating from the surface. Machining experiments require complex types of equipment and test setups. DEFORM[®] 3D is an ample tool that delivers an unbounded assortment of factors and conditions. Its graphics visualize the analysis results interestingly.

This research work is focused on several ways and approaches being used to improve the tool life of cutting inserts and machinability which are used in machining difficult-to-cut materials. To investigate the machinability of non-textured plain cutting inserts and micro-textured cutting inserts, various novel micro-textured grooves have been designed in 2D/3D and fabricated using a femtosecond laser machine on tungsten carbide inserts without amputating its coating. These inserts have (CVD) chemical vapor deposition coating of TiCN (Titanium Carbo-Nitride) and alpha-alumina up to

20 microns. The spiral triangular micro-texture covers 1.12 mm X 1.12 mm of the area with grooved edges upright to the direction of the flow of chips. 10 microns of groove width, 20 microns of wall thickness, and 10 microns of the depth of groove have been taken. Honeycomb micro-texture has covered 2.11 mm X 2.11 mm of the area on the rake face of the cutting insert. After fabrication of honeycomb micro-texture, the average groove width and wall thickness obtained is 57.7 microns and 29.49 microns respectively. The femtosecond laser machine is used to fabricate the micro-textures on the rake face of cutting inserts up to the maximum depth of 18.6 microns only. Due to the generation of several micro pools of reservoir for lubricant and long walls, the heat dissipation rate has been increased.

The turning operation has been performed using both the plain cutting inserts without any micro-texture and micro-textured cutting inserts on a Titanium Gr 2 rod of diameter 50 mm and length 510 mm. A three-jaw self-centered lathe machine has been used to conduct the experiments. The type of insert, rotational speed, and cutting feed are the main parameters. L27 orthogonal array has been used for the design of experiments. The rotational speed has the range of 350 rpm to 930 rpm and the feed has the range of 0.04 mm/rev to 0.08 mm/rev. All experiments have been performed taking the same depth of cut of 0.5 mm. Further, a complete FEM simulation has been carried out for all the factors and levels of the turning operation using DEFORM[®] 3D software.

The effect of cutting speed as well as feed on cutting tool-chip interface temperature has been studied and validated with experiments deviating an error of 3%. It is perceived that the increase in cutting speed and feed both have raised the tool-chip interface temperature. EDS (energy dispersive spectroscopy) confirms 68.2% presence of TiCN coating inside the groove with an increase of 33.7% of carbon and a decrease of 9.9% of titanium content due to laser cutting. Significant reduction in cutting tool temperature and surface roughness has been observed using micro-textured cutting inserts. The cutting insert with Honeycomb micro-texture gives superior results with a minimum cutting temperature of 210°C and a maximum of 76% improvement in surface finish. Lower cutting temperature, lesser surface roughness, and slighter flank wear have been measured while machining with a honeycomb micro-textured cutting insert. Thus the honeycomb micro-texture has improved the machinability of the cutting insert. Both the plain and honeycomb micro-textured cutting inserts have produced the

same type of chips at lower feed but when the feed has been increased, the honeycomb micro-texture has converted the chip type from a corkscrew to ribbon and long tubular which results in the reduction of crater wear of the tool. In micro-scale analysis of chip forms, various horizontal lines with more depth have been found on the convex side of the snarled ribbon chips. More and large-sized teeth have been found in long cork screw chips in comparison to the long tubular chips which results in the deformations at the rake face of the cutting insert. Vertical straight line fractures have been observed on the concave side of the corkscrew and long tubular chips.

The simulation results have been compared with experimental results. Temperature analysis has 1.11% and wear analysis has 2.19% of acceptable error. Further stress and strain analysis in DEFORM[®] 3D has been carried out. The predicted values of effective stress and strain increase with the increase in rotational speed as well as with feed. The maximum of 2.74Mpa $\times 10^3$ effective principal stress has been measured with plain cutting insert at speed of 930 rpm and 0.08 mm/rev of feed. A minimum of 2.94 $\times 10^{-5}$ mm/mm effective strain has been observed with a spiral triangular micro-textured cutting insert. From Grey Taguchi analysis the optimal parameter has been observed at run 27. The best machining results are obtained with 930 rpm of rotational speed and 0.08 mm/rev of feed using a honeycomb micro-textured cutting insert.

Keywords: Micro-texture cutting insert; Tool wear; Surface roughness; CVD coating; DEFORM 3D; Finite Element Simulation; Titanium Grade 2; Femtosecond; XRD; Honeycomb; Micro-pools; MRR; PISF; SEM; Flank Wear; Crater Wear; Chip Morphology.

Acknowledgment

First and foremost I am extremely grateful to my supervisor, **Dr. Swastik Pradhan** for his valuable advice, guidance, moral & financial support, encouragement, and scholarly inputs at every stage of research work. His healthy criticism, priceless and meticulous supervision throughout my thesis, helped me immensely to complete my work successfully.

I would like to thank **Dr. Loviraj Gupta**, Dean LFTS, Lovely Professional University, Phagwara for his motivational words, progressive approach, and providing helpful pedagogy at the university campus. I also want to thank **Dr. Vijay Kumar Singh**, Head of School Mechanical Engineering for their academic support, suggestions, and healthy criticism during my presentation of the work.

I extend my special gratitude to **Dr. Ravi Nathuram Bathe, Scientist, ARCI Hyderabad** for providing me support and cooperation in his workshop and laboratory to carry out my research work.

I acknowledge with special thanks to technical staff, non-teaching staff, and everyone who has knowingly & unknowingly helped me throughout my thesis.

I owe a lot to my parents, **Dr. Dharampal Sahil & Mrs. Rashpal Devi, Mr. Anil Kumar Sinha & Mrs. Neelima Sinha**, my family members **Mr. Ankit Kumar Sinha, Ms. Himani Sharma, Ms. Anjali Sinha, Ms. Anupama Sinha, and beloved Pankhuri Sharma** who encouraged and helped me at every stage of my personal and academic life. I am greatly indebted to them for sincerely bringing me up with care and love.

Last but not least, a word of thanks to the **authors of all those books and research articles** which I have consulted during my thesis work as well as for preparing the report.

Above all, I owe it all to Almighty God for granting me the wisdom, health, and strength to undertake this research task and enabling me to its completion.

Place: Lovely Professional University.

(*Rahul Sharma*)

Date:

Uni. Roll No. 41800527

Table of Contents

Declaration.....	ii
Certificate.....	iii
Abstract.....	iv
Acknowledgment.....	vii
Table of Contents.....	viii
List of Tables.....	xii
List of Figures.....	xiii
List of Equations.....	xvii
Nomenclature.....	xviii
Chapter 1.....	1
1. Introduction.....	1
1.1 Background and Motivation.....	1
1.2 Judging Machinability.....	2
1.2.1 Tool Life.....	2
1.2.2 Power Consumption.....	3
1.2.3 Surface Finish.....	3
1.2.4 Chip Form.....	3
1.2.5 Cutting Temperature.....	4
1.3 Difficult to Cut material.....	5
1.4 Compilation of Machining Technologies.....	5
1.5 Various Inventiveness Taken to Solve Issues.....	7
1.5.1 Hot machining.....	7
1.5.2 MQL.....	8

1.5.3 Coated Tools	9
1.5.4 High-speed machining	9
1.5.5 Flood Cooling	10
1.5.6 Micro Grooves	11
1.6 Elements Concerning Machinability.....	12
1.6.1 Workpiece and Cutting Tool Material	12
1.6.2 Micro Texturing	13
1.6.3 Cutting Tool Temperature.....	13
1.6.4 Surface Roughness.....	13
1.6.5 Material Removal Rate	14
1.6.6 Percentage Improvement in Surface Finish	14
1.6.7 Chip Morphology.....	14
1.6.8 Optimum Parameters	15
1.7 Description of Instruments and Machines	15
1.7.1 Lathe Machine	16
1.7.2 Cutting Inserts	16
1.7.3 IR Thermometer.....	16
1.7.4 Talysurf.....	16
1.7.5 Optical Microscope	16
1.7.6 Scanning Electron Microscope	17
1.7.7 X-Ray Diffraction	17
1.7.8 Solidworks	17
1.7.9 DEFORM – 3D	17
1.7.10 MasterCAM	18
1.7.11 Femtosecond Laser Machine	19
1.7.12 Ultrasonic Cleaning Apparatus	20

1.7.13 Minitab.....	20
Chapter 2.....	21
2. Literature Review.....	21
Chapter 3.....	41
3. Problem Formulation	41
3.1 Research Objectives.....	42
3.2 Organization of Dissertation	42
Chapter 4.....	43
4. Materials and Methods.....	43
4.1 Design and Fabrication of Spiral Triangular Micro Texture	43
4.1.1 Designing	43
4.1.2 Fabrication	45
4.2 Design and Fabrication of Honeycomb Micro-Texture.....	51
4.2.1 Designing	52
4.2.2 Fabrication	53
Chapter 5.....	66
5. Experimentation and Modeling.....	66
5.1 Selection of Orthogonal array and Design of Experiments	68
5.2 Material, Machine Set-up & Test Conditions	70
Chapter 6.....	75
6. Results and Discussion	75
6.1 Effect of Machining Parameters on Temperature	75
6.2 Effect of Machining Parameters on Surface Roughness.....	76
6.3 Effect of Machining Parameters on MRR	77
6.4 Effect of Machining Parameters on PISF	78
6.5 Analysis of Surface Roughness, Tool Wear and Chip Morphology.....	79

6.5.1 Surface Roughness Analysis	80
6.5.2 Tool Wear Analysis	83
6.5.3 Flank Wear	84
6.5.4 Crater Wear	87
6.5.5 Chip Morphology	89
6.6 Deform 3D Simulation Analysis for Temperature Variation	94
6.6.1 FEM Simulation	94
6.7 Comparison, Validation and Prediction of Machinability Aspects	99
6.7.1 Comparison of Experimental Setup	100
6.7.2 Comparison of Cutting Tool Temperature	103
6.7.3 Comparison of Tool Wear	109
6.8 Finding the Optimal Parameters	116
Chapter 7	124
7. Conclusions	124
7.1 Contribution to Research	126
7.2 Scope of Future Research	127
Publications	128
Published	128
Conference Proceedings	128
Communicated	129
Bibliography	130
Annexures	144
Calculation of PISF	144

List of Tables

Table 4.1: All input parameters of the femtosecond laser machine and their values. .	46
Table 4.2: Dimensions of micro-texture after actual fabrication.	49
Table 4.3: Values of operating parameters for the Femtosecond laser machine.	55
Table 4.4: Obtained values after the fabrication of honeycomb micro-texture.	56
Table 5.1: L27 Orthogonal array for the design of experiments.....	69
Table 5.2: Values of all the factors and levels used in the machining operation.....	69
Table 5.3: Detail of output results at different input values for each experiment run.	73
Table 6.1: All the attributes and remarks of this experimental setup.	80
Table 6.2: Measured values of different types of surface roughness.....	81
Table 6.3: Values of flank wear and cutting temperature for different types of cutting inserts.	85
Table 6.4: Comparison of types of chips removed at various parameters.	90
Table 6.5: Observed output temperature in simulation and experiments.	97
Table 6.6: Comparison of experimental and simulation temperatures with input parameters.	104
Table 6.7: Cutting tool wear in experiments and simulation with the percentage of error.	110

List of Figures

Figure 1.1: Main issues observed in the machining of super alloys.	6
Figure 1.2: Cutting tool having a micro-textured surface.....	11
Figure 1.3: Standard shapes and types for chip morphology.....	15
Figure 1.4: DEFORM 3D software platform for simulation.	18
Figure 1.5: Part of the CNC program output from MasterCAM	19
Figure 2.1: MQL Unit	24
Figure 2.2: Lubricant Delivery system	24
Figure 2.3: SEM Images of tool flank wear.....	26
Figure 2.4: SEM images of the chip-morphology	26
Figure 2.5: Cutting Test machine setup	29
Figure 3.1: Methodology of Research work	42
Figure 4.1: Design of micro-texture with dimensional detail.	44
Figure 4.2: 3D representation of location and orientation micro-texture design.	44
Figure 4.3: Spiral triangular Micro-texture design on the rake face of cutting insert .	45
Figure 4.4: Various trial run patterns grooved on the rake face of the cutting insert. .	47
Figure 4.5: Ultrasonic cleaning of cutting insert with micro-texture.....	47
Figure 4.6: A machine used for the topography of cutting insert with micro-texture .	48
Figure 4.7: Cutting insert without micro groove texture	48
Figure 4.8: Cutting insert with micro groove texture on rake face.	49
Figure 4.9: Dimensional measurement of micro-texture after grooving on cutting insert.	50
Figure 4.10: The topography of micro-texture grooved on cutting insert.	50
Figure 4.11: Final Design of micro-texture with dimensional detail.....	53
Figure 4.12: Honeycomb micro-texture design on the rake face of cutting insert.	54
Figure 4.13: Cutting insert with a micro honeycomb pattern.	57
Figure 4.14: Dimensional analysis of wall thickness and width of the groove.	57
Figure 4.15: Dimensional analysis of distance from cutting edge.....	58
Figure 4.16: Selected Spectrums in EDS analysis of honeycomb pattern.....	58
Figure 4.17: Element percentage component of normal spectrum-1.....	59

Figure 4.18: Element percentage component of micro-grooved spectrum-2.	60
Figure 4.19: EDS mapping results- Combined element data of all compounds.	60
Figure 4.20: EDS mapping results- Element data of the Titanium compound only.	61
Figure 4.21: EDS mapping results- Element data of Nitride compound.	61
Figure 4.22: EDS mapping results- Element data of the Carbide compound.	62
Figure 4.23: EDS mapping results - Element data of Aluminium compound.	62
Figure 4.24: EDS mapping results- Element data of Oxide compound.	63
Figure 4.25: XRD analysis of cutting insert without micro-texture.	64
Figure 4.26: XRD analysis of cutting insert with honeycomb micro-texture.	64
Figure 5.1: Design of cutting inserts (a) Non-textured (b) with Spiral Triangular micro-texture (c) with Honeycomb micro-texture.	67
Figure 5.2: TiCN coated tungsten carbide cutting inserts (a) Non-textured (b) with Spiral Triangular micro-texture (c) with Honeycomb micro-texture.	68
Figure 5.3: Titanium Gr 2 workpiece rod of diameter 50 mm and length 510 mm.	70
Figure 5.4: Square tungsten carbide cutting insert with holder.	70
Figure 5.5: Three-jaw self-centered Lathe machine set up for turning operation.	71
Figure 5.6: HTC IRX-65 digital infrared temperature measurement device.	71
Figure 5.7: Surface roughness measurement using ISR-S400 tester.	72
Figure 6.1: Variation in temperature with the type of inserts, rotational speed, and cutting feed in turning operation.	76
Figure 6.2: Variation in surface roughness with the type of inserts, rotational speed, and cutting feed in turning operation.	77
Figure 6.3: Variation in material removal rate with the type of inserts, rotational speed, and cutting feed in turning operation.	78
Figure 6.4: Variation in percentage improvement in the surface finish with the type of inserts, rotational speed, and cutting feed in turning operation.	79
Figure 6.5: Graphical representation of the variation of Ra, Rq, Rt, Rz, Rc, and Rmax.	82
Figure 6.6: Graphical representation of the variation of Rsm and Rpc.	83
Figure 6.7: Different areas of wear in a cutting insert.	83
Figure 6.8: (a), (b) Deformations occurred on the surface of the cutting insert after machining.	84

Figure 6.9: Variation of flank wear with temperature.	86
Figure 6.10: Variation of flank wear with speed and feed.	87
Figure 6.11: (a), (b) & (c) Comparison of flank, crater and nose radius wear at different speeds.	89
Figure 6.12: Variation of removed Chips type with speed and feed.	90
Figure 6.13: Shape and size of removed chips.	92
Figure 6.14: Micro-shape comparison of removed chips.	93
Figure 6.15: Main parts of simulation in DEFORM 3D.	94
Figure 6.16: Selected workpiece and cutting insert for mesh generation.	95
Figure 6.17: Generation of mesh in workpiece and cutting insert.	96
Figure 6.18: Measurement of tool chip interface temperature in DEFORM 3D software.	97
Figure 6.19: Temperature comparison graph for simulation and experimental data. ...	98
Figure 6.20: Variation in temperature with speed for three levels of feed.	99
Figure 6.21: Variation in temperature with feed for three levels of speed.	99
Figure 6.22: Dimensional comparison of Plain, Spiral Triangular, and Honeycomb micro-texture designs.	101
Figure 6.23: Effective elements on a cutting insert during machining.	101
Figure 6.24: 3D Outlook comparison of a) Plain b) Spiral Triangular and c) Honeycomb micro-texture designs.	102
Figure 6.25: Actual cutting insert comparison of with and without micro-texture. ..	102
Figure 6.26: Actual Experimentation and simulation machining process.	102
Figure 6.27: Temperature comparison for Plain cutting insert.	105
Figure 6.28: Temperature comparison for Spiral triangular micro-textured cutting insert.	105
Figure 6.29: Temperature comparison for Honeycomb micro-textured cutting insert.	105
Figure 6.30: Temperature Measurements in simulation for Plain cutting insert.	106
Figure 6.31: Temperature Measurements in for Spiral Triangular micro-textured cutting insert.	106
Figure 6.32: Temperature Measurements for Honeycomb micro-textured cutting insert.	106

Figure 6.33: Heat effected zones in Plain cutting insert.	107
Figure 6.34: Elemental temperature distribution in Plain cutting insert.	107
Figure 6.35: Heat effected zones in Spiral Triangular micro-textured cutting insert.	108
Figure 6.36: Elemental temperature distribution in Spiral Triangular micro-textured cutting insert.	108
Figure 6.37: Heat effected zones in Honeycomb micro-textured cutting insert.	108
Figure 6.38: Elemental temperature distribution in Honeycomb micro-textured cutting insert.	109
Figure 6.39: Variation in temperature for all types of cutting inserts.	109
Figure 6.40: Comparison of tool wear for Plain cutting insert.	111
Figure 6.41: Comparison of tool wear for Spiral Triangular micro-textured cutting insert.	111
Figure 6.42: Comparison of tool wear for Honeycomb micro-textured cutting insert.	112
Figure 6.43: Tool wear geometry in Plain cutting insert.	112
Figure 6.44: Tool wear geometry in Spiral Triangular micro-textured cutting insert.	113
Figure 6.45: Tool wear geometry in Honeycomb micro-textured cutting insert.	113
Figure 6.46: Tool wear comparison for experimental and simulation data.	114
Figure 6.47: Variation of effective stress in three types of cutting inserts.	116
Figure 6.48: Variation of effective strain in three types of cutting inserts.	116
Figure 6.49: Steps of Grey Taguchi method of finding optimal parameters.	119

List of Equations

Equation 5.1 : Material Removal Rate	76
Equation 5.2 : Percentage Improvement in Surface Finish	76
Equation 6.1 : Percentage Error	102
Equation 6.2 : Normalization of smaller is better	124
Equation 6.3 : Normalization of higher is better	124
Equation 6.4 : Value of delta (absolute responses)	125
Equation 6.5 : Zeta (Grey relational coefficients)	125
Equation 6.6 : Grey Relation Grade (GRG)	125

Nomenclature

°2Th	:	Degree Two Theta
°C	:	Degree Celsius
µm	:	Micrometer
3D	:	Three Dimensional
HRC	:	Hardness on Rockwell Scale C
AISI	:	American Iron Steel Institute
Al ₂ O ₃	:	Aluminium Oxide
AlCrN	:	Aluminium Chromium Nitride (Alcrona)
ANOVA	:	Analysis of Variance
BUE	:	Built up Edge
CAITA	:	Computer Aided Three-Dimensional Interactive Application
CAMQL	:	Cryogenic Air Mixed with Minimal Quantity Lubrication
CBN	:	Cubic Boron Nitride
CGI	:	Compact Graphite Iron
CNC	:	Computer Numeric Control
CNT	:	Carbon Nano Tube Coated
CO ₂	:	Carbon Dioxide
CVD	:	Chemical Vapor Deposition
D	:	Depth of Cut
DEFORM-3D	:	Design Environment for Forming
DFA	:	Desirability Function Analysis
EDM	:	Electrical Discharge Machining
EDS	:	Energy Dispersive Spectroscopy
F	:	Feed
FEA	:	Finite Element Analysis
FEM	:	Finite Element Model
Fps	:	Frame per Second
GDP	:	Gross Domestic Product
Gr	:	Grade

HSM	:	High Speed Machining
HSS	:	High Speed Steel
Hz	:	Hertz
ISO	:	International Organization for Standardization
KHz	:	Kilo Hertz
Lit	:	Liter
m/min	:	Meter per Minute
Mm	:	Millimeter
mm/rev	:	Millimeter per Revolution
MoS ₂	:	Molybdenum Disulfide
MQL	:	Minimum Quantity Lubrication
MRR	:	Material Removal Rate
MT-CVD	:	Modern Titanium Carbonitride chemical Vapor Deposition
NCT	:	Non Carbo Nano Tube
PCA	:	Principal Components Analysis
PISF	:	Percentage Improvement in Surface Finish
PVD	:	Physical Vapor Deposition
R	:	Resultant Cutting Force
Ra	:	Surface Roughness
Rev	:	Revolution
Rpm	:	Revolution per Minute
RSM	:	Response Surface Method
S/N ratio	:	Signal to Noise Ratio
SEM	:	Scanning Electron Microscope
SiO ₂	:	Silicon Dioxide
SNMA	:	S – Shape, N- Relief Angle, M – Tolerance Value, A – Clamping System
Ti ₂ N	:	Titanium Nitride
Ti ₃ Al ₂ N ₂	:	Titanium Aluminium Di-Nitride
Ti555.3	:	Near-beta Titanium Alloy
Ti6Al4V	:	Titanium Alloy (Titanium, Aluminium and Vanadium)
TiAlN	:	Titanium Aluminium Nitride

TiC	:	Titanium Carbide
TiCN	:	Titanium Carbo-Nitride
TiCrN	:	Titanium Chromium Nitride
TiN	:	Titanium Nitride
V	:	Cutting Speed
Vb	:	Measurement of Flank Wear
Vc	:	Cutting Speed
Vf	:	Feed
W	:	Watt
WC	:	Tungsten Carbide
WS ₂	:	Tungsten Disulfide
XRD	:	X-ray Diffractometer

Chapter 1

1. Introduction

1.1 Background and Motivation

Industrialization is a very significant part of any engineering understanding. Machining which includes several processes converts raw material into the looked-for shape and product with desired properties. It involves several processes, different shapes, sizes of the products. The GDP of many countries is affected by the manufacturing segment. This segment also provides maximum jobs to the people of same and other countries. That is why the “Make in India” program was launched in 2014 in INDIA also. Hence, it is required to carry out in-depth research in all manufacturing processes for making it energy efficient along with improvements in surface finish quality. Also, green manufacturing is to be developed for protecting our environment, human lives, and status. It is possible only if tribological studies of tool insert and work piece interface are done.

In machining, all processes are classified into three principle categories which are milling, turning, and drilling. All other operations come into the sub-categories of these.

- In milling operation, the cutting tool rotates so that the cutting edges of the tool stand against the workpiece for the material removal process. Milling machines are the foremost machine used for these operations.
- Turning operation is the primary method of removing material by moving the workpiece or tool against each other. Lathe machines are being widely used for this operation.
- Drilling operations use a rotating cutter to produces holes into the workpieces. Drilling operations are done in drilling machines, milling machines, and for some products even on lathes.
- These primary operations have several miscellaneous processes as shaping, boring, sawing and broaching, etc.

The perfect machining has to meet many parameters provided in technical drawings or blueprints of the product. After meeting the dimensional accuracy the desired surface finish is also a challenge in field manufacturing. The main reason for finishing errors occurs due to the use of a damaged tool, wrong selection of cutting tool, clamping error, etc. which results in irregular surface and cracks on the machined surfaces. Machinability means the ease with which any product can be machined or undergo various machining processes for removing the material for the desired and satisfactory finish. These methods must be economical enough. The machinability includes less power to cut, good surface finish, less tool wear, and high tool life. Hence all manufacturing engineers are keen observers for all parameters to improve the machinability of a process or apparatus.

Machinability can be a challenge to achieve because it has a long list of variables. These variables can be divided into two sets of categories and which are material's condition and physical properties. The condition of material means the factors like microstructure, hardness, grain size, chemical composition, heat treatment, yield, and tensile strength. Physical properties mean the properties like elasticity, work hardening, thermal conductivity, and expansion. Besides these, some other important factors which are important to be considered are the material and geometry of the cutting tool, operating conditions, and process parameters.

1.2 Judging Machinability

When the machinability is to be judged then the main factors which are to be evaluated are given below:

1.2.1 Tool Life

It is the period for which the performance of the cutting tool remains well enough to give desired results efficiently. Tool life determination becomes very difficult due to variables like tool geometry, workpiece material, conditions of machining operations, cutting speed, temperature, and depth of cut. During cutting fewer resource intakes are required. Yet, abrasive properties which are the main reason for rapid tool wear reduces the machinability of material and increases the cost of production. Tool life cannot be taken as a machinability index because of its sensitivity

to many machine variables [1]. If tools of two different materials are used then their machinability ranking cannot be compared only based on tool life like a high-speed steel tool and a sintered carbide tool is being used in two different cases [2].

1.2.2 Power Consumption

There are two reasons to include power consumption as a criterion of machinability. First, less power is required if a material is easy to move against the cutting tool. The second is the minimum machining cost per product in terms of power used.

It is good to take specific energy of metal as identification of machinability. If the material of the tool is harder than the workpiece material then it will be easily machined but hardness is not the only measure to define the tool life.

1.2.3 Surface Finish

The value of surface finish is also an important part of judging the machinability of a metal. Soft and ductile materials always tend to form an edge. But all those materials which machine with a relatively high shear zone always tend to minimize the built-up edge effects. Such materials are brass, aluminum alloys, titanium, and its alloys, cold worked steels, free-machining steels. There are many cases in which the surface finish has no importance to measure the machinability of the workpiece. Rough cuts manufacturing is an example of these. Other manufacturing in which surface finish is not the desired part of output parameters, will also not have machinability judgment based on surface finish [3].

For various materials, it is very easy to determine machinability. Surface roughness readings are measured with an instrument after machining them under very controlled cutting conditions. These values are having a reverse meaning such as high reading means not a good surface finish quality and low machinability in return. Sometimes it is better to take relative readings in materials.

1.2.4 Chip Form

Machinability can also be judged based on chip form obtained in machining operation. If long string type chips are formed then its machinability rating is low. And if very fine chips in form of powder are obtained then it means their machinability is

better. Those materials would have a top rating, which inherently forms nicely broken chips. The process of disposal and handling of chips is a little expensive. String-type chips are very difficult to remove off from the machine, workpiece and can produce hazardous to the operator. But these are required to be removed from the freshly machined surface. Chips formation depends on the material of the workpiece, machine parameters so the machinability can be improved by taking the appropriate method of removing them.

If the rating is given based on ease of chip removal then it is qualitative. The type of chip obtained also depends on the machining operation as in drilling operation, spiral shape chips are always considered to be a better type as they will not block the hole.

1.2.5 Cutting Temperature

The cutting temperature is the most effective parameter of determining the machinability as it affects most on tool life and job surface finish also. The main part of the heat generated is disposed of through the chips. But as chips are to be removed earlier during machining to the obtained good quality surface, so it cannot add more effectiveness in the reduction of cutting temperature. So the chips taken away must happen when the maximum part of the heat is disposed of away through chips so that effect on tool and workpiece can be minimized. The main effect of high cutting temperature on the tool are:

- The material of the cutting tool will become soft and wear out will increase.
- Cutting edges of the tool will deteriorate
- Reduction in tool life.

The main effects of cutting temperature on the work piece are:

- Distortion in shape and inaccuracy in dimensions due to the expansion and contraction because of high temperature.
- Oxidation and burning of the surface may result in the rapid corrosion of the workpiece.
- Generation of micro cracks.
- Initiation of tensile residual stresses.

No doubt the rise in cutting temperature will reduce the cutting force required for machining by softening the work material and reducing the shear strain which leads to the reduction in power consumption. But if the cutting edge of the tool is soft then the rate of wear will also increase. The soft tool will not be able to last for a long time while machining and will get fractures easily. So modern research of reducing the cutting temperature can lead to the improvement of machinability [4].

1.3 Difficult to Cut material

Any material in general which is difficult to machine with existing methods of machining is known as difficult to cut material. Stainless steel was also considered as the material of this category when sufficient methods were not developed for its machining. But due to the developments of manufacturing techniques, it is excluded from that list.

The main difficult-to-cut materials are Inconel, Titanium, Super Invar, Nickel, and Low thermal expansion coefficient material, etc. People from the United States had difficulty finding proper cutting methods of such material.

Super alloys are having superior properties due to which these are one of the high-performance materials used in various industries. These properties are like high tensile and strength to weight ratio, high compressive strength, high fatigue resistance in the sea, lower density, and high corrosion resistance. Super alloys are also in this category because of their poor thermal conductivity during machining, low modulus of elasticity of the material, and at a high temperature, they have a strong tendency of chemical reaction to tool materials [5].

1.4 Compilation of Machining Technologies

During the machining of such materials, the traditional methods cannot give the required results. Vibrant factors need to be taken into consideration for desired results. These factors are like rigidity and stiffness of cutting tools, repairs and appropriate selection of machining parts, etc. Super alloys have properties of higher melting temperature due to which these are used in the manufacturing of aerospace and naval machine components. These materials are mainly of four main types: Nickel, Cobalt, Titanium, and Iron-based alloys. These super alloys are important modern materials to

meet the demands of extreme applications. Despite their excellent properties against corrosion and fatigue, high temperature strength, and lower heat sensitivity, they are extremely difficult to machine. By definition, these materials will be machined at high speeds due to the rapid wear risk, even though the actual machining speed could be substantially lower than the typical high processing speeds of aluminum.

In machining, cutting tool plays an important role the reason is that cutting speed completely depends on the material of the cutting tool. That is why all researchers are continuously trying to find out the tool work piece interaction parameters for obtaining a better-machined surface. To improve the machinability of such materials there is a requirement of proper selection of tool, machine tool with all cutting conditions. Figure 1.1 shows the various factors in the field of the machining area.

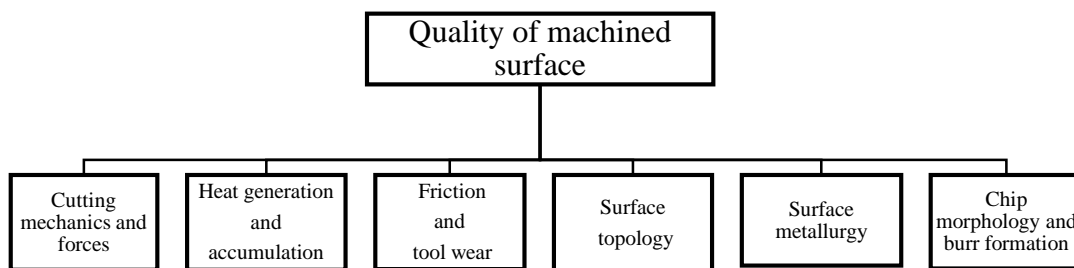


Figure 1.1: Main issues observed in the machining of super alloys.

All super alloys or difficult-to-cut materials have high strength at high temperatures. Due to this property, machining mostly produces segmented chips and produces high dynamic forces. These materials have the property of poor heat conductivity. Due to its large hardness, it generates high temperatures at the time of machining. All these properties of super alloys create the notch wear possessing a large depth of cut. Moreover, due to poor thermal property, these metals have a high and concentrated temperature at the tool/chip interface. Which increases the tool wear and machining cost.

1.5 Various Inventiveness Taken to Solve Issues

1.5.1 Hot machining

Different machining approaches have been used to overcome these problems, one of them is called “hot machining”. Hot machining is a method to externally heat the workpiece material before or during the machining operation. This machining method is very useful to cut difficult to machine materials because they are harder and have higher tensile strength than other engineering materials. They become softer when external heating on the workpiece material is applied [6]. As a result, the application of external heat would promote the machinability of the material. The application of external heat on workpiece material is simply named “Hot machining”. This description is sometimes called “thermally enhanced machining”, “heat-assisted machining”, “elevated temperature machining”, “plasma-assisted machining” or “laser-assisted machining”. In this study, hot machining is preferred due to covering all other descriptions. The advantages of hot machining can be mentioned as follow:

- a. Reducing mechanical properties of workpiece materials for easy machining operation.
- b. Increasing the machinability property of the material
- c. Increasing to select higher machining parameters (higher cutting speed, depth of cut, and feed)
- d. Reducing tool wear
- e. Increasing productivity
- f. Eliminating cutting fluid application
- g. Reducing total production cost

These advantages are important when expensive materials are machined and production costs are high. The disadvantages of hot machining, in turn, can be mentioned below:

- a. Increasing machine tool cost due to external heating technique cost
- b. Difficult to control dimensional accuracy due to heat on the workpiece material
- c. Difficult to determine surface finish
- d. Require more safety precautions because of heating Equipment

1.5.2 MQL

Many years ago, the concept of MQL (Minimum quantity of lubricant) came into play because of some environmental issues and occupational hazards. No doubt the minimization of cutting fluid will give economic benefits by saving the cost of lubricant. MQL also saves time for machine cleaning, workpiece, and tool mounting. It is also known as “near dry lubrication” or in some cases Micro lubrication. In the MQL technique, a small quantity of lubricant of a flow rate of 50ml/hr to 500 ml/hr towards the cutting zone is used. One or more nozzles are used to provide lubricant in an external system. If the normal lubricating system has been compared with MQL then it has been observed that it is only 1/3 to 1/4 in terms of the amount of lubricant used. Due to this method, the cost, time, and disposal of cutting heat are affected which in return affects the machinability [7].

Advantages of MQL System:

Financial advantages

- a. Due to the controlled supply of coolant saving of coolant and other resources is there.
- b. Higher tool life can be achieved.
- c. It reduces the time of the machine cycle up to 30%.
- d. The purchase and handling cost of lubricant will be reduced.
- e. Disposal costs of the coolant will also be reduced.
- f. Dry metal chips can be easily recyclable as compared to wet metal chips.
- g. The leakage of coolant leads to accidents that can be avoided.
- h. Operators can be protected from skin diseases.

However, there are numerous benefits of a minimum quantity lubrication system but still, it has many challenges to adopt in actual practice.

- a. Machining Special tools required.
- b. High investment costs.
- c. Suitability of the machine is required [8,9].
- d. MQL produces a very fine wastage, which is very difficult to filter out from lubricants.

- e. MQL setup requires many changes in machine tool setup and machine area.

1.5.3 Coated Tools

Coated tools are already being used in many manufacturing operations. The main concern here is that it must be of such a layer thickness that it possesses very low thermal conductivity. Due to which it prevents the ingress of heat into the material of the tool. The most common materials which are used are TiAlN, TiN, TiAlCrN, etc. Coated cemented carbides are widely used cutting tools for major manufacturing areas. Moreover, these give high levels of productivity, which make affordable products for the customers. Coated carbide inserts are widely used while working with all ferrous materials. Uncoated carbide inserts are good for machining non-ferrous materials, such as aluminum. These coated tools are having two categories as Chemical Vapor Deposition (CVD) and Physical Vapor Deposition (PVD). Both have several benefits. In the thick category, the CVD coatings have a layer of 9 – 20 microns and these have high wear resistance. PVD coatings are of thin type coatings having a layer of 2 – 3 microns.

Advantages:

- a. Coated tools reduce the job setup times hence reduces manufacturing costs.
- b. Different grades of the same insert can be used for the machining of different materials which in return reduces the tool inventory.

Disadvantage:

The rigidity and power of the CNC milling machine must be sufficient for the use of coated tools. These machines should also be able to produce controlled cutting feed.

1.5.4 High-speed machining

In the HSM machining process, the engaging time is reduced and the cuts are narrow. A high cutting feed is selected. So a very little cutting force is required which gives a small tool deflection. This is one of the highly productive and safe processes which has a constant stock. HSM cannot be one of the particular processes because it is a combination of several processes to be done in less time. It can be defined as:

- Operations to be performed at a high cutting speed (v_c).
- Operations to be performed with a high spindle speed (n).
- Operations to be performed with a high cutting feed (v_f).

- Operations to be performed with a high removal rate (Q)

Advantages of HSM:

Radial forces are low in HSM. Spindle forces are also very low which saves the guide ways and spindle bearings. High-speed machining gives the best results when applied with an axial milling operation. It also reduces the amount of vibration produced. High-speed machining is mainly used in small-sized parts in which the material removal rate is very low. HSM is used to get a fine surface finish in the range of 0.2 microns. It also makes it possible to machine very thin surfaces. In high-speed machining, the contact time plays an important role which must be minimized to avoid unnecessary vibrations.

Disadvantages of HSM:

In HSM the maintenance cost increases due to faster wear of ball screws, spindle bearings. HSM cannot be applied without having complete knowledge of the process. It needs a faster data transfer rate and programming setup. Hence an experienced and trained operator is required. A proper work plan is required considering all of the precautions and safety conditions. All machine parts and fasteners are required to be checked regularly to avoid any accident. Proper mentioned tools can be used.

1.5.5 Flood Cooling

The flood cooling method is commonly used in industries to reduce the cutting temperature. It includes the use of soluble oil. These have a huge quantity of lubricant to be supplied to reduce the temperature and to remove chips by flushing on the cutting interface. When a flood of coolant is supplied, it reduces the thermal shock on the milling cutter. Ignition of the chips reduces. But this method is not appropriate in machining titanium. As flood cooling does not have the precise and uni-directional application of coolant, machining of titanium has a short contact area so the removed chips act as an obstacle of applying coolant to the cutting area so the temperature is not minimized and tool life gets reduced during machining. Moreover, a large quantity of coolant is to be processed for reuse.

1.5.6 Micro Grooves

There are many fields in which the perfect mechanical properties are required. Food processing industries, aeronautical fields, and medical operations have a requirement of a high surface finish with a corrosion-resistant surface. During machining of steels, it is not easy to get the required surface finish with traditional methods because of high tensile strength. It has low thermal conductivity [10].

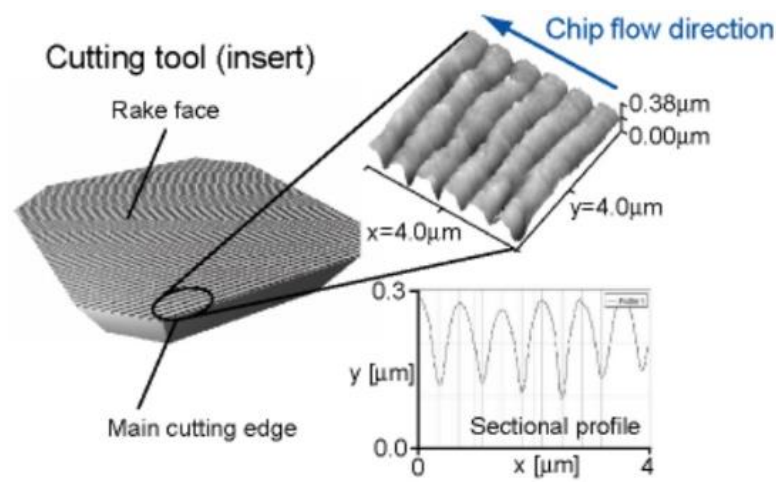


Figure 1.2: Cutting tool having a micro-textured surface [12].

For the enhancement in machinability, many methods have been tried like surface coating or tool geometry modifications. But that does not produce much effect. Biermann et al. [11] done experiments using various categories of hard coatings like TiN, AlCrN, and TiAlN. It was declared that TiAlN coatings and AlTiN gives better machining result because of their high hardness. Sugihara and Enomoto [12] have generated a micro-texture to improve the anti-adhesion property. They found a major decrease in chip adhesion on the face of the cutting tool. They have machined the aluminum alloy with micro-grooved tools. Their study proved that the modified tool surface with micro grooves is a modern method of enhancing the adhesion resistance. Figure 1.2 shows such a micro-groove texture. Zhang et al. [13] produced a macro/micro-sized texture on the surface of coated TiAlN tools. Hence it results in to rise in anti-adhesion resistance properties. An experiment was performed on AISI 316. It increases the lubrication on the interface of the tool and chips zone. Because of these microtextures, the contact area decreases. Some dimple and channel-type patterns were

grooved on the surface of the tool which was then used to machine plain carbon steel. They conclude that dry machining with a microgroove tool improved the heat transfer capabilities. And the machining in MQL with micro groove tool reduces the cutting temperature, cutting forces, and contact area of tool and chips. If we list down the benefits of textured tools with traditional tools then it can be concluded that the micro-grooved tools give an effective reduction in tool chip interface, provide hydrodynamic lift, produces effective lubrication, tool wear, cutting forces, etc.

1.6 Elements Concerning Machinability

To learn the machinability of any cutting insert, attempt to improve its tool life, and giving conclusions in this respect, subsequent factors or terms are essential to be deliberated.

1.6.1 Workpiece and Cutting Tool Material

Difficult to cut materials have numerous applications in the arena of manufacturing. These have enhanced properties than conventional materials. Titanium alloys Ti6Al4V have around 90% of titanium, 5-6% of aluminum, and 4-5% of vanadium. It has various grades starting from grade 2 to grade 23, depending upon the composition and properties. Titanium grade 2 is a pure metal that has high strength and excellent cold-forming properties. It also has good welding and resistance to oxidation properties. It is available in rod, pipe, flat bar, and sheet forms. It is being used in aerospace industries, automobiles, and the medical field. It has tremendous applications in architecture and manufacturing areas. The titanium grade 2 rod of diameter 50 mm has been used. A material composition identification test has been conducted using NITIN-X-XRF Analyzer of Model DC2000. Similarly, the cutting tools are generally made up of hard metals or alloys. Some cutting inserts undergo some chemical processes to achieve better properties. In cutting inserts, the cutting edges, flank and rake face, different angles, holding style, and many more properties are important. Tungsten carbide inserts are the widely used type of cutting insert. These are economical and good-performing cutting inserts. There are CVD coated, PVD coated and without coating cemented carbide cutting inserts available for manufacturing industries. TiCN, Al₂O₃, and TiN are the most commonly used coating materials on

these cutting inserts. Cutting inserts have many shapes and sizes. The SNMA is the standard notation that represents the shape, angle, tolerance, and holding method in a cutting insert. Many companies like Widia, ISCAR, etc are producing the SNMA 120408 cutting inserts with PVD, CVD, and without coating classification. Here 12 represents the side of the square, 4 is the thickness, and 8 is the value representing the nose radius.

1.6.2 Micro Texturing

Micro texturing is the process of designing and fabrication the textures or patterns of micro size. It is the most challenging part of this thesis. These micro textures are so small that can be analyzed with a microscope only. Mostly the micro-textures covers 1 to 2 mm² area near the cutting edge of the cutting inserts depending upon the design and patterns. These micro-textures are designed using the platforms like AutoCAD or Solidworks® in 2D and 3D. The size of the micro pattern also depends on the available size of cutting inserts. After designing the micro-texture is to be manufactured using a laser machine. Many machines have been used like the Nd-Yag Laser machine, femtosecond laser machine, micro-EDM machine, etc. for these laser machines, a G and M code program (CNC Programme) is required as per the design.

1.6.3 Cutting Tool Temperature

Cutting tool temperature plays an important role in declaring the cutting tool life or in other terms we can say the machinability of cutting insert. Cutting tool temperature is the real-time value of the temperature which a cutting insert acquires during the cutting operation. It depends on the material of the workpiece, cutting insert, and coatings. It also depends on the machining factors like speed, feed, the coolant used, the shape of chips, etc. If a cutting insert is capable of removing the heat generated during the machining operation, its cutting edge shape, wear, and coating layers can be protected for a long time, and ultimately its performance in terms of surface finish, power consumption, cost of machining, etc can be improved.

1.6.4 Surface Roughness

Surface roughness is the measure of the quality of machining which we obtained using a particular type of cutting insert. In many areas like food industries, automobile

industries, marine and aerospace industries, medical fields, a good surface finish is required. Surface roughness is the measure of crests and troughs on the surface of machined material. All cutting inserts give a good surface finish at the start of its machining operation but after that, it depends on various factors.

1.6.5 Material Removal Rate

The material removal rate is the rate with which a cutting insert can remove the material from the surface of the workpiece. It is also denoted as MRR. In a few of the machining cases, more material removal rate is good and in others, the lesser material removal rate is considered to be good. It is calculated in various ways. In the case of a round bar or rod, it can be calculated as the ratio of reduced diameter to the original diameter. Equation 5.1 is showing the formula to calculate MRR for this thesis work.

1.6.6 Percentage Improvement in Surface Finish

More percentage improvement in surface finish represents good characteristics of cutting insert. The successful increase of PISF using innovative methods or by making few changes in conventional methods means the machinability of the cutting insert has been improved. So it is also an important element to declare the performance of the cutting insert. PISF is calculated as the difference in surface roughness to the initial surface roughness. Equation 5.2 is elaborating the method to calculate.

1.6.7 Chip Morphology

The quality of the obtained surface finish also depends on the shape of the removed chips. The long chips are always be considered not good for machining as they can undergo welding with the finished surface. These reduce the heat removal rate causing the rise in cutting insert temperature. Long chips are also hazardous to the machine operator as they may cause accidents in many ways. So chips must be of small size or powder form for good machining results. Chips morphology is the study of size, shape, category of removed chips at the micro and macro levels. Its saw teeth shape become a major reason behind its shape. To categorize the removed chips after machining on titanium grade 2 rod, the standard used shapes, types, and size chart has been shown in figure 1.3.




















1	2	3	4	5	6	7	8
RIBBON CHIPS	TUBULAR CHIPS	CORK SCREW CHIPS	HELICAL CHIPS	SPIRAL CHIPS	ARC CHIPS	ELEMENTAL CHIPS	NEEDLE CHIPS
							
Short	Short	Short	Short	Flat	Loose		
							
Long	Long	Long	Long	Conical	Connected		
							
Snarled	Snarled	Snarled	Snarled	Short			

Figure 1.3: Standard shapes and types for chip morphology [14].

1.6.8 Optimum Parameters

Optimum parameter defining is the stage of declaring a few sets of values. A combination of all those values under the same machining conditions gives the best output results in the same category of a workpiece and cutting insert material. It also includes the most and least effective factors. There are many ways to find out the optimum parameters. Grey relational analysis using Taguchi is one of the most effective methods widely used in such a set of experiments where a large set of factors and levels of parameters comes into play.

1.7 Description of Instruments and Machines

During machining processes on difficult to cut material using textured / non-textured cutting inserts and to check the performance, to analyze the results, various instruments and machines are to be used. An introduction to very important instruments have been added to this section.

1.7.1 Lathe Machine

For basic machining operations like turning, facing, drilling, etc the widely used machine is the lathe machine. It has various types and categories depending upon its usage. For this research work, a three-jaw self-centered lathe machine has been used. The same types of operation can also be performed on a CNC lathe machine but the setup required to measure some real-time values during machining becomes complex in comparison to a normal lathe machine. Lathe machines have their standard speed and feed values. So those values are calculated in advance for the input parameter levels and the designing of a set of experiments.

1.7.2 Cutting Inserts

SNMA 120408 CVD coating of TiCN, Tungsten carbide of WIDIA Company has been used. It has the standard double square shape. The size of a side of the square is 12.7 mm and the thickness of the insert is 4.76 mm. It has a nose radius of 0.8 mm. It has zero relief angle means the rake face and flank face are perpendicular to each other. 0.003 mm is the tolerance limit with a cylindrical hole without any chip breaker.

1.7.3 IR Thermometer

Real-time measurement of cutting insert temperature is not possible with the in contact thermometer so a contactless HTC IRX – 65 Infra-red ray thermometer has been used. This is having a temperature value range of 10 °C to 1100 °C. It also has a wire probe to check the pointed end temperature. Results from this thermometer have been tested and verified before actual use during machining.

1.7.4 Talysurf

To measure the surface roughness values of titanium grade 2 rods before and after machining, INSIZE ISR-S-400 talysurf has been used. The cut-off length of 0.8 mm, 3 no of cut with 2.97 μm calibration Ra is taken. It gives us all the other roughness values like Rz, Rt, Rq, etc.

1.7.5 Optical Microscope

The designed and fabricated texture is of micron size so an optical microscope is required to test the pattern as well as for dimensional analysis. For this, the Olympus

topography machine has been used. It helps to compare the designed and fabricated micro-texture in 3D. Width and depth of the groove in micro-texture, the thickness of the wall, distance from cutting edge, and dimensional variation of actual from designed micro-texture have been carried out on this machine. After this, the Celestron microscope has been used for chip morphology.

1.7.6 Scanning Electron Microscope

Scanning electron microscope prepares a raster scan pattern using a beam of electrons and this beam produces a signal after striking on the atom. Catching and converting these signals into a high-quality image is done by this machine. JEOL JSM-6084LV SEM machine has been used. It has a magnification range of up to 300000X. Using the images from this machine, an analysis of the presence of a thin coating on the surface of the cutting insert has been validated.

1.7.7 X-Ray Diffraction

XRD analysis has been performed for the material characterization of the cutting insert. An Ultima IV XRD machine has been used which is a fully automated and computer-controlled measurement machine. With this XRD analysis, the presence of various oxides, other metals, and the reason behind the formation of new compounds has been studied.

1.7.8 Solidworks

For the fabrication of micro-texture on the rake face of the cutting insert, a 3D design has been prepared and used in .dxf format with the help of Solidworks® 2015 Software. The design alteration after trial runs become easy with Solidworks® 2015 platform. It also creates the 2D and 3D designs required for the simulation process in .stl format.

1.7.9 DEFORM – 3D

The actual experimental analysis of difficult-to-cut material is quite expensive as well as time-consuming. Moreover, only limited setups can be generated and the actual data can be gathered for analysis. For this reason, a 3D simulation has been performed. The results have been matched and compared with the actual experimental

results. After validating the simulation, it is easy to predict the other results for those the set up was not possible.

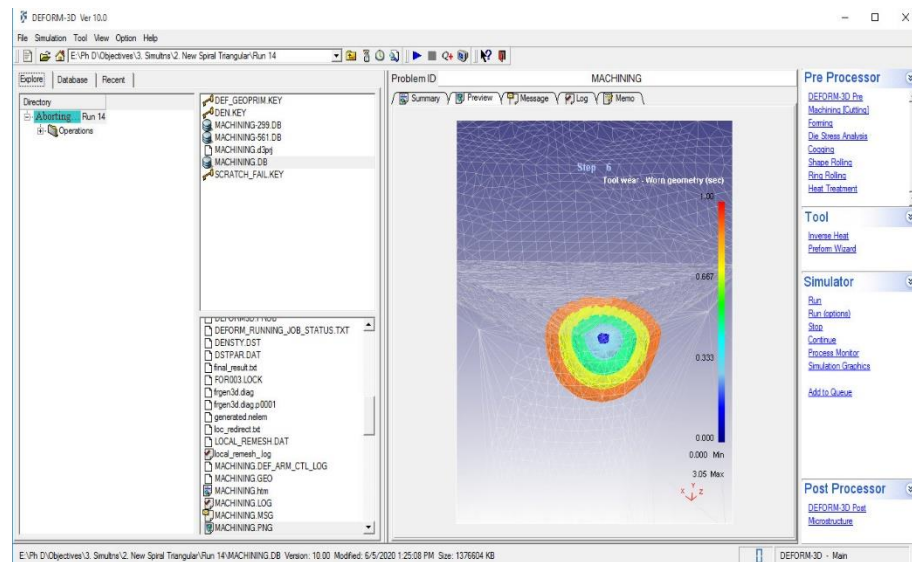


Figure 1.4: DEFORM 3D software platform for simulation.

For this simulation analysis, the DEFORM[®] 3D tool platform has been used. First, the output results of temperature and tool wear have been compared. After validating, the conclusions have been made for other factors like stress, strain analysis, etc. The simulation interface of DEFORM[®] 3D software is shown in figure 1.4.

1.7.10 MasterCAM

Fabrication of microtexture on cutting insert has been done on the Femtosecond laser machine. That laser machine has a computer-controlled system that takes commands in the G-Code and M-Code form. For this MasterCAM has been used which creates the program into NC format required to feed into the femtosecond laser machine. The start of such CNC program containing G-Code and M-Code is shown in figure 1.5. It is only the start of code giving the origin point to the laser beam jet.

```
%  
( DATE: 10-12-19 TIME: 14:55 )  
(T2|LASER BEAM|H2|D2|TOOL DIA. - .035|XY STOCK - 0.|Z STOCK - 0.)  
DVAR $Var1  
M14;MOTION LAMP ON  
TIMER 0 CLEAR  
MSGLAMP 11 GREEN  
M8 ;SHIELD GAS ON  
DWELL 2  
G360  
G71  
G90  
G109  
G0G17G40G49G80G90  
M05  
G0X.043Y.237  
M04  
G1Y.235  
G3X.097Y.111I.169J0.  
G1X.102Y.116  
X.106Y.121  
X.111Y.126  
X.104Y.132  
X.098Y.14  
X.092Y.147  
X.087Y.155  
X.082Y.163  
X.077Y.172  
X.074Y.18  
X.07Y.189  
X.068Y.199  
X.066Y.208  
X.064Y.217  
X.063Y.227  
Y.236  
X.06Y.244
```

Figure 1.5: Part of the CNC program output from MasterCAM

1.7.11 Femtosecond Laser Machine

The complete analysis is based on the fabrication of micro-texture on the rake face of the cutting insert. If it has been fabricated, only then the complete analysis was carried out. This has been done on the femtosecond laser machine. There are several other machines on which the micro-texturing can be performed but good and precise dimensional results have been obtained by many of the researchers on this machine. This machine has a computer-controlled programming base that controls the whole process. It takes the CNC program into .NC format which has been generated on MasterCAM. Along with the CNC program it also needs the values of power transmission, pulse width, feed, repetition rate, tool diameter, compressed air flow rate, etc. which have been finalized after several trial runs. It has various units combined to operate on a laser bed. There is a minimum of four computer systems and several

electronic types of equipment attached in set to operate the micro-texture laser cutting machine.

1.7.12 Ultrasonic Cleaning Apparatus

The fabrication process removes material in powder form. It also has burnt oxides and other scattered particles on the surface of the cutting insert. For the accurate dimensional, topographic, SEM, and XRD analysis, it is required to clean the cutting insert. So an ultrasonic cleaning has been carried out using acetone solution and ultrasound from 20-40 kHz for a maximum of 5 minutes per insert.

1.7.13 Minitab

Minitab has been used to find out the optimum parameters with Taguchi Grey relational analysis. Minitab makes the analysis for most and least affecting parameter. It becomes very difficult to analyze when the number of runs is so high. Moreover when the input factors and their levels have a big orthogonal array then this method is quite useful for the analysis.

Chapter 2

2. Literature Review

Machining difficult-to-cut material is a challenge. Sahoo and Pradhan [14] have taken cutting speed, feed, and depth of cut as the process parameter and found their effect on the flank wear and surface finish while turning of Al/SiCp metal using uncoated tungsten carbide inserts. The experiments were carried out in a dry environment. The design of experiments was taken using the L9 array of Taguchi. Premature failure of tool did not happen. The observed optimal parametric combination is v3–f1–d3 and v1–f1–d3 for surface roughness and flank wear respectively. Sahoo et al. [15] have done the conventional casting process and develop a metal matrix of Al/SiCp. They have done the turning operation and studied the machinability characteristics of the carbide cutting insert with TiN coating. Experiments were conducted in a dry machining environment.

Whereas Zhang et al. [13] studied the saw-tooth chip formation in the experiment. They used Inconel 718 as raw material and N/TiN coated cutting tool. They have performed experiments using dry experimental conditions. Following observations are obtained (1) At high-speed cutting, saw-tooth chips are formed because of the formation of cyclic crack. (2) During the turning process, they studied cutting force components keeping all parameters constant. The periodical deviation of the chip thickness results in the fluctuation of the cutting force components.

In continuation to this Zetek et al. [16] have done an optimization process to find out that what is important during the optimization process. Standard finishing processes were carried out but cutting edge radiuses were under main consideration. It is necessary to use a perfect suitable device to view a complex cutting tool and cutting process. In the experiment, the results define the selection criteria of cutting tool and tool geometry for machining of Inconel. In experiments they used a tool with shape edged cutting tip. The tool wear is affected by all of these selected parameters. For

better dependability, it is necessary to get tool wear without notches or other defects. It increases tool efficiency and overall safety in the machining of super alloys.

Experiments are quite expensive to conduct as they need costly setups so Parida and Maity [17] have used Inconel 718 in the room as well as at elevated temperatures. Analysis was done both by experiments and FEM simulation. Cutting force, chip size, shape, temperature, and thrust force were taken under observation. On comparing simulation data and experimental outputs, it was found to be partial validation. Hence the Simulation is good to predict results for those experiment conditions in which the experiments are costly, difficult, and time-consuming. It was also found that when the workpiece temperature increases the chip thickness decreased. Maity and Pradhan [18] have performed experiments on titanium alloy (Ti-6Al-4V) using WM25CT cutting inserts. The main factors under consideration were cutting speed, depth of cut applied to feed and their effect on cutting force, chip reduction, surface roughness, and tool wear. The response surface methodology (RSM) was used to carry out the experiments with a central composite design. The obtained quadratic equations were compared with the experimental values. Chip morphology shows that the side flow of chips and gap between the chips varied when process parameters are changed also the type of chip obtained varied with a change in process parameters. Damage of nose was observed when cutting speed was 160 m/min. During this, the feed was 0.14 mm/rev with a depth of cut 0.75 mm.

Similarly, Maity and Pradhan [19] have tried to explain the machining of titanium alloy grade 5. To machine the titanium rod they have taken the CVD coated cutting inserts. The design of experiments has been created with the help of Minitab using Taguchi L9 array. Maity and Pradhan [20] have performed experiments on Ti-6Al-4V alloy using carbide inserts by mist cooling lubrication. The considered process parameters were cutting forces, surface roughness, material removal rate, tool wear, and chip reduction. It was concluded that the best result was found when the cutting speed of the tool was taken 160 m/min and the feed was given to be 0.16 mm/rev. With these, the cutting depth of 1.6 mm was taken. Various effects were observed on chip formation due to cutting speed along with the depth of cut. Long tubular and helical chips were obtained.

Ribeiro et al. [21] depict the effect on titanium material during machining. He declared the best cutting conditions while machining titanium alloys. He concluded that dry turning operation with 90 meters/min of cutting speed was the best comparable machining condition. It gives a better surface finish. However, when the experiment was done by increasing the cutting speed to 110 meter/min the recorded data of surface finish was increased but along with this cutting tool edge deteriorate very quickly.

Whereas Haron and Jawaid [22] have performed experiments of rough machining on titanium alloy and studied the surface reliability using uncoated carbide inserts. The cutting speed was taken from 45 meters/min to 100meter/min. The applied feed was 0.35 to 0.25 mm/rev with a constant cutting depth of 2 mm. As titanium has a less machinability index so the surface finish was not of good quality. The value of surface roughness was in the limit of 6 microns. When SEM was taken, severe microstructure alterations were observed. Silva et al. [23] performed experiments taking dry as well as wet conditions. The measuring parameters were wear in the tool and changes in surface quality.

The supply of fluids was controlled by reduced flow rate, MQL, and flooding method. Figure 2.1 shows such an MQL setup. They declared that longer values and higher material removal rate were obtained when experiments are performed reduced flow rate. Doing experiments under these conditions prevents the chipping. Figure 2.2 enlighten all the components in such a cooling system. After machining, continuous saw tooth chips were gathered and these are of fragmented type. From the values obtained, it has been declared that the cutting speed and feed have maximum effect on tool wear and surface roughness respectively. A higher R² value gives the highly significant regression model. After experiments, it was also concluded that the obtained values in experiments are very close to the predicted values.

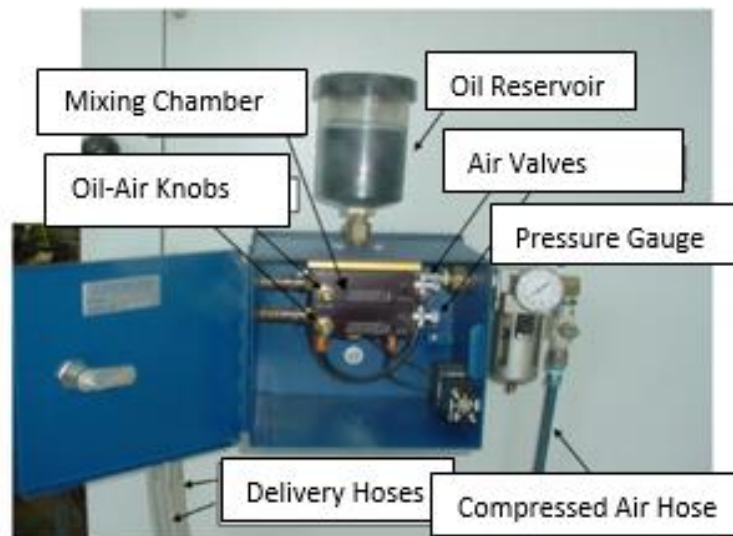


Figure 2.1: MQL Unit [23].

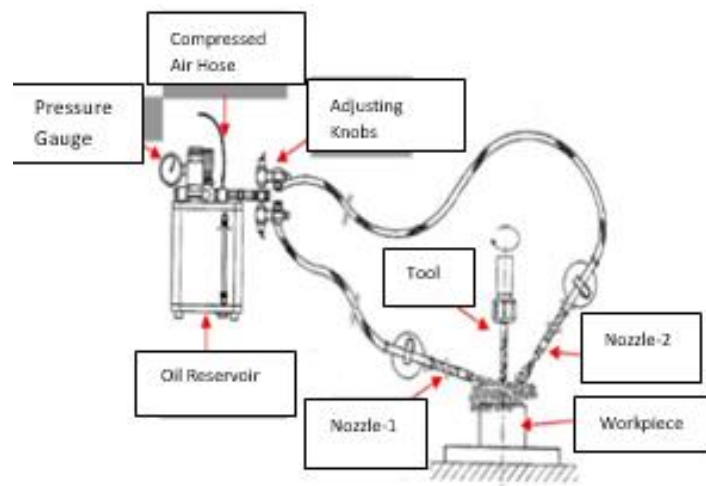


Figure 2.2: Lubricant Delivery system [23].

Chip's shape size and type are very important in determining the machinability of a cutting insert that is why Gente and Hoffmeister [24] explained the chip formation while machining of grade 5 titanium alloy using the cutting speed which varies from 300-6000 m/min. They measure the specific cutting forces. It introduced a novel and rapid method in which deceleration was there in a very short distance. It delivers new data regarding the construction of the segmented chips. During experiments when cutting speed exceeds 2000 m/min a new change in the structure of the segmented chips was observed. Whereas no change in the specific cutting energy was observed, though

it affects the structure of the segmented chips. Hua et al. [25] studied the chip morphology while machining titanium alloy. He has concluded that when cutting speed is low, generally discontinuous chips were produced, whereas at high cutting speed formation of serrated chips takes place. In his study of finite element simulation, the segmented chip generation occurred based on the implicit, Lagrangian non-isothermal rigid visco-plastic model of flow stress. The formation of cracks in the chip occurred due to the ductile fracture criteria based on the strain energy. From the simulation result, it was revealed that stress near the tool tip change, and the crack propagates towards the free surface of the deformed chip in the shear zone as the cutting speed increased.

Sun et al. [26] performed experiments at low cutting speed but high feed. They found the segmented continuous chips. The slipping angle of continuous chips was 38 degrees. But the same for segmented chips was 55 degrees. During experimentation, it was observed that the peak cyclic force over continuous chips was 1.18 times lesser than the segmented chips. Segmented chip length does not depend on the cutting speed and depth of the cut. Cutting speed increases and a decrease in cutting forces occurs due to the thermal softening of materials. Herbert et al. [27] produced a new cutting tool having a micro hole pattern. This micro-hole pattern controls the tribological characteristics. Various dimensions and numbers of the micro-holes pattern in various orientations were manufactured. Then a comparison study has been done between a micro-hole pattern insert and the normal insert. After that, the leading parameter on the machining of Titanium alloy (Ti-6Al-4 V) is tested. During process MQL method is followed for the supply of lubricant.

The adhesion and abrasion tool wear was observed. If the comparison is done for the results obtained from normal insert with micro-textured inserts then results show less flank wear. In experiments, the cutting insert with micro-hole type texture designs 1 and 2 as given in figure 2.3 was used. Higher cutting temperature is the leading factor in judging machinability. It is apparent from the output Table that in the case of micro-hole textured insert, the adhesion of chips is less. Along with this, the machining performance is better even at a higher speed which improves productivity. The chips obtained from the first design have extra shear bands in contrast to the second design as shown in figure 2.4.

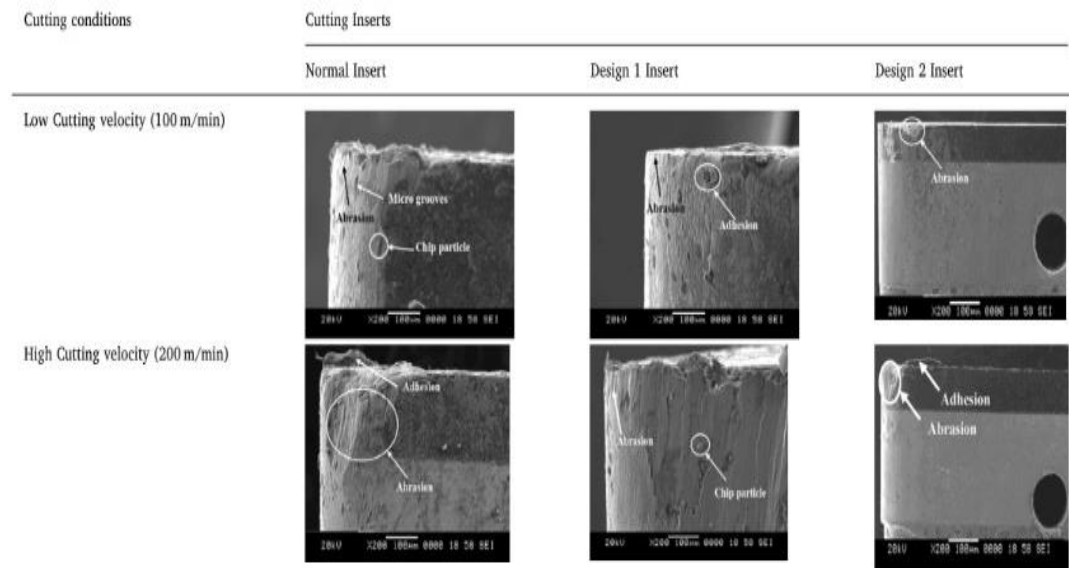


Figure 2.3: SEM Images of tool flank wear [27].

It was declared that the insert with micro-hole reduced the friction which results in a reduction in vibration up to 30-50%, also the surface finish is improved to 40%, with a 30% reduction in cutting temperature. For further improvement in machinability, liquid lubricant can be used. All these parameters improve the tool life without any negative effect on performance.

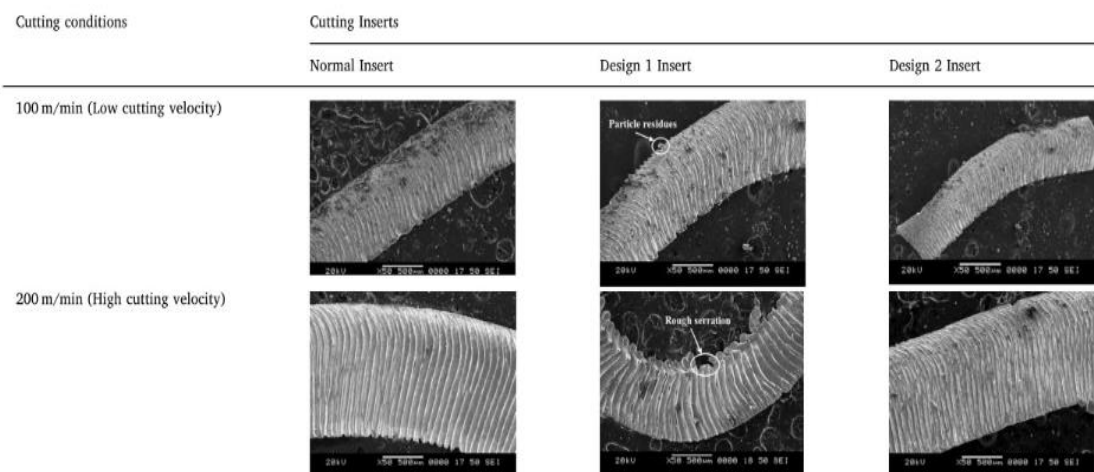


Figure 2.4: SEM images of the chip-morphology [27].

Schulze and Zanger [28] performed experiments on titanium alloy with variable cutting speed and segmented chips were formed. The mechanical and thermal load variation were studied. A finite element model with a self-developed continuous remeshing method was developed to form the serrated chips. Tool wear, Stresses, temperatures,

and velocity of the tool face with tool tip had been investigated. Maity and Pradhan [29] have presented conduct the turning operation on titanium grade 5 alloys. Uncoated carbide inserts are used. The output parameters under observation are taken like speed, depth, and feed given on wear of tool, surface finish and chip reduction coefficient was studied using Taguchi L9 orthogonal array design. Multi-objective optimization based on ratio analysis (MOORA) technique has been used as an optimization tool, It is a multi-objective optimization technique that considers all the attributes along with their relative importance. The optimal cutting conditions of the cutting parameters were obtained by using MOORA coupled with the Taguchi method. The used parameters are cutting speed of 112 meters/min, cutting depth of 1.6 mm with given input feed of 0.04 mm/rev, and cut depth of 1.6 mm. Results declared that the depth of cut gives maximum effect on surface roughness. When cutting speed increased and given feed is also increased the wear rate of the cutting inserts increases. By increasing the given feed and cutting speed, there is a decrease in the chip reduction coefficient. The optical microscopic image of the chips shows that serrated chips were formed during the machining of Ti-6Al-4V.

Pradhan and Maity [29] have performed experiments on titanium alloy of grade 5 using PVD Al-Ti-N coating carbide insert (KC5010) to study the effect of the cutting variables on surface roughness. Along with this tool wear and chip reduction coefficient were also studied. Taguchi L27 is used for the design of experiments. Analysis of variance (ANNOVA) is applied for the cutting variable influencing the responses. Optimal conditions were validated with a confirmation test. It is declared that the optimum parameters setting has significantly improved the machining performance of titanium alloy.

Obikawa et al. [30] proposed the manufacturing of micro-textured tools using a laser of femtosecond machine. Milling experiments were carried on aluminum alloy. Results proved that a micro-grooved surface endorsed the anti-adhesive effects but still there was a problem of adhesion in all experiments. They studied the different ways of improving anti-adhesive effects. They found that the micro-textured tool expressively improved the lubricity and anti-adhesive property. Umbrello [31] studied the finite element analysis of Ti-6Al-4V during high-speed machining. The study deals with the cutting force, tool wear, segmented chip formed, and the morphology of the chip.

Material characterization for FEM analysis was done by using Johnson- cook material model equation. To study the behavior of titanium alloy during high speed machining three different sets of material constant was being implemented. The results revealed that the prediction of both principal cutting force and morphology of the segmented chip agreed well with the experimental results.

Calamaz et al. [32] have done the numerical simulation of serrated chips in the process of machining titanium alloy. They performed all simulations and conclude numerical solutions using FORGE 2005 software. The main of the new materials models is to produce segmented chips during the machining of titanium alloy with a wide range of cutting speed and feed. During modeling, it was assumed that the segmentation of chips was induced only by adiabatic shear banding. And it was also fixed that there is no materials failure in the primary shear zone. The results were calculated based on strain rate, temperature, strain, strain-softening effect. After that, the results were validated with experiments under the same conditions. Schulze and Zanger [33] had determined the material model parameter of the Johnson cook model for titanium alloy by performing split Hopkinson bar tests. They have done the simulation of cutting tools and workpiece taking constant material to predict the surface veracity of the finished surface. It was concluded that surface integrity depends upon the material model and the value of the material constant. Strain rate and cutting temperature was showing opposing mechanisms with the variation of the cutting velocity and the depth of the plastic deformation was rapidly increased.

Caliskan and Kucukkose [34] have used the CN/TiAlN coated carbide tools and studied Wear behavior with cutting performance in milling operation of Ti6Al4V taking dry conditions during machining. The investigation is done for the surface finish concerning cutting forces. SEM was conducted along with EDS to study the structural and compositional characterization of worn workpieces. Results show that the abrasive wear is dominant in the tool failure on coated tools. Milling of Ti6Al4V was done using CN/TiAlN coated carbide tools and the 15% longer lifetime was obtained with tool wear. Zhan et al. [35] have used micro-grooved tools in turning operation. Their main focus was on the production and consumption of cutting energy. The models were Reliable through sensible cutting experiments as shown in Figure 2.5. Results also show the significant effect of speed, depth taken, and applied feed on cutting energy.

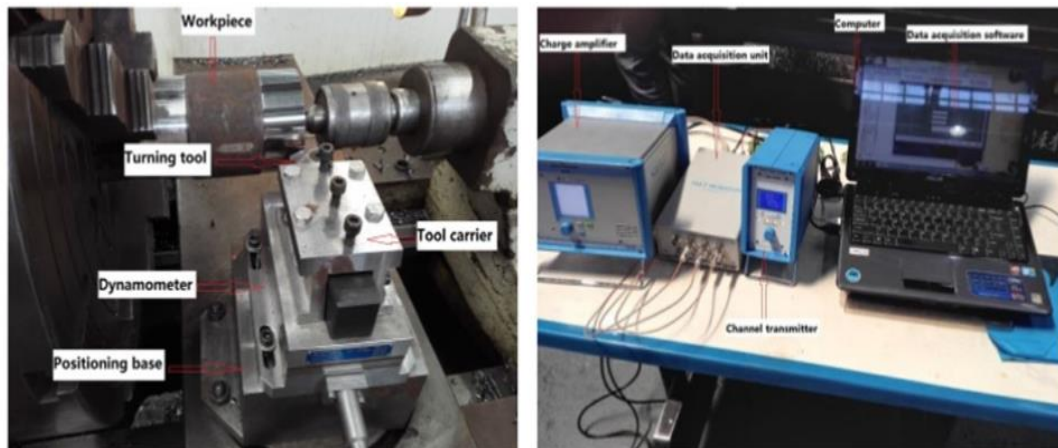


Figure 2.5: Cutting Test machine setup [35].

The industrialization growth of any nation merely depends on how we evolve new methods and techniques to machine metals with better and desired properties. To machine difficult to cut metals, various methods are there in practice like high-speed machining, minimum quantity lubricant, hot machining, etc. But in comparison, machining with a micro-textured insert gives the best result among all others. This method of machining shows a variation in results when different shapes and sizes of micro-textures have been taken. K. Zhang et al. used micro-textured CNT (Carbon Nano Tube Coated) tools and comparison has been done with NCT (Non-Carbon Nano Tube Coated) tools. An extensive decline in the values of cutting forces and cutting temperatures is detected. Also, the coefficient of friction at the tool and chip interface is reduced. In this study, it has been affirmed that the geometry of the micro-grooved pattern has a foremost effect on machinability. Coated tools with micro-texture give better results than the texture taken parallel to chip flow [36].

N. H. Duong et al. executed experiments and found that machining with a micro-grooved cutting tool engenders lower cutting force and thrust force. Hence less energy is required for machining. The micro-textured groove width, shape, depth, area covered and edge distance affect cutting force [37]. C. Zhang et al. declared the improvement in stress distribution of rake face of cutting tool when machined with micro-textured cutting insert. Simulation has also been done. Results proved that machining with high speed and using micro-textured insert decreases the cutting force and direction of pattern decide the tool wear as well as the cutting temperature. Cutting with a micro-textured tool also changes the chip morphology [38]. C. Qiu et al.

performed the experiments and proved that tensile stress can be reduced by using micro-textured cutting inserts. It also tempts to have compressive residual stress on the surface of the machined workpiece. The residual stress has a maximum effect due to the width, depth, and distance from the cutting edge of the insert [39]. H. Jiang et al. has used ANOVA (Analysis of Variance) of single-factor and the test results declare that all factors like speed, feed, and depth values are taken, have a significant effect on cutting energy in experiments. But when it has been measured for surface energy, it was found to be very less [35].

C. Darshan et al. prepared a micro-texture design that has parallel lines. The best result is found at a speed of 80 m/min. The measured average surface roughness was 3.148 micrometers. Taking this combination of parameters the cutting temperature was 45.42 degrees [40]. K. Orra and S. K. Choudhury have proved the reduction in coefficient of friction up to 11.9% with micro-textured insert as compare to normal cutting insert. It reduced cutting force, suppress flank and nose wear for both the lower as well as the higher cutting speeds. When the same experiments have been done using MoS₂ lubricant, the machinability factor gets reduced at a higher speed [41]. C. M. Rao et al. have proved that the micro-textured cutting insert has reduced the friction between tool and chip along with a reduction in vibration up to 30% to 50%. During machining, the temperature is also reduced up to 30%. S. Karthikeyan et al. made a comparison of machining results with and without micro-textured inserts on aluminum. It has been declared that the coefficient of friction is reduced by 12% in machining with textured insert than the non-textured insert. Then a gap of micro-texture has been filled with graphite powder which improves the cutting velocities along with feed [27].

K. Maity and S. Pradhan have used titanium alloy as workpiece material and done FEM (Finite Element Model) simulation using cutting insert with micro-texture. In machining, cutting speed of 125.6 m/min is taken and feed was of 0.23 mm/revolution. Simulation results were taken at 2 mm of the depth of cut. Then simulation results were compared with experimental data. Considerable improvement in machinability was found [42]. K. Patel et al. have prepared cutting inserts with different ranges of micro-texture width from 50 micrometers to 100 micrometers, depth from 10 micrometers to 30 micrometers, and gap of 15 micrometers to 100 micrometers. All these inserts are used for machining of titanium alloys [43]. N. T.

Alagan et al. three different micro-textures have been designed and fabricated on rake face and flank face. Then machining has been done on Alloy 718 with high-pressure coolant. A noticeable improvement in the surface finish has been observed [44].

Turning is the most common machining operation used in industries for the manufacturing of products with desired properties. The nature of the material used in manufacturing also plays an important role. Due to less weight to strength ratio, modern metals like Titanium has a prevalent variety of application in the arena of industries, medical equipment, and marine parts, etc [45]. Titanium alloys have low thermal conductivity and a highly reactive nature because of that machining of such metals with traditional techniques becomes very difficult. The raised temperature during machining reduces the tool life, so the temperature analysis is of great significance in a way to increase the machinability [46]. Abundant research has been carried out to date but the experimental setup, testing, and analysis methods are extremely expensive. So the modern finite element analysis using various software becomes very effective. These simulation methods provide a nodal observation for various parameters and plot them graphically.

A platform like DEFORM 3D enables us to analyze, compare, and make conclusions for any elemental mesh in the workpiece, cutting insert, and chips. It permits us to use a wide range of input factors and their levels. Numerous research has been conducted in this area to enhance tool life and machinability [47,48]. Tounsi and otho (2000) have done machining to deduce the most effective parameter in the machining process. They have considered a cutting tool, machine chuck along with workpiece under observation, and found that vibration is the most effective variable to be considered during machining [49]. K. Maity and S. Pradhan (2017) have studied the types of chips produced during the machining at a cutting speed of 160 m/min and feed was taken as 0.14 mm/rev. They have taken a constant depth of cut of 0.75 mm during their experiments [18]. Enomoto and Sugihara (2010) have used Aluminium alloy as the workpiece material and performed milling operations using the micro-textured insert. They considered surface finish as the required factor of judging the performance and declared that lubrication has improved the finishing capability of cutting insert [50].

H. Caliskan and M. Kucukkose (2015) have done milling of Ti6Al4V using CN/TiAlN coated tools. They declared the adhesive and abrasive wear as the main

reason for tool failure [51]. M. Zetek et al. (2014) concluded that the edge radius of 15 μ m is not the standard parameter that all producers are using but all parameters must be in an optimal value. Moreover, if this is used in polishing and other processes, it can increase the tool life [16]. Sima and Ozel (2010) have performed experiments on Titanium alloy and tried to modify the material depending upon the temperature. They conducted experiments using coated and uncoated cutting inserts. Finite element analysis is performed in DEFORM software and material flow stress is predicted [52]. D. Umbrello (2008) has done the FEM analysis for the high-speed machining of Ti6Al4V. He has considered tool wear rate, cutting force, and obtained shapes of the chip into consideration. All the simulation results have been validated with experimental results [31]. Ribeiro et al. (2003) declared that the increase in cutting speed results in tool wear which in return reduces its life. They directed experiments on titanium and 90 m/min was found as the promising cutting condition [21]. Schulze and Zanger (2011) determined the surface veracity of the machined titanium surface in simulation using DEFORM software. They declared that the strain rate and cutting temperature reduced with the upsurge in the cutting velocity. Material constant was used in the FEA simulation [33].

K. Maity and S. Pradhan (2018) used DEFORM 3D software for the simulation of titanium alloy. In the machining process, they have used a micro-grooved insert and all the DEFORM 3D simulations show fractional covenant with experimental results [42].

For the industrial evolution of any nation, innovative materials/metals, methods of machining, machinability improvement techniques, etc are essential to be developed. Numerous metals are there which can replace the traditional one because of their superior properties. Likewise, the difficult-to-cut materials have a great possibility of application in aerospace, naval, medical, and industrial areas. Nevertheless machining of difficult to cut metals is still a challenge [36]. Several machining methods have been developed by researchers to improve machinability. Most frequently used are High-speed machining, MQL (Minimum quantity lubrication), Flood lubrication, Hot machining, Coated tool machining, and many more. According to P. Sivaiah et. al. [53], the MQL system is very effective as compared to the conventional methods of cooling. Any machining operation using a micro-textured insert has amplified the machinability

among all of the other methods [54,38]. S. Karthikeyan et al. [55] have prepared straight lines in micro-texture. Whereas Wenlong Chang et al. [56] prepared micro-grooves of different orientations such as horizontal, perpendicular, and inclined lines at a 45-degree angle to the rake face, and reduction in tool wear was observed. Deng Jianxin et al. [57] and Na Zhang et. al. [58] found that parallel and dot type micro-textured cutting tools have less coefficient of friction. According to Junsheng Zhang et. al. [59], machining with micro-textured cutting inserts has reduced the diffusion wear. They have prepared the line and circular pit type of grooves in which the line orientation has increased the heat dissipation rate but the circular pits provide more area for the application of lubricants while machining.

These micro textures can be produced by various methods and machines. C. Darshan et al. [40] have used micro EDM, Nd-Yag laser machine, V tip micro grinding machine, etc. to prepare circular holes on the tool surface. An increase in cutting speed decreases the microhardness for ferrite and austenite but not in the machining of difficult-to-cut metals [60]. So, Adam Khan M and Kapil Gupta [61] focused on tool wear and tool life while performing the experiments and demonstrated that with an increase of velocity, tool wear increased, and insert with dimple micro-texture is having maximum tool life. In a comparative study of micro and nanoscale textures for the machining of aluminum alloy, it is found that the cutting force requirement in the nanotextured cutting tool was less than the micro-textured cutting tools [62].

Not only the experimentation but simulation has also been conducted by A.K. Parida et. al. [63] on DEFORM which proves that tool life is increased with nano dimples. 3D finite element simulation has been conducted on Ti-6Al-4V alloy in dry turning and validated with experiments [64]. Microgroove width, depth, and distance from the cutting edge are the most significant parameters on cutting forces. In addition to that C. M. Rao et al. [27] found the surface finish is varying by changing the size and orientation of the microgroove.

The selection of micro-texture design, its orientation, and laser machine parameters, etc. must be done in such a way that it must not abolish the micro CVD coating from the surface of the cutting tool [65]. After the fabrication of the grooves, the percentage of carbon and oxides produced inside the groove should not be more than a particular value. Because it will block the heat dissipation from that area which

will reduce the cutting tool life and ultimately machinability will decrease [35]. K. Orra and S. K. Choudhury et al. [41] have grooved the micro-textures using an Epilog laser machine at low speed and high power and declared that the characteristics of the cutting tool have not been distorted but according to V. Sharma and P. M. Pandey [66], the deviation in dimensions was observed during the fabrication of micro-texture. The various design parameters taken were the distance from the cutting edge, width of the micro groove, diameter of the curved part, and depth of the texture. In the fabrication of micro texture, the laser power and frequency have a good influence on contact angle [67].

Difficult to machine metals like Titanium Grade 2 has high corrosion resistance, good formability, and good strength to weight ratio maintained even at high temperatures, etc [68]. Due to these properties, it is being preferred in a variety of applications like medical equipment, human body parts replacements, aero engines, and industrial manufacturing [69,70]. N. J. Hallab and J. J. Jacobs [71] explained that since 2007, 1.5 million knee replacement using such metals has occurred. But to make the best use of such metals, high-quality surface finish, precise dimensional machining at an economical price range are required.

Machining of such metals is still a challenge as tool life reduces due to its low thermal conductivity [72]. Many non-traditional methods of machining like minimum quantity lubricant, hot machining, flood machining, etc. have been developed which tried to reduce the tool chip interface temperature but the increase of use of lubricants and energy consumption have been observed [73,74]. B. S. Nishanth et. al. [75] have compared electro discharge, electro Chemical, ultrasonic turning, and Water jet Machining.

The main problems in traditional machining methods are the harmful effect of the use of coolants on human life, issues of aquatic organisms, and the cost of machining, etc. are explained by Imran Masood [76]. Among all of the non-traditional machining methods for difficult to cut metals, textured cutting inserts have shown better results [77]. D. Arulkirubakaran et. al. [78] have conducted the numerical simulation of the machining process using DEFORM 3D software and declared that the cutting temperature and force have been reduced using textured insert. Whereas Z. Wu et. al. [79] explained that cutting of removed chips using textured cutting insert becomes easy

which prevents the welding of chips on the surface. A drilling tool with microtexture has been generated by S. Niketh et. al. [80] and they declared that 10-12% of reduction of thrust force is observed in dry machining and micropools of lubricants in the textured cutting insert are the reason.

C. Darshan [40] has prepared the parallel line pattern of micro-texture whereas A. Olleak and T. Ozel [81] have fabricated parallel, perpendicular, and diagonal lines and pits to the cutting edge. T. Sugihara and T. Enomoto [82] have investigated the performance of a cutting insert with micro stripe texture. These stripes have parallel and orthogonal orientations to the cutting edge of the insert. Anti-adhesive properties both in dry and wet cutting conditions have also been examined. It has been observed that only a few standard shapes like straight lines, circular pits, sinusoidal waves, the parallel and perpendicular micro-texture have been fabricated [27]. Moreover, P.Sivaiah et. al. [83] have done machining using variously textured and non-textured inserts on AISI 304 SS workpiece. As Titanium Gr 2 has a wide range of areas of applications, it is required to work on its machining using cutting inserts having new micro-textures designs. A. K. Prida et. al. [84] have compared the FEM simulation results with experimental using dimple type microtextures and declared the better results with textured insert. N. Ghate and A. Shrivastva [85] have tried to find out the process parameter for the fabrication of various titanium implant surfaces.

Difficult to cut metals have numerous usages in the medical, automobile, production, and other industries but due to their high machining costs, applications get minimized. Various metals/alloys have been tested to expand their applications as S. N. Rosa et. al. [86] have replaced the usual grey cast iron with compact graphite cast iron having a residual level of titanium content. They declared that the higher content of titanium is responsible for the shorter tool life but it has no influence on the surface roughness of CGI. P. J. Arrazola et. al. [87] have done machining of Ti555.3 and compared the results with Ti6Al4V. They found quite a similarity between the machining results of these two metals. Wear properties using multi-layered carbide cutting inserts on hard steel of 55HRC have been studied by A. P. Kenel et. al. [88]. Tool life and surface roughness are investigated while performing face turning operations on AISI 51100 and AISI 52100 steels [89].

It is important to analyze the cause of damages that occurred in cutting insert while machining the Ti alloys so, the microscopic and macroscopic features have been studied. A minimum quantity lubrication system has also been introduced to study the shapes of removed chips [90]. A. C. Hoyne et. al. [91] have declared that, at high machining temperatures, titanium becomes very reactive which increases the effective tool wear. So, they have generated an atomization-based cutting fluid spray system in the cutting zone and declared it more effective than flood cooling and dry conditions. T. Nguyen et. al. [92] performed machining operations on the Ti-6Al-4V bar using uncoated carbide and PCD inserts. A confocal microscope has been used to study the microstructure of titanium before and after machining. Assuming that, the rate of cutting tool wear may also depend on machining process parameters, A. Kumar and G. Sehrawat [93] have tried to find out the relation between process parameters like feed & cutting speed on the surface roughness & tool wear while machining of Ti-6Al-4V using coated carbide cutting tools. After SEM analysis it has been declared that the tool wear increased with an increase in feed. To reduce the machining cost, experiments with cryogenic machining in place of wet machining have also been carried out. Improvement in tool life and the surface finish has been observed [94]. Cryogenic cooling with CO₂ has also increased the tool life while machining titanium alloy [95]. M. Lotfi et. al. [96] found that the experimental analysis is costly so they have done the finite element analysis to study the wear of a TiAlN coated carbide insert with Inconel 625 and declared the depth of cut as the most responsible factor for wear. Along with this, few researchers have also compared the effectiveness of PCD cutting tools with uncoated tungsten carbide cutting tools in machining Ti-6Al-4V alloy considering the cutting speed, surface finish, tool wear, and chip morphology as the parameters [97]. Tool wear analysis and comparison between coated and uncoated cutting insert has also been carried out [98].

Machinability of cutting inserts when used with difficult-to-cut materials is required to be increased to minimize the manufacturing cost of required products. The main reason for smaller cutting insert life is the tool wear which occurs due to many reasons such as high machining temperature, various material properties, etc. The cutting insert wear can be identified and controlled with the study of shape, size, and type of removed chips. J. Barry et. al. [99] observed that the chip shape has been

changed from aperiodic to periodic saw-tooth with the increase of speed and feed. Variation in thickness of chips has also been declared. Morphology of top, back, and the cross-sectional surface of chips after performing the milling operation on titanium with mill cutter under flood cooling system has been conducted [100]. Whereas S. Joshi et. al. [101] performed the optical and scanning electron microscopy of removed chips. They concluded that at room temperature high shear occurs in chips which have been compared with other temperature values. R. W. Maruda et. al. [102] tool wear analysis has been carried out for cemented carbide inserts in the machining of AISI 1045 carbon steel. They found that the wear has been reduced by minimum quantity cooling-lubrication method. The significant effect on tool wear is caused by the droplet diameter of the coolant. To monitor the tool wear, a thermocouple has been designed and installed on a polycrystalline cubic boron nitride cutting tool. In this, AISI O2 steel has been used as workpiece material and the effect of temperature on tool wear has been studied [103].

In addition to that S. Sun et. al. [104] focused on material removal rate, cutting speed, chip geometries. The dimple-shaped deformations have been studied and found that the number of dimples reduced with the increase of material removal rate which helps to reduce the tool wear. The response relationship analysis on residual stress distribution characteristics to control tool wear has also been introduced [105]. H. Lin et. al. [106] prefer oils on water cooling method in comparison to the MQL or CAMQL methods to reduce the machining cost, hazards and pollution. Then the effect on-chip shapes, types have been studied. They declared that the external oils on the water method have reduced the tool wear effectively. A relationship between the tool wear and high-frequency vibrations has been found. The change in tool geometry represents the change in the shape of removed chips. They tried to control the vibrations to minimize the tool wear and improve the tool life [107]. Attention has also been given to the study of the role of cutting force in chip formation. For this, the machining of Inconel 718 followed by the analysis of cutting force components has been conducted. It was found that the sawtooth chips at high cutting speed influence the fluctuation in cutting forces [13].

Modern production industries continuously demand contemporary manufacturing techniques on smart material. To formulate such affirmations, a variety

of experiments are essential to be performed which involve the high investment of resources. Distinct machining and test setups are required. Whereas the FEA (Finite element simulation analysis) using DEFORM 3D software provides an assortment of data analysis tools. Predictions always come after validation. So, first, the simulation results have been validated with experimental observations then several predictions using the same data and on the same software, can be accomplished.

C. S. Kumar et.al. [108] have performed experiments on AISI 52100 steel with coated and uncoated AlTiN cutting tools under dry machining conditions. Temperature variation has been analyzed. The complete machining process took place on a heavy-duty lathe machine. A different setup has been made to measure the values during experiments whereas A. K. Parida and K. Maity [109] have executed experiments on Ti-5553 using a hot machining process. They consider that the nose radius of cutting tool inserts also affects thrust force and tool chip contact length [17]. While machining of Inconel 718 and chip geometry, chip thickness, shear plane length, and cutting forces have been studied [110]. According to high stress and strains are difficult to find out experimentally so FEM simulation using any software is a better tool in such analysis. Similarly, Y. M. Arisoy and T. Ozel [111] have done experiments and simulations to study the micro-hardness in titanium alloy. They have focused on the cutting conditions to find its relation with grain size in machining distinct effects. T Thepsonthi and T. Ozel [112] have performed the milling operation in three dimensional simulation for titanium alloy and predict the chip flow. The simulation results have been compared with the experimental results and concluded the tool wear is the main parameter to affect the cutting temperature and wear rate. They gave visualization effects to their assumptions using simulation software. A. K. Parida et. al. [113] have used the DEFORM software to conduct the simulation analysis. They performed experiments on AISI steel and declared the simulation results with 10% of error. M. Lotfi et. al. [96] intended to produce a FEM model for the prediction of tool wear while machining Inconel 625 using TiAlN coated carbide inserts. They tabulate the results and found the depth of cut as most affecting factor for cutting tool temperature the most.

Z. Wu et. al. [79] have performed the FEM simulation on Ti6Al4V and validated the results with cutting temperatures, cutting forces, and tool-chip contact lengths with a 10% of error. K. Maity and S. Pradhan [42] have performed the

simulation on DEFORM-3D for machining of titanium alloys with microgroove cutting inserts. They have taken constant cutting speed, feed, and depth of cut for all the runs. They found the partial agreement of simulation results with experimental output values. A. K. Parida and K. P. Maity [114] have taken the Inconel 718 as the workpiece material. They conduct the turning operation in actual experiments and FEM simulation. They focused on 2D modeling rather than 3D modeling to validate the simulation results. No preheat condition has been applied. In another analysis, they have considered Al 6061 alloy as the most demanding material and performed the FEM simulation on DEFORM-3D software to study the forces and chip morphology [115].

Tool life in the machining of Inconel 625 alloy on DEFORM software has also been studied with chip formation [116]. Identification of variation in cutting energy, cutting force, and chip analysis under hot flame and room temperature machining conditions on nickel base alloy have been studied. They conduct the experiments and simulation both for the same parameters [117]. B. S. Prasad et. al. [118] have declared that the vibration signals also have a noticeable effect on tool wear in turning operation. They performed the experiments in AISI 1040 and validate with simulation. Using DEFORM-3D software as a platform, a 3D cutting finite element model was established for the machining process of titanium alloy whirlwind milling with three elements. The effects of cutting speed, feed and radial depth on the cutting temperature were analyzed. The results showed that the cutting speed had the greatest influence on the cutting temperature, the axial feed and the radial cutting depth [119].

J. Obiko et. al. [120] have taken declared the Deform 3D as an effective platform for analysis of deformations of X20CrMoV121 steel. They take 850 °C as the preheat temperature and conduct the simulation process to study the strain/stress distribution. U. Kumar et. al. [121] have tried to implement the FEM approach on forging processes. They have studied a wide range of process parameters to minimize the machining cost and declared that the results of DEFORM simulation are approximately acceptable. J. O. Obiko et. al. [122] have used the FEM tool to find out the relation between turning parameters and forces. S. Kosaraju et. al. [123] have found a 9.07% to 9.94% error in comparing the experimental and simulation results while investigating the machining of Titanium alloys. J. O. Obiko and F. M. Mwema [124] have performed a 3D simulation on DEFORM to compare the proposed metal upsetting process with the

conventional process. They declared that the modified upsetting process results in fewer deformations and FEM simulation provide convincing confirmations of that. K. K. Prasad et. al. [125] have compared the simulation results with experimental results of machining of difficult-to-cut metals like titanium taking power consumption as one of the major parameters. Drilling process analysis has also been done using the FEM simulation process [126] whereas U. Khanawapee and S. Butdee [127] have conducted the simulation analysis of the cold upsetting process for Al7075 fitted with S15C.

Chapter 3

3. Problem Formulation

Recently numerous non-traditional techniques are available such as MQL, coated and uncoated cutting tools, flood lubrication, etc. But all these approaches have constraints such as unavailability of resources, the requirement of special set up, the problem of disposal of coolants, trained operator requirement, etc. (Chetan et. al.) [40]. Therefore, the non-traditional technique like the micro-grooved surface of cutting inserts appears to be a better technique than the conventional methods as it will be helpful in reducing the cutting tool temperature. It will also reduce the tool wear rate. Ultimately the machinability of the cutting tool would be increased as it will increase the heat dissipation rate. But the micro texturing is also a typical task as it requires a special machine for the fabrication of patterns. The chip morphology also describes the rank of machinability. In near future, the research can be followed on metals like Titanium and its alloys, Inconel, Nickel, and all material with low thermal expansion coefficient on which such machining improvement techniques are still to be discovered. Also, work has to be done on the design and simulation of several micro-grooved patterns subsequent investigation of tool wear, chip forms for the textured insert.

After ample study of prevailing literature on textured and non-micro-textured cutting tools, the following interpretations have been made:

- For efficient machining, a good surface finish is an essential requirement.
- The quality of the surface finish declines as the wear increases. It may be due to poor lubricating conditions or lack of cooling at the cutting interface.
- Micro-textured cutting inserts have given good results in terms of increase of surface roughness and tool life while machining the difficult-to-cut metals.
- The use of micro-textured cutting inserts with solid lubricants has also reduced the power required to machine the surface of difficult-to-cut metals. It also reduces the co-efficient of friction.
- The attributes for the above-mentioned improvements are:

- a. Contact area decreases between tool and chip.
- b. Self-lubricating property at the cutting zone of tools and chips.
- The effectiveness of textured tools merely depends on designs of textures, alignment with cutting edge, area of texture, and orientation.
- The design and orientation of texture according to the direction of chip flow are very significant for the enrichment in machinability of the cutting tools. Because of fewer adherences in perpendicular texture orientation, it is more effective than parallel textures.

3.1 Research Objectives

- a) Design of various micro-grooved patterns on the surface of cutting inserts.
- b) 3D modeling, FEM Simulation, and comparison of all micro-textured cutting inserts with experiments.
- c) To study the effects of cutting variables on machinability during machining titanium alloy.
- d) To find out the optimum parameters settings using the Grey Taguchi method.

3.2 Organization of Dissertation

Various steps to achieve all of the above-mentioned objectives are organized in figure 3.1. Following these steps, a detailed study analysis has been included in the next chapters. It starts from literature reviews and determination of objectives, includes various designing, fabrication, testing, analysis, and conclusion reports.

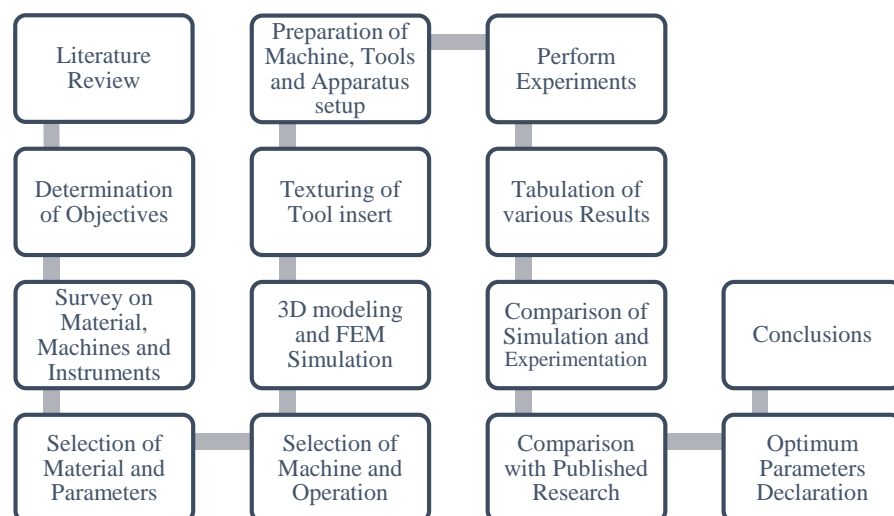


Figure 3.1: Methodology of Research work

Chapter 4

4. Materials and Methods

4.1 Design and Fabrication of Spiral Triangular Micro Texture

In this section, a Spiral triangular micro-texture has been designed and then fabricated on the rake face of CVD (Chemical Vapor Deposition) coated with TiCN and alpha-alumina on a tungsten cutting insert. Best input parameter values are found and verified with the help of topography. The spiral triangular texture will act as a reservoir of lubricant and will provide more area for heat dissipation rate. Topography confirmed that using the femtosecond laser machine for the micro-texture on the surface of the cutting insert has not eradicated the coating.

To fabricate the micro-texture on the rake face of cutting insert, all the parametric study has been performed and standard dimensions have been taken. It started with a 2 D (Dimensional) design of the micro pattern and then grooved on a 3D (Dimensional) cutting insert. The actual fabrication process started after doing some trial analysis. After making corrections and final fabrication of micro-texture on cutting insert, verification of all parameters has done with the help of topography.

4.1.1 Designing

Solidworks[®] software is used to design the pattern in 2D and 3D shapes. Dimensions have been taken as per the standard dimensions available for the cutting insert of SNMA 120408 HK1500. The material of this cutting insert is tungsten carbide material with a chemical vapor deposition coating of TiCN and alpha-alumina up to 20 microns. It has a 12.7 X 12.7 mm side. The thickness of the insert is 4.76 mm. The available radius at the cutting edge is 0.8 mm. So first of all, a texture covering the cutting edge side of 1.12 mm on both sides is taken and a spiral design in triangular form has been chosen. This design provides maximum area for the reservoir of lubricant or coolant. Moreover, it has a continuous wall for heat dissipation of the thickness of 20 microns. The groove has a width of 10 microns. A gap of 0.08 mm has been left

between the cutting edge and the edge of the texture. The depth of micro-texture is chosen to be 10 microns only to prevent the removal of chemical vapor deposition coating from the rake face of the cutting insert. Figure 4.1 shows the design of the selected spiral triangular textures with dimensions. Figure 4.2 gives the 3D view of actual texture grooving and figure 4.3 explains the location and orientation of the design.

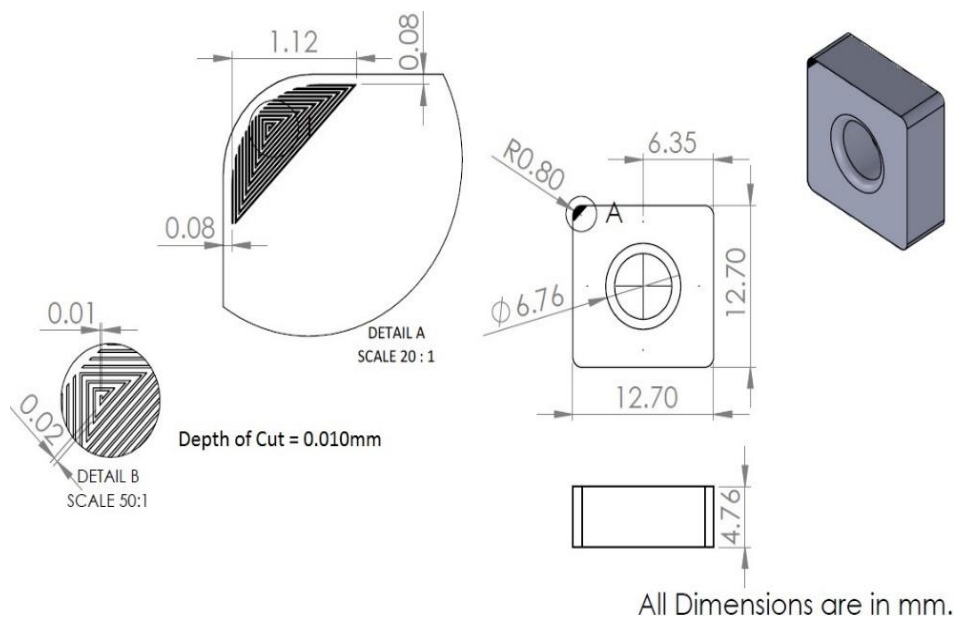


Figure 4.1: Design of micro-texture with dimensional detail.

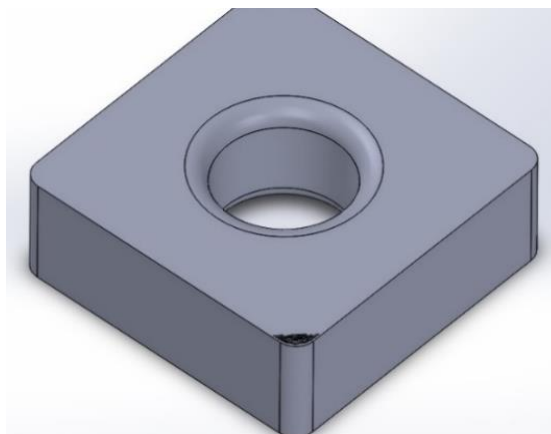


Figure 4.2: 3D representation of location and orientation micro-texture design.

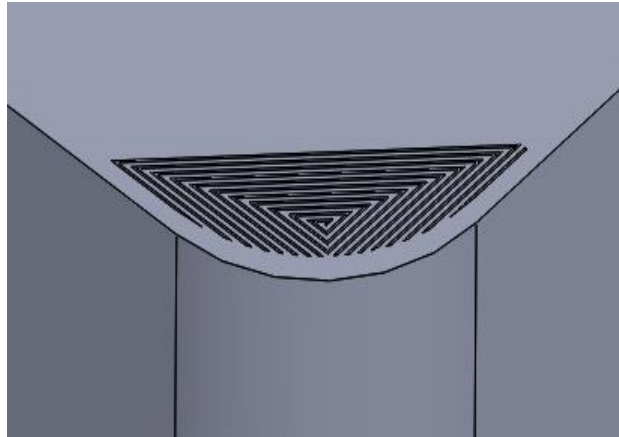


Figure 4.3: Spiral triangular Micro-texture design on the rake face of cutting insert

After designing the pattern as per the actual dimensions of the cutting insert, a G-Code CNC (Computerized Numerical Control) program has been generated using MasterCAM software. All input parameters such as co-ordinates of laser bed, a distance of origin from cutting edge, feed, repetition rate, tool diameter, shutter count, dimensions of tool and workpiece, margin from cutting edge, depth of cut, etc. are taken into consideration while making a CNC program. After writing this, few trial runs have been conducted to check and make changes for final input variables and then the CNC program has been finalized accordingly.

4.1.2 Fabrication

Laser grooving has been done by the Femtosecond laser cutting machine on the surface of the cutting insert. First, several trial runs have been done in straight line patterns and after checking in topography one combination has been finalized and all the patterns are then prepared using those input parameters. In femtosecond laser machine power transmission, pulse width, feed, and repetition rate are entered as the input parameter. The compressed air flow is applied to make a spatter-free grooving with a gap taken from the cutting edge of the laser. Distance from the origin of the laser bed is taken as 10 microns in finalized design. By taking all these input variables the pattern obtained on the cutting insert surface is having chamfered square shape of the groove. It takes 4.52 sec per sample to make the micro-groove. An average output width of the groove is obtained as 15.5 microns with a depth of 11.036 microns. The obtained average actual gap from the cutting edge of the insert is 24 microns. In the whole process, the shutter count used was 1. After this, cutting inserts have been prepared for

experiments. Table 4.1 shows all the input parameter values of the femtosecond laser machine taken for trial runs and the finalized parameter set. Figure 4.4 shows all the trial run fabrication of micro-textures on the rake face of the cutting insert.

From all of these, the best value combination which is giving the required result has been taken for final grooving of texture and that is 2W of power transmission, 100 fs of pulse rate with 2.5 mm/sec of feed. The repetition rate has been decided as 10000 Hz and a tool diameter of 12 mm is taken. During the grooving, a compressed airflow of 12 lit/min has been passed. In this micro-texture grooving, the gap from the cutting edge of the insert has been taken equal to 30 microns and in the femtosecond laser machine, the distance of the start of a laser beam from the origin of the bed has been taken as 10 microns.

Table 4.1: All input parameters of the femtosecond laser machine and their values.

Femtosecond Laser Machine Specifications and Input Parameters								
Design Pattern	Power Transmission (W)	Pulse Width (fs)	Feed (mm/Sec)	Repetition Rate (Hz)	Tool Dia (mm)	Compressed Air Flow Rate (lit/min)	Gap taken from cutting edge of Insert (micron)	Distance of Origin from cutting edge
Spiral Triangle	2	100	2	10000	0.015	12	30	10
	2	100	2.5	10000	0.015	12	30	10
	3	100	2.5	10000	0.015	12	30	10
	3.5	100	2.5	10000	0.015	12	30	10
	4	100	2.5	10000	0.015	12	30	10
	4.5	100	2.5	10000	0.015	12	30	10
	5	100	2	10000	0.015	12	30	10

The main reason for selecting this set of values is the power transmission and feed. Less power consumption with more feed will be economical and it is giving the best result in terms of microtexture groove depth and shape. After making all the micro-groove patterns on the surface of cutting inserts, these are followed by ultrasonic cleaning to make the insert's surface clear from all removed material particles and spatters during laser grooving.

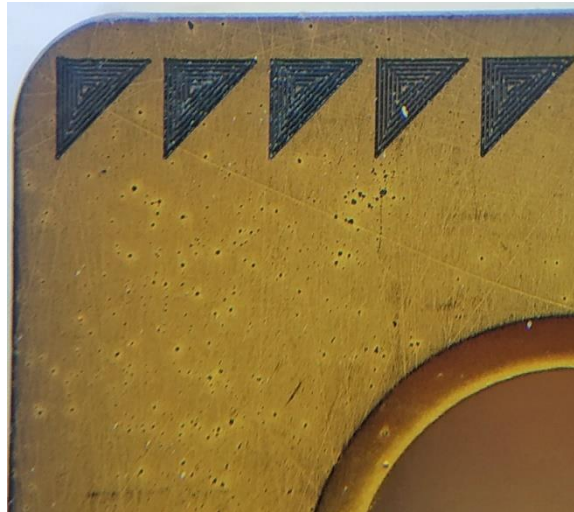


Figure 4.4: Various trial run patterns grooved on the rake face of the cutting insert.

This process uses acetone solution and ultrasound from 20-40 kHz for a maximum of 5 minutes per insert. Figure 4.5 shows the ultrasonic cleaning of cutting inserts after making micro grooves on the surface of the femtosecond laser machine.

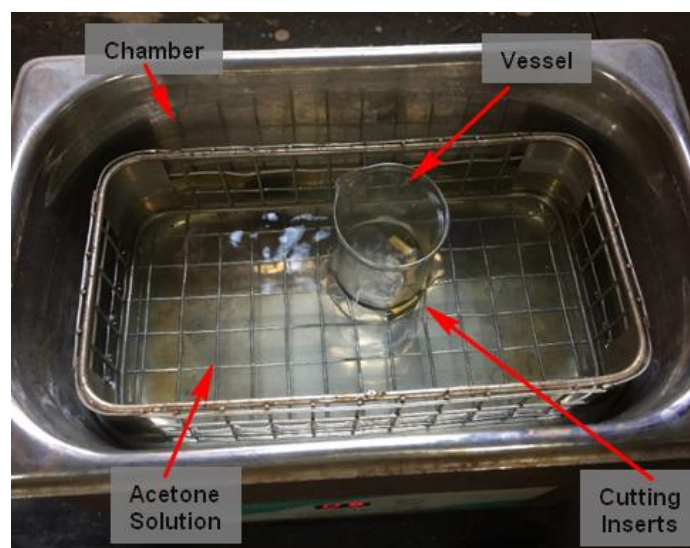


Figure 4.5: Ultrasonic cleaning of cutting insert with micro-texture.

After ultrasonic cleaning of inserts, it undergoes a topographic process in which various dimensions and other parameters have been evaluated as per the requirement of machining of difficult to hard metals like Inconel, Titanium, etc. Figure 4.6 shows the topographic machine used to check various values such as depth of cut, width of groove pattern, wall thickness and cutting edge distance, etc.

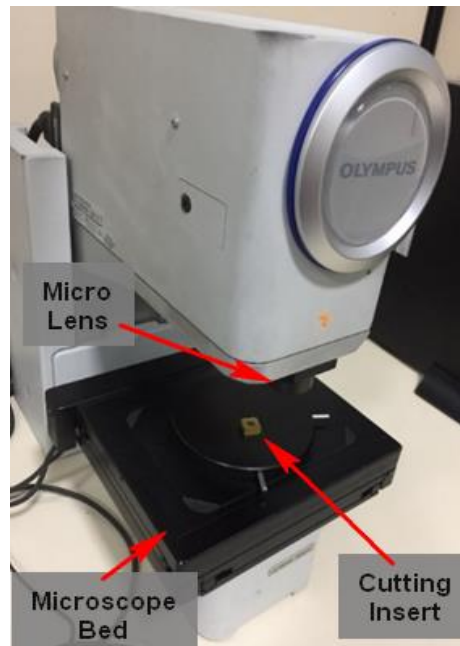


Figure 4.6: A machine used for the topography of cutting insert with micro-texture

The design step has been completed in two steps. First, the design of the spiral triangular pattern has been prepared. Then several trial fabrication run has been done. It was followed by the topographic inspection of all trial runs which gave us the best combination of input parameters. Taking all of those parameters, necessary design and dimension changes have been done and then final fabrication is completed. After the actual fabrication of the micro groove texture on the rake face of the cutting insert, the obtained values of different parameters are explained in table 4.2.



Figure 4.7: Cutting insert without micro groove texture

Table 4.2: Dimensions of micro-texture after actual fabrication.

Results							
Design Pattern	Time Taken Per Sample (Sec)	Shape of Groove	Average Output Width of Groove (micron)	Average Output Depth of Groove (micron)	Average Wall Thickness (micron)	Average Actual Gap obtained from cutting edge of Insert (micron)	Shutter Counts
Spiral Triangle	5.10	Chamfered Square	35	7	13.52	24	1
	4.52	Chamfered Square	15.5	11.036	21.34	24	1
	4.41	Chamfered Square	38.4	11.1	8.97	24	1
	4.02	Chamfered Square	38.05	11.7	8.15	24	1
	3.54	Chamfered Square	39.6	12.37	8.21	24	1
	3.3	Chamfered Square	38.5	12.6	9.07	24	1
	3.0	Chamfered Square	46	12.5	5.94	24	1

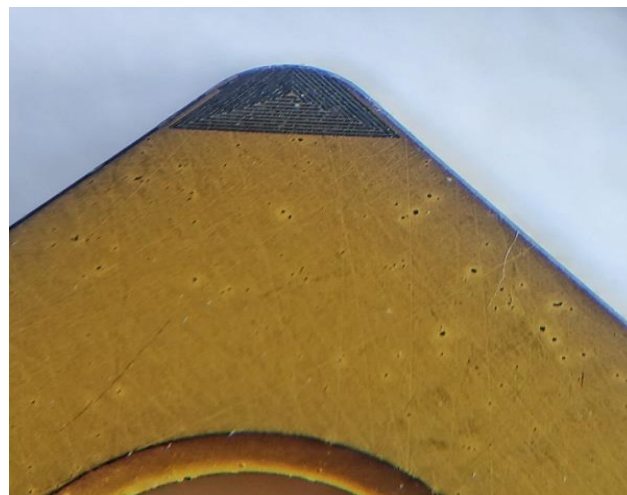


Figure 4.8: Cutting insert with micro groove texture on rake face.

Figure 4.7 has cutting inserts before and figure 4.8 has after the fabrication of micro-texture. After fabricating the micro-texture, it has to be assured that the size of the

actual micro-texture obtained must be the same as in design. So for this, dimensional analysis has been done with the help of topography shown in figure 4.9.

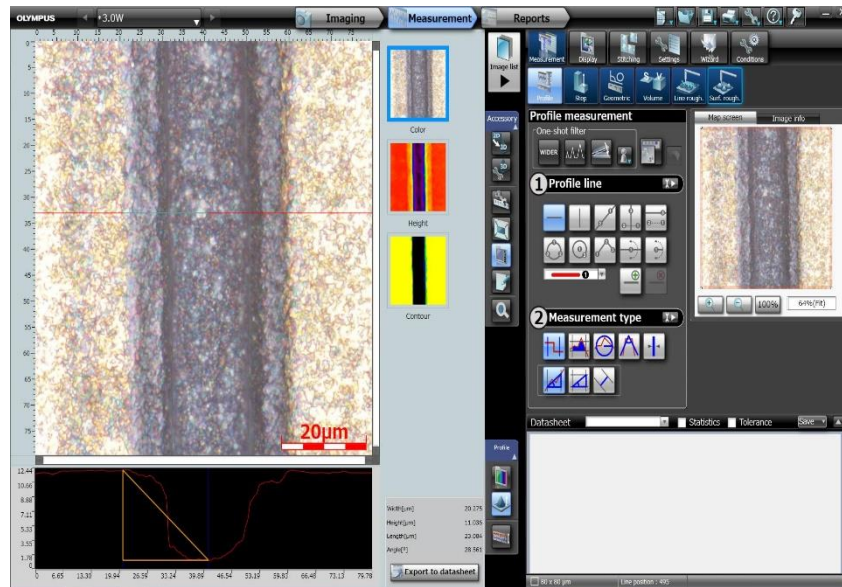


Figure 4.9: Dimensional measurement of micro-texture after grooving on cutting insert.

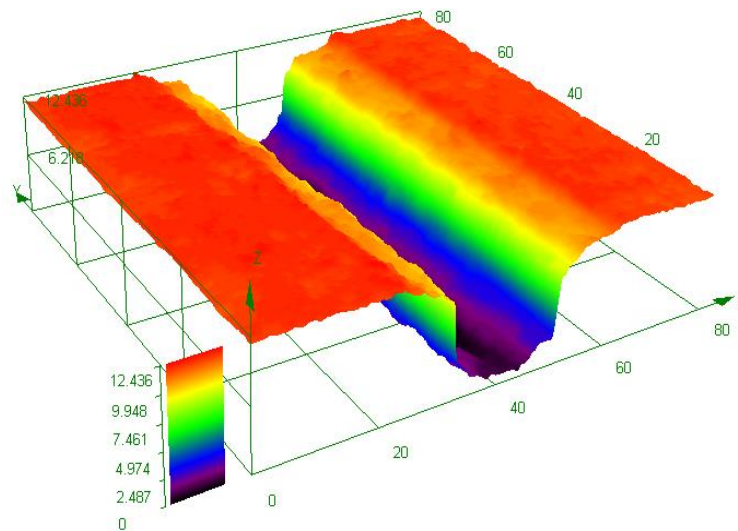


Figure 4.10: The topography of micro-texture grooved on cutting insert.

All the dimensions are in the range of designed values and no further alteration is required. Very clean and precise texture has been obtained. Further to make the surface analysis of the prepared groove, the 3D topography has been done. It gave a clear comparison of all the obtained results in X-Y coordinates. It also helps to understand

the shape of the groove and identify those regions where depth is varying. As micro-texture grooving with the laser has to be done in steps and laser beam has to follow a path within the given range so, at those turns where design has a bend, depth of groove decreases. Figure 4.10 shows all those areas with distance from a particular origin taken in the topographic image.

After all the trial runs, the best parameter set has been decided based on less power consumption with more feed so that the fabrication can be performed in less time. It will be more economical in comparison to others. Moreover, these values produce the required shape of pattern, less than 20 microns of depth, and orientation of the micro groove pattern in actual fabrication. The topographic test of all the runs has proved that the required dimensions of micro-texture have been attained without any major transformation in the parent cutting insert. Fabrication has been performed by taking 30 microns of distance from the cutting edge, using 2W of power, 100 fs of pulse width with a feed of 2.5 mm per second. The repetition rate was taken at 10000 Hz with a tool diameter of 0.015 mm. After fabrication, the micro spiral triangular pattern obtained on the cutting insert surface has a chamfered square shape of the groove. It took 4.52 sec per sample to make a micro groove. The average output width of the groove has been obtained as 15.5 microns with a depth of 11.036 microns. The obtained average actual gap from the cutting edge of the insert was 24 microns. In the whole process, the shutter count used was 1 only. Topography confirmed the coating is still evaded on the cutting insert surface. All other results have required depth but along with that the groove width also increased. Due to which the pattern design will be having fewer walls to dissipate the heat. So there will be no effect of such a pattern on the cutting insert surface. Hence a combination of 15.5 microns of width and 11.036 microns of depth has been selected [128]

4.2 Design and Fabrication of Honeycomb Micro-Texture

This section focuses on the design of the micro-texture pattern, its orientation, laser machine input parameters, and preservation of CVD coating during fabrication. As Krolczyk, G. et al. [129] found the interaction between the machined and material of wedge at the rake face of the cutting insert so, first the novel honeycomb 3D micro-texture is designed using Solidworks[®], and then actual fabrication has been performed

using a femtosecond laser machine on the rake face of cutting insert. The result has been analyzed in the laboratory. The complete process is done on the rake face of TiCN coated tungsten carbide cutting inserts. For the selection of the best input parameter values, all dimensional analysis has been carried out with surface topography. EDS test study shows the elemental increase of carbon and decrease of titanium in the coating. The novel honeycomb micro-texture provides several micro pool reservoirs for lubricant. The obtained wall thickness has increased the number of fins and their lengths to maximize the heat dissipation rate while machining. Although, the new formation of oxides and 33.7% increase of carbon element has been observed inside the groove, the effect of an increase of surface area and fin length is comparatively more [42]. Hence CVD coating and its properties are still present after the micro-grooving.

4.2.1 Designing

Designing micro-texture plays a major role in getting the required results of machining. Some design parameters are purely based on available specifications of the cutting tool, holder, and machine. Some of them are decided based on all of the previous research conclusions. The design of texture is done on Solidworks 2015[®] in the 2D and 3D frameworks. All design parameters have been taken as per the standard dimensions of SNMA HK1500 Tungsten carbide with CVD coating of TiCN of 20 microns cutting insert [43,44]. It is a square insert of 12.7 mm side and 4.76 mm of thickness with 8 available cutting edges. The nose radius is 0.8 mm. Based on all these parameters, a novel honeycomb pattern has been designed in Solidworks[®] software. Before grooving this on the actual insert and also to finalize the femtosecond laser machine parameters, some trial runs have been performed. After the actual preparation of a sample of micro grooves on the surface of cutting inserts, some dimensional alterations in design have been done for getting accurate results. From literature, It has been observed that the maximum effect of raised temperature during machining is observed up to a distance of 3 mm to 4 mm only which is measured from the cutting edge of the insert [130]. So, the honeycomb pattern has been designed to have a continuous series of small hexagonal structures. These hexagons are placed to cover 2.11 mm of the area along both of the cutting edges of the tool rake face. This novel honeycomb design pattern has several micro hexagonal pools that will provide maximum area for lubricant or

coolant on the rake face of the cutting insert as compared to all the patterns from the literature. It has been designed in such a way that a continuous wall has been obtained with an average thickness of 29.49 microns which is spread out in the complete design pattern. As thin fins have more heat dissipation rate, this micro-texture will help in decreasing the temperature of inserts during machining. The groove has an average width of 57.7 microns. From the tool cutting edge to the start of microgroove texture an average gap of 63.6 microns has been taken to avoid the damage of this honeycomb texture during machining. As the CVD coating thickness is up to 20 microns only so while fabrication of texture the groove depth is chosen to be 18.6 microns only so that it should not abolish the TiCN layer from the cutting insert.

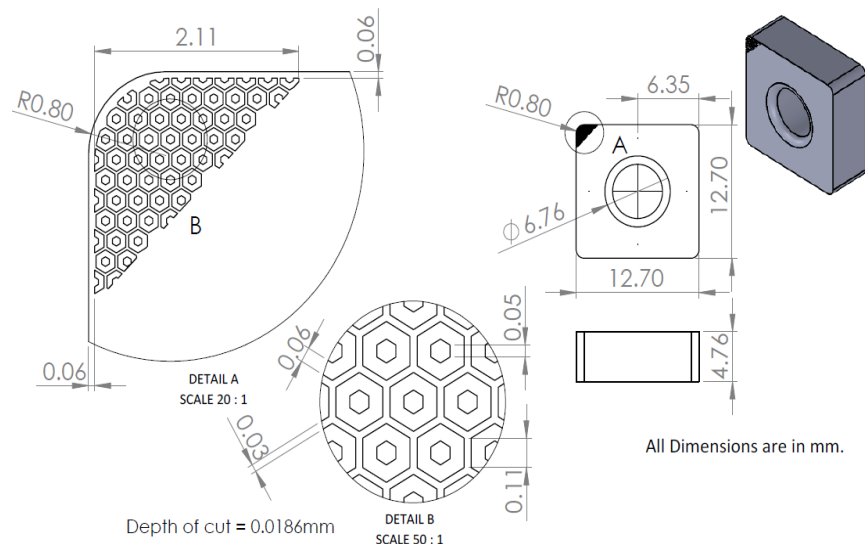


Figure 4.11: Final Design of micro-texture with dimensional detail.

Figure 4.11 shows the final design of the selected honeycomb texture with dimensions. The detail of the size of micro hexagons, location of micro-texture, groove wall thickness, and width is given. Figure 4.12 explains the orientation of the design on the rake face along with the area covered.

4.2.2 Fabrication

MasterCAM[®] software has been used to generate the CNC program in G-Code and M-Code for laser grooving on a femtosecond laser machine [12]. Values of distance from the origin, the distance of bed from the edge of the cutting insert, the shortest path with minimum shutter counts, etc in co-ordinates forms have been measured and

entered. Before finalizing the parameter values, several trials run in the form of the straight-line pattern are fabricated and evaluated dimensionally using surface topography [19].

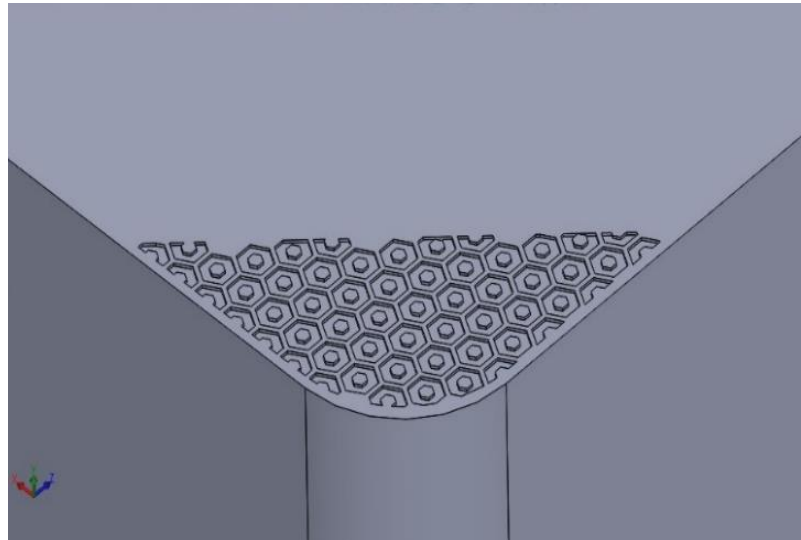


Figure 4.12: Honeycomb micro-texture design on the rake face of cutting insert.

In a femtosecond laser machine, a distance of 2184 microns is taken from the origin and laser bed to get sufficient space to mount and unmount the cutting inserts from the laser bed. The chamfered square shape of the groove has been obtained in straight line trial patterns and a filleted square with varying depth shape is obtained in the fabrication of a novel honeycomb pattern. The average time taken to fabricate the design on one insert is 42.08 sec. The obtained average micro groove width is 57.7 microns with 18.6 microns of depth. After fabrication, the gap between the cutting edge and the start of the groove is measured to equals 63.6 mm. The complete fabrication process took a total shutter count of 64. Table 4.3 shows all the femtosecond laser machine input parameters with the trial runs and final selected values. For the economical production of such grooves, less power consumption with more feed is preferred. Due to this 2W of power transmission and 2.5 mm/sec of feed has been taken for the fabrication of all cutting inserts. During Fabrication an airflow of 12 lit/min helps to clean the laser bed as well as insert also.

The repetition rate of 10000 Hz and tool diameter of 0.015 mm has been taken for all the trials and final fabrication processes. Then the femtosecond laser machine is set to run for the given time and a cutting insert with micro-texture of honeycomb style

is obtained. Ultrasonic cleaning is done using acetone solution for 5 min to 7 min per insert at the 20-40 kHz of frequency. Then it undergoes topographic analysis in which all the dimensional parameters are evaluated [23]. Olympus topographic machine is used to analyze the fabricated groove.

Table 4.3: Values of operating parameters for the Femtosecond laser machine.

Femtosecond Laser Machine parameters and values						
Design Pattern	Power Transmission (W)	Pulse Width (fs)	Feed (mm/Sec)	Compressed Air Flow Rate (lit/min)	Gap has taken from the cutting edge of Insert (micron)	Distance of Origin from cutting edge (micron)
Straight Line (Trial Patterns)	2	100	2	12	30	10
	3	100	2.5	12	30	10
	3.5	100	2.5	12	30	10
	4	100	2.5	12	30	10
	4.5	100	2.5	12	30	10
	5	100	2	12	30	10
Honey Comb	2	100	2	12	90	2184
	4.5	100	2.5	12	70	2184
	5	100	2	12	60	2184

After fabrication of the actual novel honeycomb micro-texture on the cutting insert, the dimensional analysis has been performed on the surface topographic machine and results show that the required depth of 18.6 microns is obtained in 42.08 sec with an average width of 57.7 microns. The average gap of 63.6 microns from the cutting edge of the insert has been obtained. Table 4.4 is showing all the dimensional results obtained after the actual fabrication of the insert along with the best match with the required parameters.

After fabrication of the micro-textures of the honeycomb pattern the cutting insert has an area covered with the series of such patterns is shown in figure 4.13 focused at a range of 1 mm. For the dimensional analysis of the cutting inserts, surface topography has been performed at the 100 μm range

Table 4.4: Obtained values after the fabrication of honeycomb micro-texture.

Results						
Design Pattern	Time Taken Per Sample (Sec)	Average Width of Groove (microns)	Average Depth of Groove (microns)	Average Wall Thickness (microns)	Average Actual Gap from cutting edge of Insert (microns)	Shutter Counts (Numbers)
Straight Line (Trial Patterns)	0.56	35	7	--	0	1
	0.52	38.4	11.1	--	0	1
	0.46	38.05	11.7	--	0	1
	0.32	39.6	12.37	--	0	1
	0.24	38.5	12.6	--	0	1
	0.16	46	12.5	--	0	1
	42.08	57.7	18.6	29.49	63.6	64
Honey Comb	46.63	61.53	28.4	18.44	42	64
	51.81	62.02	36.14	16.21	27	64

. A dimensional analysis of generated groove width and wall thickness has been carried out using the surface topographic machine at a range of 100 micrometers. Varying dimensions are obtained. Taking all the dimensions as shown in figure 4.14 and then an average of all values has been calculated. An average groove width of 57.7 microns and a wall thickness of 29.49 microns has been obtained. Similarly, dimensional analysis is shown in figure 4.15. An average gap of 63.6 microns has been obtained from the edge of the honeycomb micro-groove pattern and the cutting edge of the insert.

Various values of all the parameters have been measured in different honeycomb patterns and then an average of all parameters has been calculated. It shows that at the corners of the groove, the depth of the groove is less as compared to other areas. This is due to the reason that when cutting laser beam passes from a straight-line path it gives a uniform depth of groove but when it has to bend or rotate from an edge, to cover the same path in the shortest time frame it does not go to that much depth of surface [33].

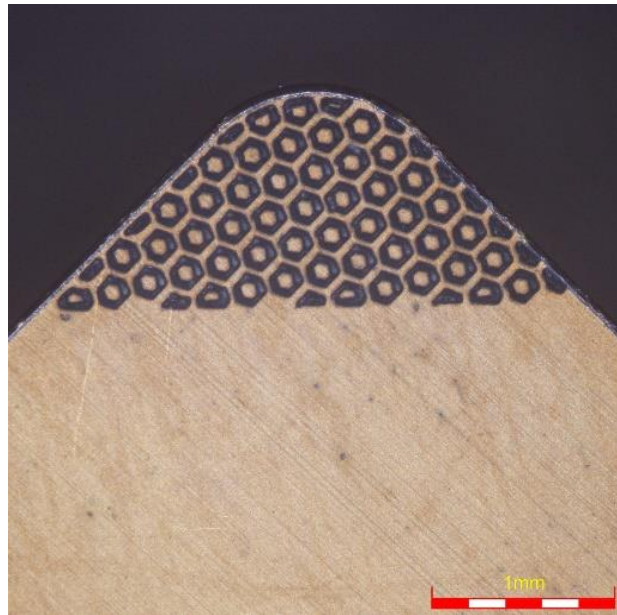


Figure 4.13: Cutting insert with a micro honeycomb pattern.

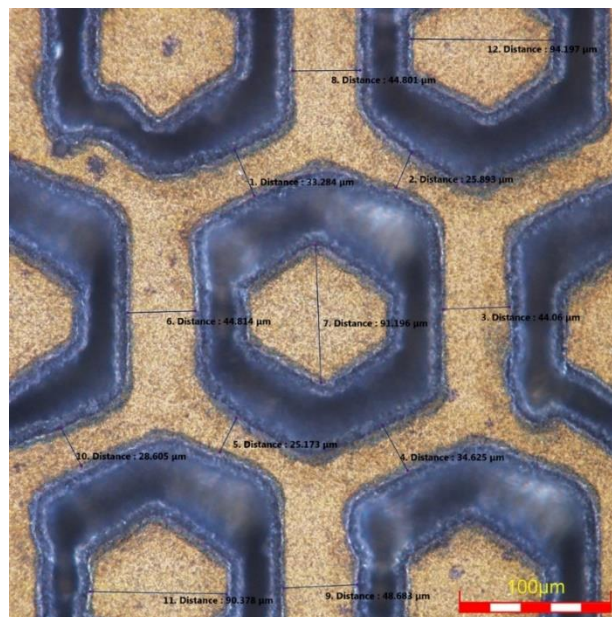


Figure 4.14: Dimensional analysis of wall thickness and width of the groove.

It also helps to protect the coating of the cutting insert because if more time has been given at these bends, the depth of the groove at the other part of the pattern increases. So this type of varying depth of the groove is accepted to protect TiCN coating on the surface of the cutting insert.



Figure 4.15: Dimensional analysis of distance from cutting edge.

After this EDS analysis has been carried out at a focus range of 100 μm . Figure 4.16 shows the selected spectrum for study, Spectrum 1 has been selected from the normal area where no grooving is there and spectrum 2 is taken from the inner side of the honeycomb pattern. It clearly shows several dark spots where the depth of the groove is more in comparison to the light-colored areas with lesser depth.

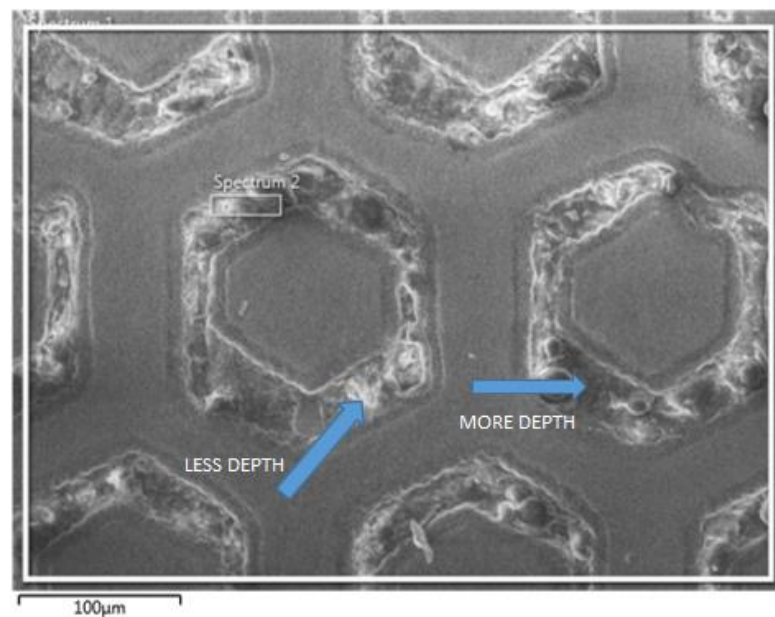


Figure 4.16: Selected Spectrums in EDS analysis of honeycomb pattern.

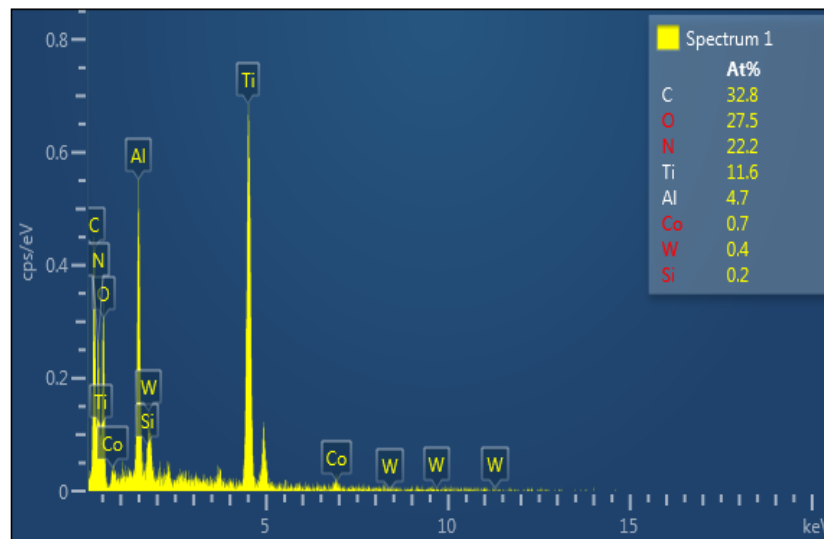


Figure 4.17: Element percentage component of normal spectrum-1.

Then, the percentage of all elements present in spectrum 1 is shown in figure 4.17. It shows that there is a presence of 11.6% of titanium, 32.8% carbon, and 22.2% of nitrogen. When the honeycomb micro-textured has been fabricated then inside the grooved honeycomb pattern (spectrum 2), the presence of a thin coating of TiCN is still found. It has 1.7% of titanium, 66.5% of carbon. There is a decrease of 9.9% of titanium and an increase of 33.7% of carbon elements have been observed. It is due to the burning of metal during laser grooving in the femtosecond laser machining [15,28]. This increase of carbon element inside the groove will not have much effect because the effect of the increase of surface area and fin length is more on the heat dissipation rate. Figure 4.18 shows the percentage of all the elements in spectrum 2 inside the groove.

In the EDS mapping analysis, it has been observed that before micro grooving Titanium is present all over the surface of the cutting insert, and even after micro grooving with femtosecond laser machine this element is present inside the grooved area of the honeycomb pattern. Figure 4.19 shows a combined element data of all the present compounds and figure 4.20 gives the detail of all the spots where the Titanium element is present. Here the dense color shows the non-grooved part of the cutting insert. As the same color element is present inside the groove of the honeycomb pattern also, it proves the presence of the titanium element of the thin coating inside the micro-grooved area. Figure 4.21 gives the detail of all those spots where the nitride is present

and figure 4.22 shows the presence of carbon in the cutting insert. In comparing figures 4.23 and figure 4.24 the increase of carbon element due to laser grooving is proved as now more area has that color symbol.

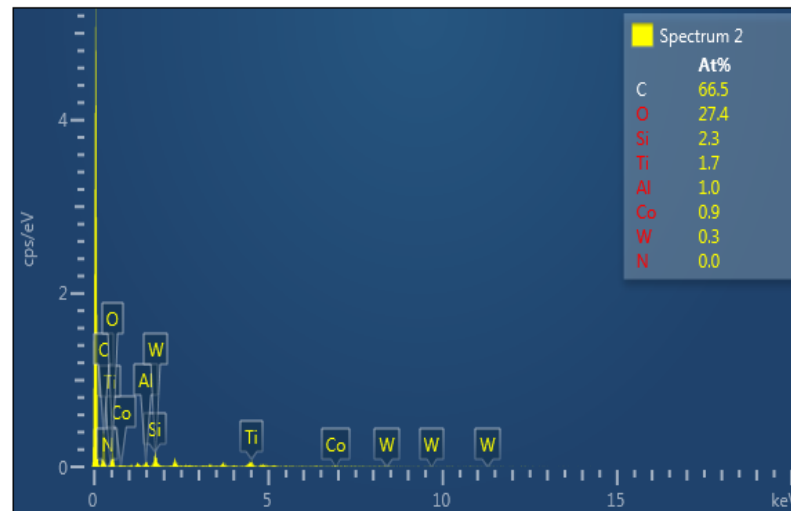


Figure 4.18: Element percentage component of micro-grooved spectrum-2.

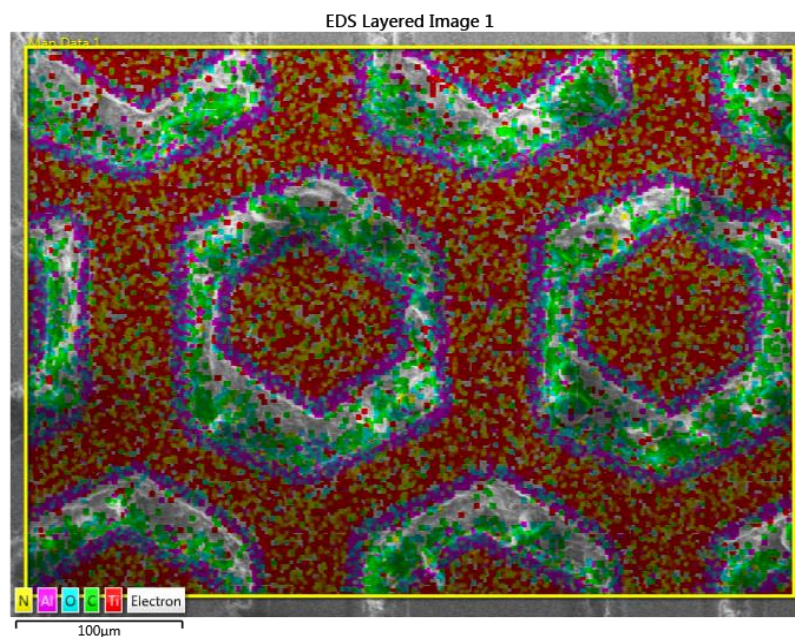


Figure 4.19: EDS mapping results- Combined element data of all compounds.

In figure 4.23 the presence of alumina is shown only at the corners of the microgroove. While grooving, the laser beam was focused at the center of the width of the groove. So oxidation and reduction have occurred more inside the grooved area only. At the edges, aluminium appears as a thin layer of coating is diminished. Figure 4.24 shows

the oxides formed inside the micro-grooved area. It was present earlier also but due to laser grooving its percentage.

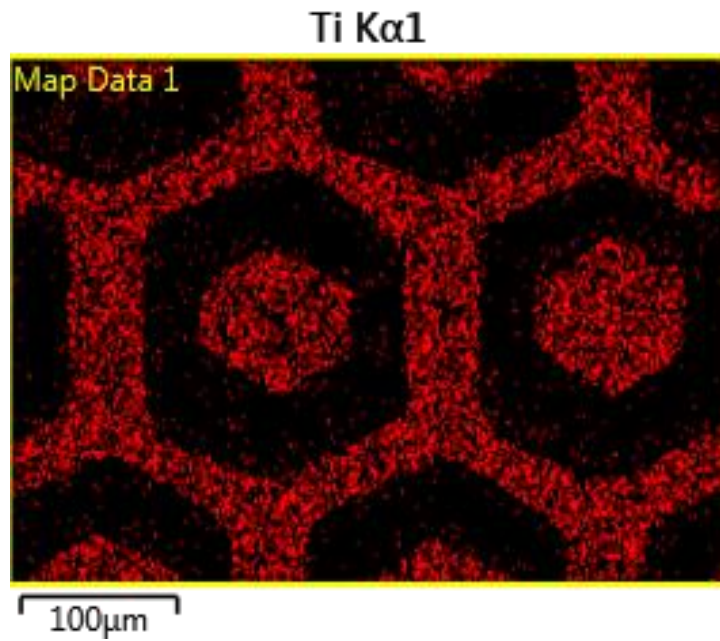


Figure 4.20: EDS mapping results- Element data of the Titanium compound only.

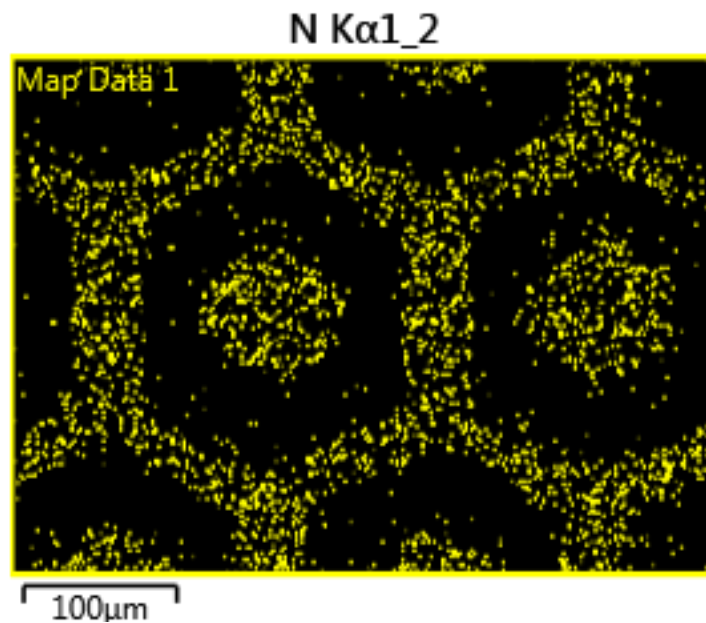


Figure 4.21: EDS mapping results- Element data of Nitride compound.

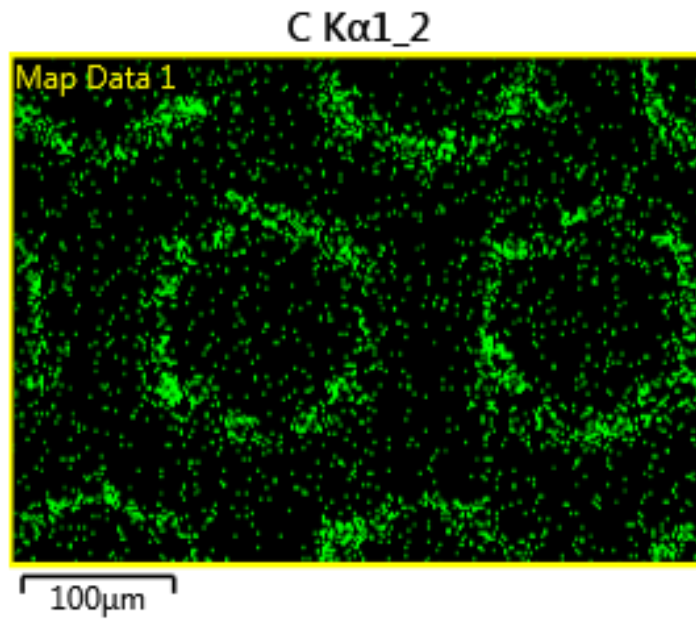


Figure 4.22: EDS mapping results- Element data of the Carbide compound.

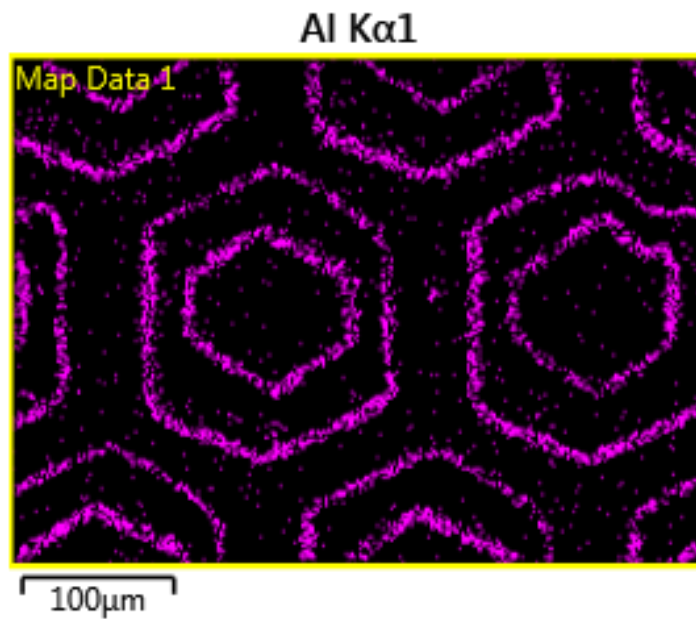


Figure 4.23: EDS mapping results - Element data of Aluminium compound.

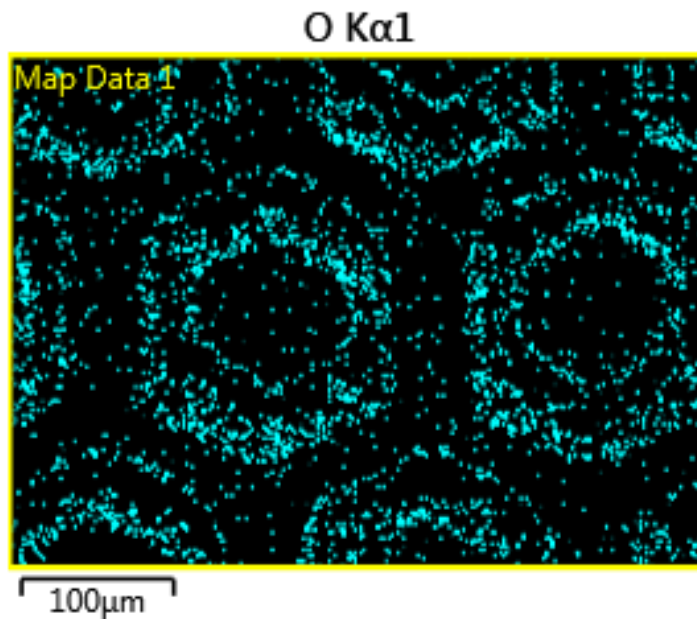


Figure 4.24: EDS mapping results- Element data of Oxide compound.

XRD (X-Ray Diffraction) analysis also clears that before grooving it was present with aluminium in the form of alumina but after oxidation, it is converted into silicon dioxide shown in figure 4.25 and figure 4.26. A study of compounds in cutting insert using XRD is done which verifies the presence of a thin layer of TiCN even after microlaser grooving of a honeycomb pattern on the rake face of tungsten carbide insert. PSD fast mode. It started at a 10° angle and ends at a 119.990° angle in total 57.60 sec.

The first XRD analysis of a plain insert has been executed. It shows the presence of Titanium Carbo-Nitride, Alumina compound on the surface of the cutting insert. Figure 4.25 shows the various diffraction pattern at various values of position angle 2θ and intensity (counts per second) with the presence of compounds in cutting insert without micro-texture. Then at the same machine parameters, the compound study of cutting insert after grooving of honeycomb micro-texture is done. It confirms the presence of $Ti_3Al_2N_2$ (Titanium Aluminium Di-Nitride) and Ti_2N (Titanium Nitride).

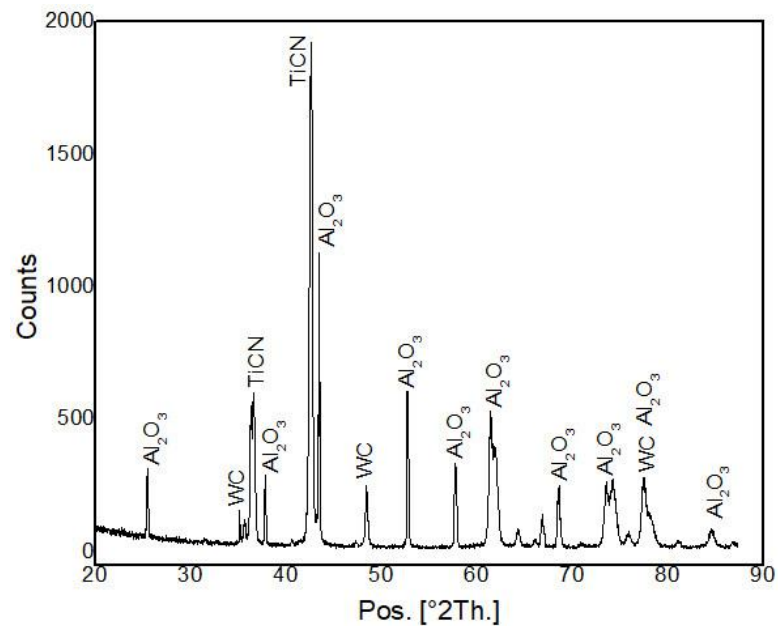


Figure 4.25: XRD analysis of cutting insert without micro-texture.

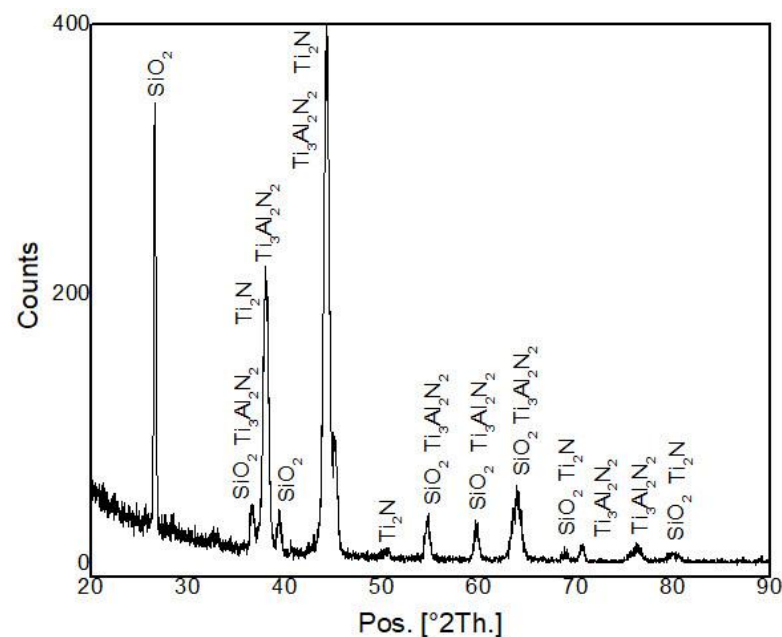


Figure 4.26: XRD analysis of cutting insert with honeycomb micro-texture

The generation of SiO₂ (Silicon Dioxide) is also observed. These modifications in compounds occur due to microlaser grooving. TiCN has been reduced to Ti₃Al₂N₂ and Ti₂N. Similarly, Al₂O₃ gets oxidized and SiO₂ has formed. Figure 5.26 shows numerous diffraction patterns and the presence of compounds at various values of angle 2theta (2θ) (2θ) and intensity (counts per second) in cutting insert with honeycomb micro-texture. The newly formed Ti₃Al₂N₂, SiO₂, and Ti₂N compounds have high hardness and

low friction coefficient. These have other common properties like high deformation resistance and high compressive strength. Whereas, corrosion resistance and abrasive wear are the properties of TiCN and Al₂O₃ respectively [131,132]. So after grooving the novel honeycomb micro-texture on the cutting insert, major properties will remain the same.

It is not changing any physical, chemical as well as mechanical properties of thin coating also. Design and fabrication of a spiral triangular pattern have been done successfully using the femtosecond laser machine [133]. Experiments with plain and simple micro-texture have shown improvement in machinability [134]. So this study has a scope of experimentation as well as FEA simulation analysis to be done [135].

Chapter 5

5. Experimentation and Modeling

This chapter focuses on machining Titanium Gr 2 using few new types of microtextures. These novel microtextures have been fabricated on the rake face of the double-sided square cutting insert and their machinability is compared. First, the spiral triangular and honeycomb micro-textures have been designed using Solidworks® software and then fabricated using a femtosecond laser machine without amputating its TiCN coating [136,67]. Taking rotational speed range of 325rpm to 930rpm and cutting feed of 0.04 mm/rev to 0.08 mm/rev, a dry turning process on a self-centered lathe machine have been conducted. The machinability of all types of cutting inserts has been compared based on cutting temperature, surface roughness, material removal rate (MRR), and percentage improvement on the surface finish (PISF).

To compare the machinability aspects of the micro-textured cutting insert with non-textured cutting insert in the turning operation of Titanium Gr 2, first of all, the spiral triangular and honeycomb micro-texture designs have been prepared using Solidworks® software. The dimensions of the micro-texture design have been finalized according to the trial runs performed in the femtosecond laser machine. Figure 5.1 (a) shows the design of the non-textured plain insert, figure 5.1 (b) shows the design of cutting insert with novel spiral triangular micro-texture, and figure 5.1 (c) explains the design of cutting insert with novel honeycomb micro-texture on the rake face. The XRD and EDS tests performed after the actual fabrication of these micro-textures give evidential proof of the presence of a layer of TiCN (Titanium Carbo-Nitride) coating on the cutting insert. Hence no change in the characteristics of the TiCN coated tungsten carbide cutting inserts is confirmed. Figure 5.2 (a) is showing the non-textured cutting insert, figure 5.2 (b) displays the cutting insert with novel spiral triangular micro-texture, and figure 5.2 (c) displays the cutting insert with novel honeycomb micro-texture on the rake face[135].

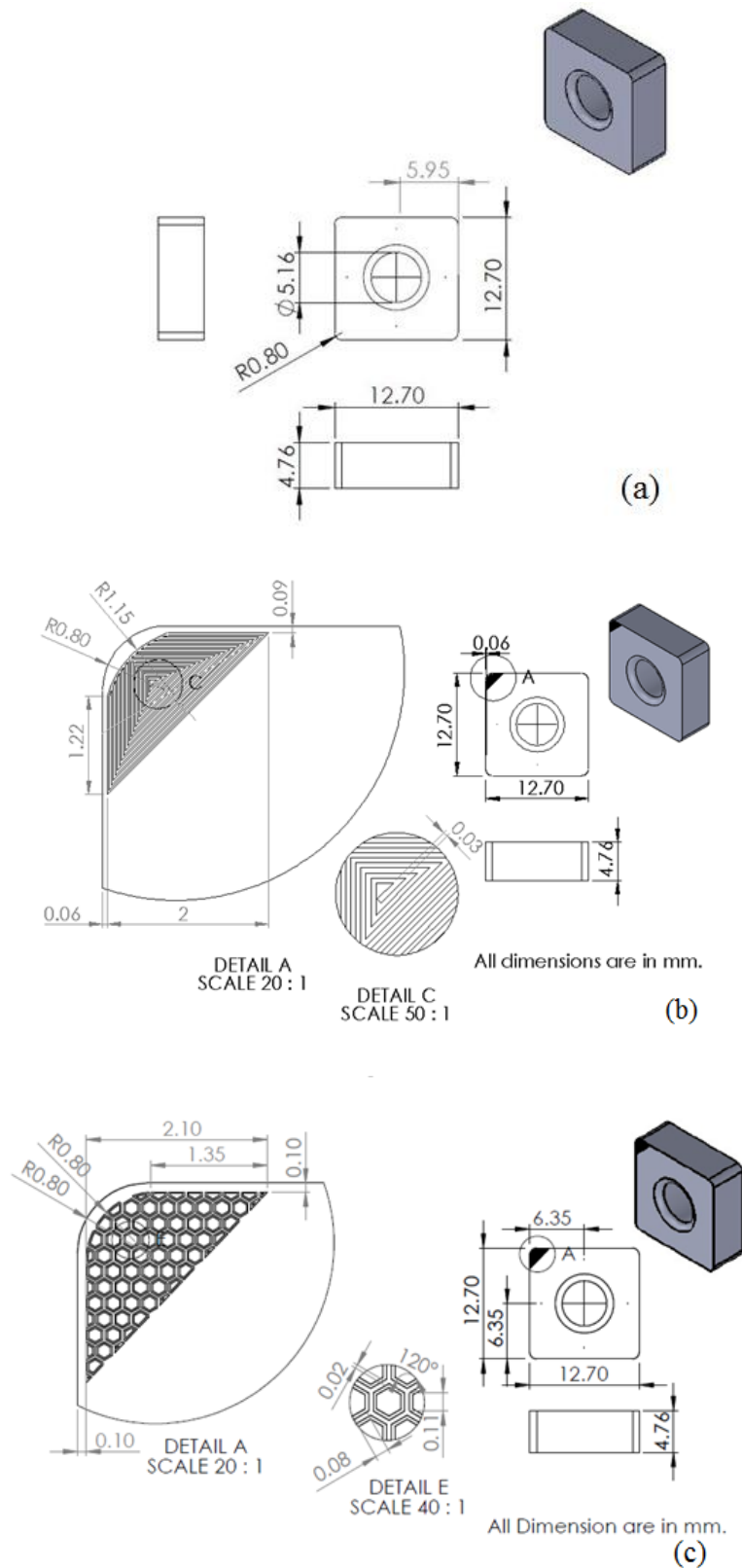


Figure 5.1: Design of cutting inserts (a) Non-textured (b) with Spiral Triangular micro-texture (c) with Honeycomb micro-texture

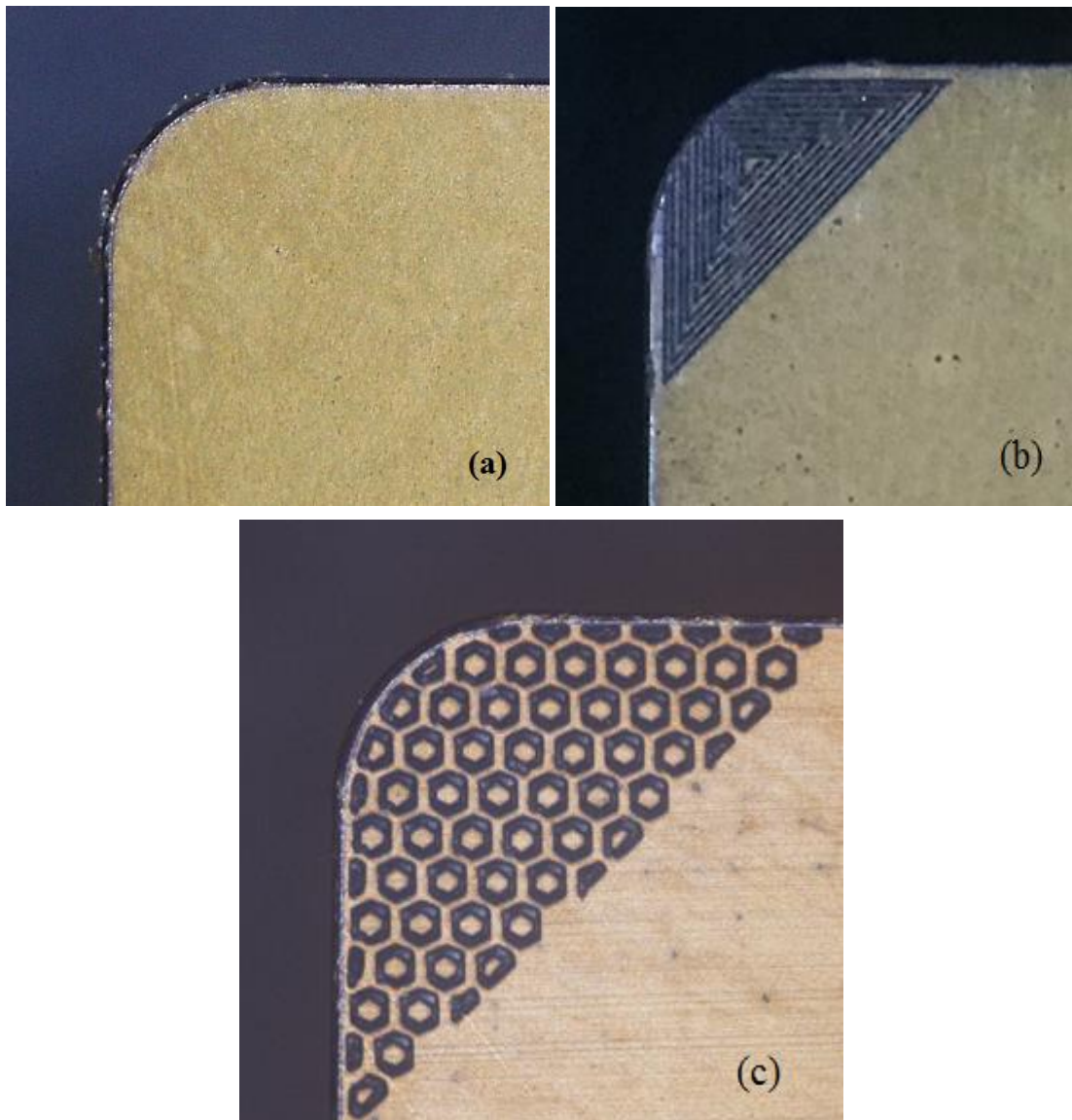


Figure 5.2: TiCN coated tungsten carbide cutting inserts (a) Non-textured (b) with Spiral Triangular micro-texture (c) with Honeycomb micro-texture.

5.1 Selection of Orthogonal array and Design of Experiments

For the design of experiments L27, the orthogonal array has been selected taking three levels of the rotational speed of the workpiece that is Titanium Gr 2 rod, and three levels of cutting feed. Three types of cutting insert have been used for turning operation on a three-jaw self-centered lathe machine. Table 5.1 shows the design of the experiment with a total of 27 runs. Table 5.2 explains all the factors and levels used in this experiment.

Table 5.1: L27 Orthogonal array for the design of experiments

Design of Experiments			
Run	Parameters		
	Rotational Speed (rpm)	Feed (mm/rev)	Type of insert
1	1	1	1
2	1	1	2
3	1	1	3
4	1	2	1
5	1	2	2
6	1	2	3
7	1	3	1
8	1	3	2
9	1	3	3
10	2	1	1
11	2	1	2
12	2	1	3
13	2	2	1
14	2	2	2
15	2	2	3
16	2	3	1
17	2	3	2
18	2	3	3
19	3	1	1
20	3	1	2
21	3	1	3
22	3	2	1
23	3	2	2
24	3	2	3
25	3	3	1
26	3	3	2
27	3	3	3

Table 5.2: Values of all the factors and levels used in the machining operation.

Rotational Speed (rpm)	Feed (mm/rev)	Type of Insert
1 = 325	1 = 0.04	1 = Plain Insert
2 = 550	2 = 0.06	2 = Insert with spiral triangular pattern
3 = 930	3 = 0.08	3 = Insert with Honeycomb pattern

5.2 Material, Machine Set-up & Test Conditions

The turning operation has been performed on the three-jaw self-centered lathe machine taking three different rotational speed levels. The material of the workpiece used is Titanium Gr 2 (Ti-6Al-4V) which is having low thermal conductivity and heat dissipation rate. Figure 5.3 shows the Titanium Gr 2 workpiece rod of diameter 50 mm. The length of the rod equals 510 mm which is then divided into few sets as per the length of each experiment run. SNMA 120408 tungsten carbide square cutting inserts have been used. These inserts have a CVD coating of TiCN (Titanium Carbo-Nitride) up to 20 microns. The square insert is of 12.7 X 12.7 X 4.76 mm dimensions. The nose radius of the insert is 0.8 mm with a 75 degree of approach angle. Figure 5.4 shows the symmetry of the tungsten carbide square cutting insert with the holder. All the turning operations are carried out at a room temperature of 25 degrees. The novel micro-texture designs have been prepared using Solidworks® software as per the available dimension data of the double-sided square cutting insert giving an extreme level of attention that after fabrication of micro-textures, no change in the properties of the cutting insert may occur.



Figure 5.3: Titanium Gr 2 workpiece rod of diameter 50 mm and length 510 mm.

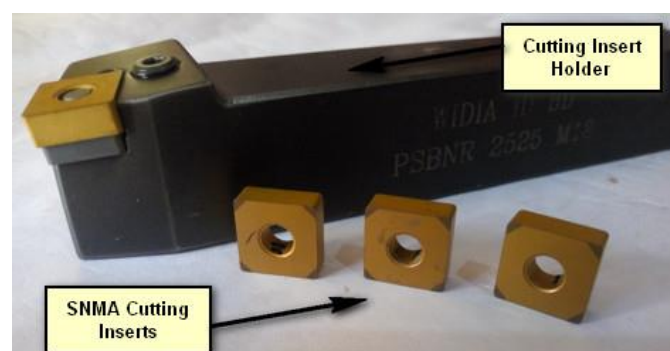


Figure 5.4: Square tungsten carbide cutting insert with holder.

The dry turning operations have been performed in the available rotational speed range of 300 – 1000 rpm. The cutting feed varies from 0.4 – 0.8 mm/rev. The depth of cut has been taken 0.5 mm for all the runs. Figure 5.5 is having the schematic representation of the setup to perform the machining operation on a three-jaw self-centered lathe machine.

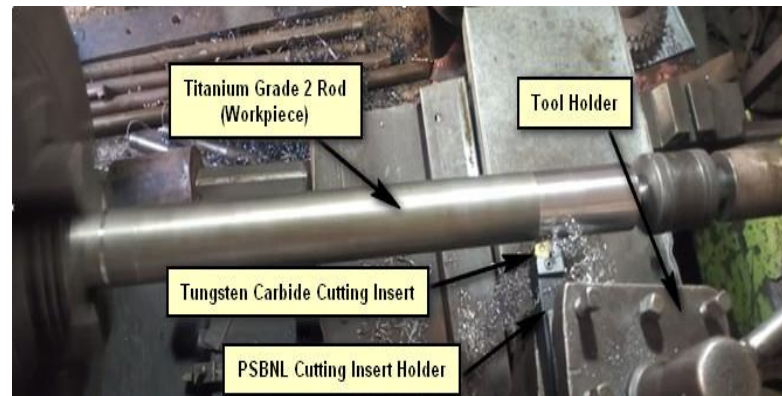


Figure 5.5: Three-jaw self-centered Lathe machine set up for turning operation.

Cutting temperature is the main parameter to check the machinability of any cutting insert. For this purpose, the HTC IRX-65 digital infrared temperature measurement device having a range of -50°C to 1250°C has been used. It provides the contactless measurement of temperature while machining on the tip of the cutting insert. Figure 5.6 shows the device use for the measurement of temperature.

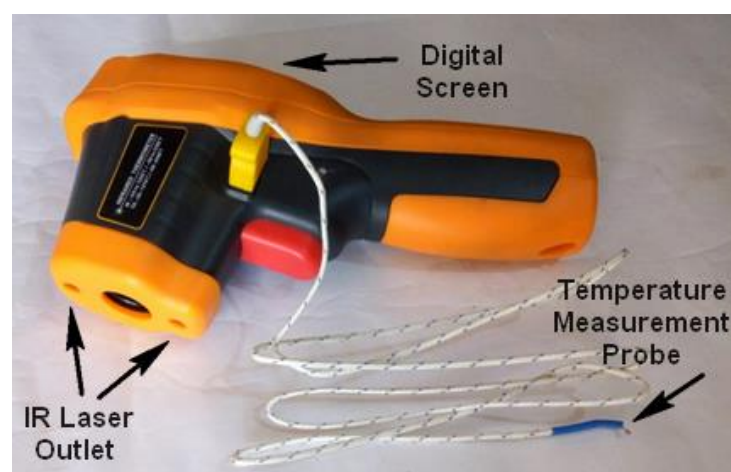


Figure 5.6: HTC IRX-65 digital infrared temperature measurement device.

For the measurement of surface roughness, the Insize ISR-S400 surface roughness device has been used. The cut-off length of 0.8 mm, 3 no of cut with $2.97\ \mu\text{m}$ calibration

Ra is taken. Figure 5.7 explains the surface roughness measurement process after the turning operation on Titanium Gr 2 rod using different types of cutting inserts with different factors and their levels.

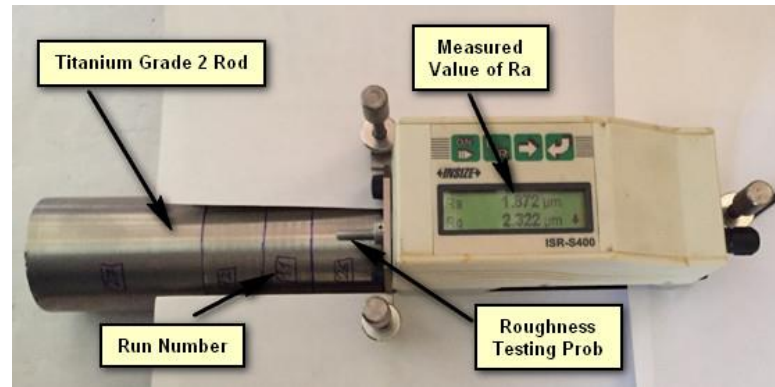


Figure 5.7: Surface roughness measurement using ISR-S400 tester.

The values of the diameter of Titanium Gr 2 rod before and after each turning operation run is measured using Insize vernier caliper. The standard equation 5.1 has been used to calculate the values of MRR (material removal rate) for all the experiment runs.

$$MRR = V \times F \times \left(\frac{\text{Change in Diameter}}{2} \right) \quad (\text{Eq. 5.1})$$

$$PISF = \frac{\text{Change in Surface Finish}}{\text{Avg Surface Finish}} \times 100 \quad (\text{Eq. 5.2})$$

For the calculation of PISF (percentage improvement in surface finish), values of surface roughness before and after the turning operation have been measured. The average of three values measured at different positions has been taken. The surface roughness of the Titanium Gr 2 rod before machining is found to be 4.03 μm . Using equation 5.2, PISF has been calculated for all runs. Table 5.3 give the detail of all the measured output values in respect to the factors and levels of each run. The maximum cutting temperature is observed while machining with a non-textured insert at 930 rpm taking 0.06 mm/rev of cutting feed and minimum with Honeycomb micro-texture at 325 rpm and 0.04 mm/rev of cutting feed. The cutting insert with Honeycomb micro-texture gives the maximum of 76% improvement in the surface finish at 930 rpm and 0.04 mm/rev of cutting feed. Machining of Titanium Gr 2 shows the minimum material removal rate of 6.799 mm³/min with a non-textured insert and a maximum of 39.58 mm³/min with honeycomb micro-texture.

Table 5.3: Detail of output results at different input values for each experiment run.

Run	Parameters			Output Results			
	Rotational Speed (rpm)	Feed (mm/rev)	Type of insert	Temperature (°C)	Surface Roughness Ra (µm)	PISF (%)	Material Removal Rate (mm ³ Per min)
1	325	0.04	Plain Insert	230	2.942	27.00	6.799
2	325	0.04	Spiral Triangular	227	1.687	58.14	6.916
3	325	0.04	Honeycomb	210	1.228	69.53	6.786
4	325	0.06	Plain Insert	264	2.17	46.15	9.633
5	325	0.06	Spiral Triangular	254	2.093	48.06	9.496
6	325	0.06	Honeycomb	240	1.892	53.05	9.672
7	325	0.08	Plain Insert	327	3.062	24.02	13.884
8	325	0.08	Spiral Triangular	295	2.886	28.39	13.26
9	325	0.08	Honeycomb	268	2.522	37.42	13.286
10	550	0.04	Plain Insert	378	2.062	48.83	10.978
11	550	0.04	Spiral Triangular	336	1.654	58.96	10.67
12	550	0.04	Honeycomb	295	1.911	52.58	10.788
13	550	0.06	Plain Insert	404	2.439	39.48	16.566
14	550	0.06	Spiral Triangular	372	1.38	65.76	16.203
15	550	0.06	Honeycomb	317	2.209	45.19	16.104
16	550	0.08	Plain Insert	363	2.895	28.16	22
17	550	0.08	Spiral Triangular	313	2.203	45.33	21.56
18	550	0.08	Honeycomb	340	2.054	49.03	21.648
19	930	0.04	Plain Insert	475	2.964	26.45	19.344
20	930	0.04	Spiral Triangular	404	2.034	49.53	18.972
21	930	0.04	Honeycomb	591	0.967	76.00	18.451
22	930	0.06	Plain Insert	625	3.822	5.16	28.625

23	930	0.06	Spiral Triangular	476	1.54	61.79	27.955
24	930	0.06	Honeycomb	548	2.297	43.00	27.676
25	930	0.08	Plain Insert	604	3.158	21.64	37.423
26	930	0.08	Spiral Triangular	502	2.946	26.90	38.985
27	930	0.08	Honeycomb	577	1.02	74.69	39.58

Chapter 6

6. Results and Discussion

6.1 Effect of Machining Parameters on Temperature

The range of cutting temperatures while performing the turning operation on Titanium Gr 2 with honeycomb micro-textured insert is less in comparison to other types of inserts. At rotational speed 550 rpm and cutting feed 0.04 mm/rev it shows the minimum cutting temperature in comparison to another type of cutting inserts at the same parameters. This is due to the reason that Honeycomb micro-texture has maximum heat dissipation rate due to its long fin shape walls type design. As Titanium Gr 2 has a low heat dissipation rate characteristic so, at high rotational speed, the time available for conduction of heat is less and more heat will gather at the cutting zone [137]. So, a rise in cutting temperature is perceived with an increase in rotational speed with all types of cutting inserts. An increase in the cutting feed also increases the cutting temperature of all types of cutting inserts. Figure 6.1 shows the variation in cutting temperature with the type of inserts, rotational speed, and cutting feed levels.

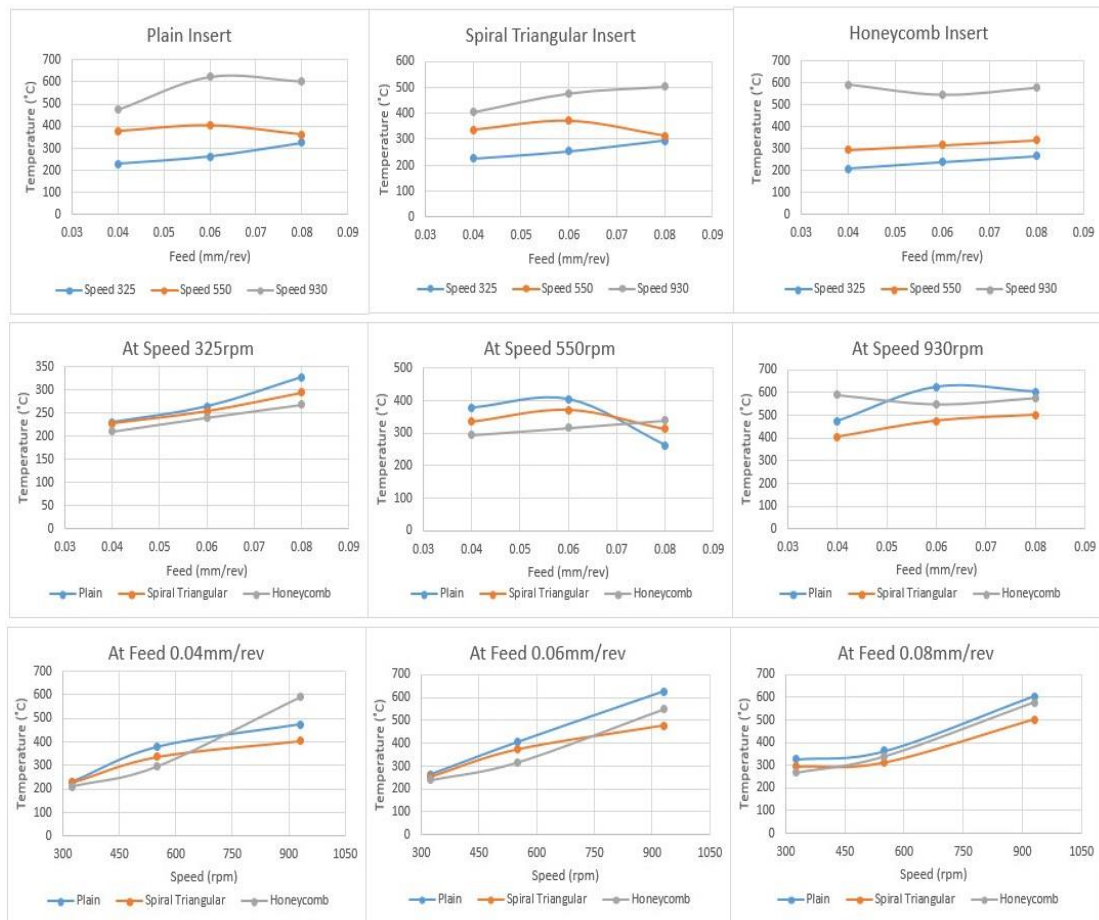


Figure 6.1: Variation in temperature with the type of inserts, rotational speed, and cutting feed in turning operation.

6.2 Effect of Machining Parameters on Surface Roughness

The measured surface roughness values have a maximum range of $2\ \mu\text{m}$ to $4\ \mu\text{m}$ after machining of Titanium Gr 2 rod with non-textured plain insert, whereas $1.5\ \mu\text{m}$ to $3\ \mu\text{m}$ with spiral triangular and minimum of $1\ \mu\text{m}$ to $2.5\ \mu\text{m}$ with honeycomb micro-textured cutting insert. It is mainly due to the increase of heat dissipation rate with honeycomb micro-texture. Because of that, the tool wear reduces and hence smooth surface has been obtained [138]. Surface roughness increases with an increase in rotational speed as at high rotational speed material removal rate increases [139] but while machining with honeycomb micro-textured insert at rotational speed 930 rpm, surface roughness first increases up to 0.06 mm/rev of cutting feed and then start decreasing on a further increase of cutting feed. This is due to the reason that when rotational speed and cutting feed both are high then the cutting tool get less time to remain in contact with the workpiece material. The cutting tool moved forward quickly

so the material removed from a particular area is less. Figure 6.2 shows the variation of surface roughness with the type of insert, rotational speed, and cutting feed.

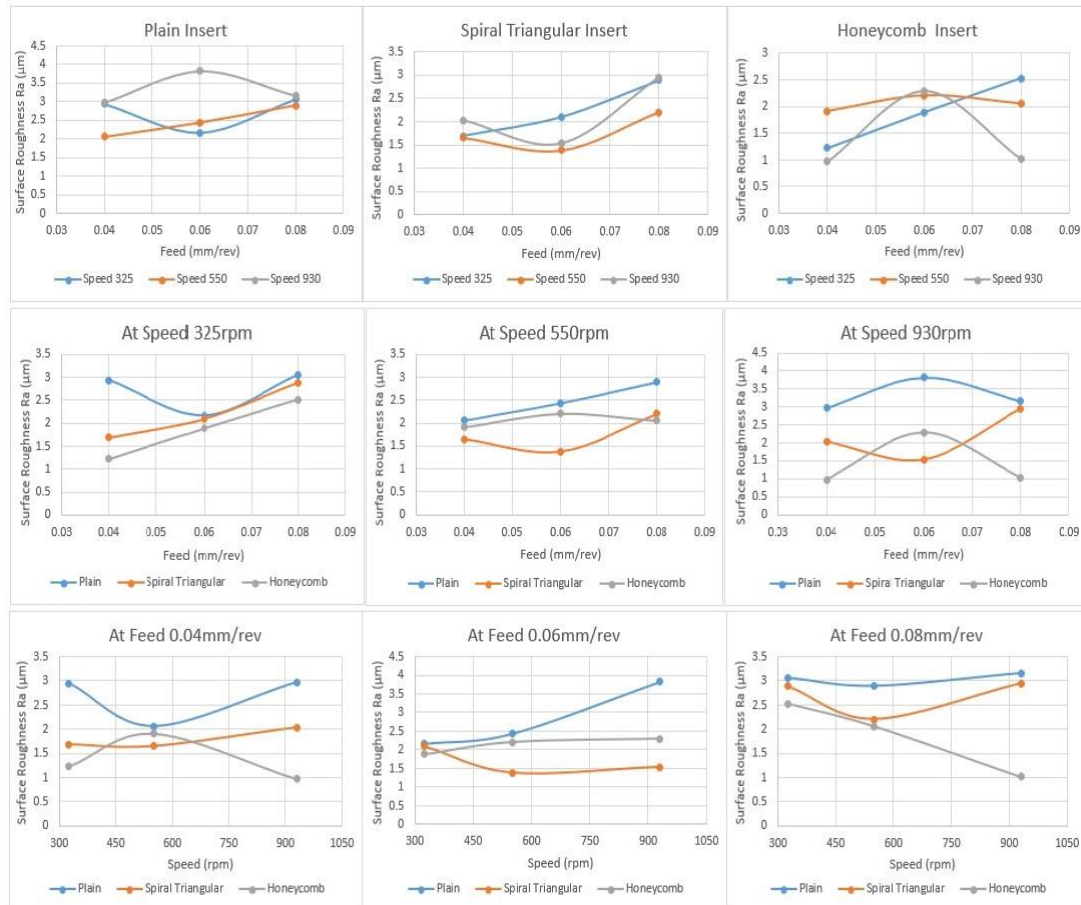


Figure 6.2: Variation in surface roughness with the type of inserts, rotational speed, and cutting feed in turning operation.

6.3 Effect of Machining Parameters on MRR

For all types of cutting inserts, the material removal rate has been increased with an increase in rotational speed and cutting feed [140]. Graphs drawn in figure 6.3 show that the MRR is maximum when machining with Honeycomb micro-textured insert than spiral triangular micro-texture and minimum with non-textured plain insert.

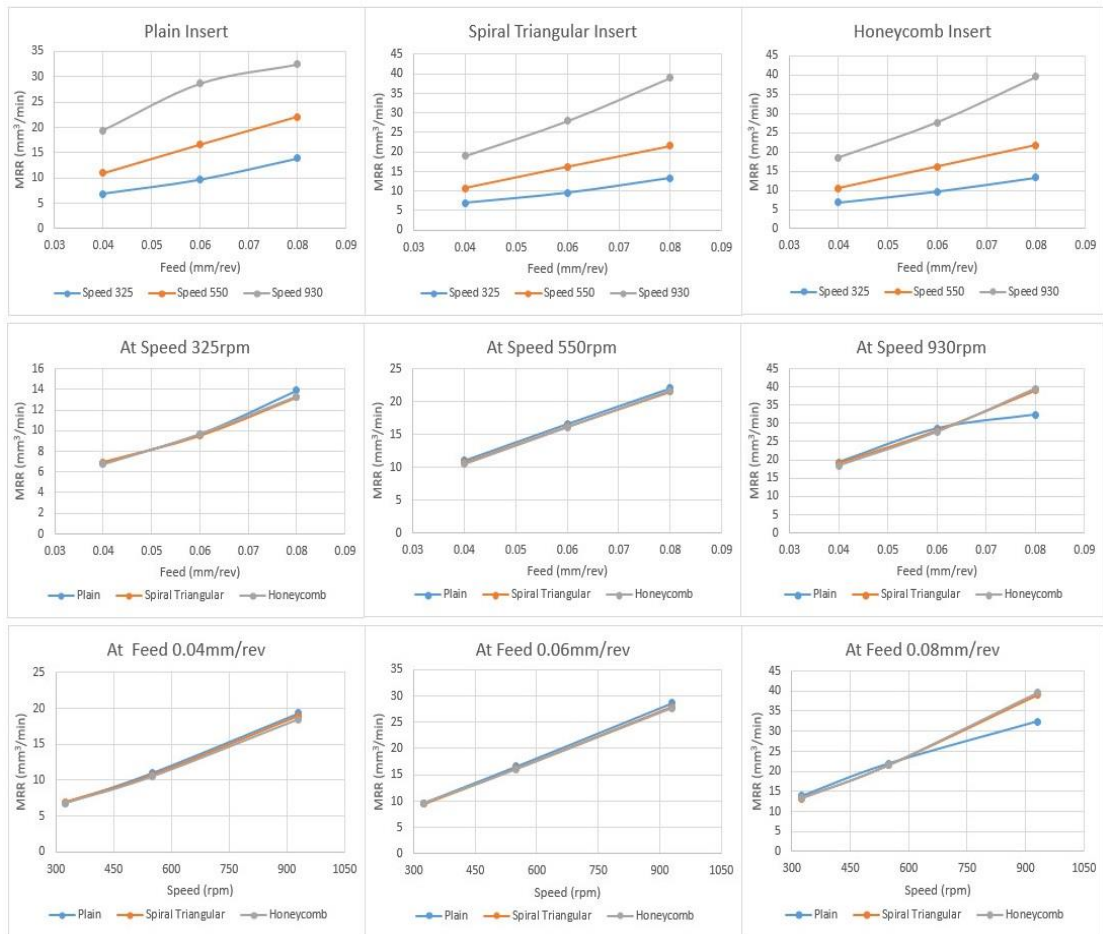


Figure 6.3: Variation in material removal rate with the type of inserts, rotational speed, and cutting feed in turning operation.

6.4 Effect of Machining Parameters on PISF

PISF with non-textured plain and spiral triangular cutting inserts increases and then decreases with cutting feed but with honeycomb micro-textured insert, it decreases and then increases with feed. At rotational speed, 325rpm and 930rpm cutting insert with honeycomb micro-texture give maximum PISF but at 550rpm insert with spiral triangular micro-texture show the maximum PISF. Figure 6.4 shows the variation of PISF with rotational speed, cutting feed, and type of insert in all machining runs.

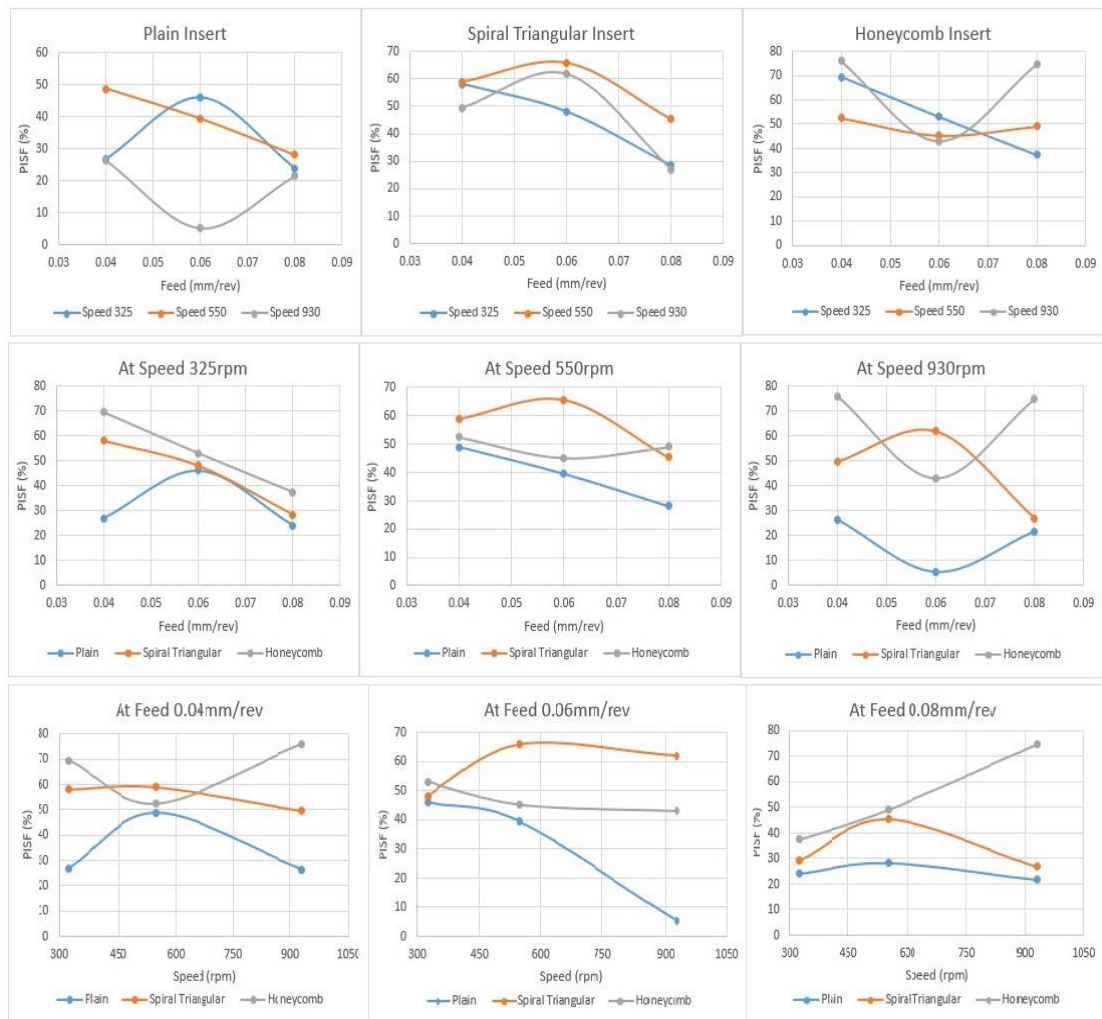


Figure 6.4: Variation in percentage improvement in the surface finish with the type of inserts, rotational speed, and cutting feed in turning operation.

6.5 Analysis of Surface Roughness, Tool Wear and Chip Morphology

Most of the researchers have worked on the study of tool wear and chip morphology by trying different methods of machining, changing the machining environments, cooling systems, and very little attention has been given to analyze the machinability of cutting inserts after modifying them at the micro-level. In this chapter, the analysis on surface roughness, cutting insert wear, and chip morphology have been done while machining titanium grade 2 with a tungsten carbide insert. A honeycomb micro-texture has been fabricated on the rake face of the cutting insert. The machinability of these two types of cutting inserts has been compared considering cutting speed, feed, and cutting temperature. Macro and micro-level chip morphology has also been conducted.

To analyze the surface roughness, tool wear, and chip properties the turning operation has been carried on the Titanium Gr2 rod. Tungsten carbide square insert has been used in dry conditions. The operation has been done on a three-jaw self-centered chuck-type lathe machine at room temperature. All the attributes and values have been summarized in table 6.1.

Table 6.1: All the attributes and remarks of this experimental setup.

Attribute	Remarks
Workpiece Material	Titanium Gr 2 (Ti6Al4V)
Workpiece Dimensions	Diameter 50 mm, Length 510 mm
Cutting Insert Material	Tungsten Carbide with TiCN coating
Cutting Insert Dimensions	12.7 mm X 12.7 mm X 4.76 mm
Type of Operation	Turning
Machine Used	Self-Centered 3jaw Lathe machine
Workpiece Rotational Speed	325 rpm, 550 rpm, 930 rpm
Cutting Speed	51.025 m/min, 86.35 m/min, 146.01 m/min
Cutting Feed	0.04 mm/rev, 0.06 mm/rev, 0.08 mm/rev
Depth of Cut	0.5 mm
Type of Insert	Plain Insert (Without Micro Groove), Microgroove Insert (Honeycomb Groove)
Responses	Surface Roughness, Tool wear, Chip Morphology

Three levels of available cutting speed from 325 rpm to 930 rpm have been used. Similarly, the range of feed used is 0.04 mm/rpm to 0.08 mm/rpm. To compare the responses, two types of cutting inserts have been used. First of all, a honeycomb microgroove pattern has been designed and fabricated on the rake face of the cutting insert [135]. After that analysis has been carried out for the confirmation of the presence of thin TiCN coating and then the turning operation has been performed. The surface roughness, tool wear, and chip morphology are taken as the output responses.

6.5.1 Surface Roughness Analysis

The machinability characteristics of a cutting tool can be declared on its performance in form of the surface roughness and life of the tool. Hence the values of surface roughness have been measured using the Insize ISR-S400 surface roughness tester. The different surface roughness values like Ra, Rq, Rt, Rz, Rc, Rmax, Rsm, and

R_{pc}, etc have been measured. The R_a is the arithmetic mean of absolute values and it is mostly used to declare the roughness of any surface. After R_a, the R_z which is the mean of the roughness depth is being used. Similarly, the R_t is the total height of the roughness profile, R_c is the mean height and R_{max} is the maximum roughness depth. Whereas the R_{sm} is the mean of peak width, R_{pc} is the average number of peaks and R_q is the root mean square of the roughness values. All the measured values of various surface roughness after machining of the Titanium Grade 2 are shown in table 6.2.

It has been observed that the variation in the values of R_a, R_q, R_t, R_z, R_c, and R_{max} follow the same pattern. This is due to the reason that all these values are related to the height and depth in the surface roughness graph. Figure 6.5 shows the graphical representation of the roughness values in different machining run numbers. But when roughness values of R_{sm} and R_{pc} have been compared, merely opposite behavior of both has been observed. It is due to the reason that R_{sm} is the mean of peak width which is inversely related to the R_{pc} that is the average number of peaks. If the number of peaks will increases then the width of each peak will reduce in a particular length. Figure 6.6 shows the variation of R_{sm} and R_{pc} graphically. The cutting insert with honeycomb micro-texture gives better results of surface finish in comparison to the plain cutting insert [141].

Table 6.2: Measured values of different types of surface roughness.

Run	Machining Conditions			Obtained Results							
	Parameters			Surface Roughness in Experiment							
	Speed (rpm)	Feed (mm/rev)	Type of insert	R _a (μm)	R _q (μm)	R _t (μm)	R _z (μm)	R _c (μm)	R _{max} (μm)	R _{sm} (μm)	R _{pc} (per cm)
1	325	0.04	Plain Insert	2.942	2.6	14.84	12.297	5.05	14.84	80	120
2	325	0.04	Honey Comb	1.228	2.877	14.42	11.127	5.791	14.26	162	54
3	325	0.06	Plain Insert	2.17	2.388	13.92	12.481	4.753	13.92	95	104
4	325	0.06	Honey Comb	1.892	2.598	14.95	11.593	3.847	14.07	96	95
5	325	0.08	Plain Insert	3.062	3.605	18.25	15.315	8.593	16.51	186	50
6	325	0.08	Honey Comb	2.522	3.018	13.48	12.223	8.81	12.71	160	58

7	550	0.04	Plain Insert	2.062	2.41	11.56	10.659	4.008	11.18	96	91
8	550	0.04	Honey Comb	1.911	2.54	13.56	11.756	4.318	12.59	69	137
9	550	0.06	Plain Insert	2.439	3.093	18.66	15.677	6.069	18.57	62	166
10	550	0.06	Honey Comb	2.209	2.679	12.54	10.812	5.564	11.52	85	112
11	550	0.08	Plain Insert	2.895	3.547	18.69	15.017	5.759	17.53	106	100
12	550	0.08	Honey Comb	2.054	3.72	18.83	15.365	6.495	18.83	101	83
13	930	0.04	Plain Insert	2.964	2.434	11.67	10.12	4.474	11.31	114	83
14	930	0.04	Honey Comb	0.967	3.636	19.6	16.576	6.863	19.6	103	100
15	930	0.06	Plain Insert	3.822	4.561	22.66	18.494	11.723	20.51	280	37
16	930	0.06	Honey Comb	2.297	2.883	15.58	13.814	4.586	15.58	81	112
17	930	0.08	Plain Insert	3.158	3.712	25.23	16.332	6.217	25.23	113	95
18	930	0.08	Honey Comb	1.02	3.863	17.87	16.558	8.45	17.79	126	79

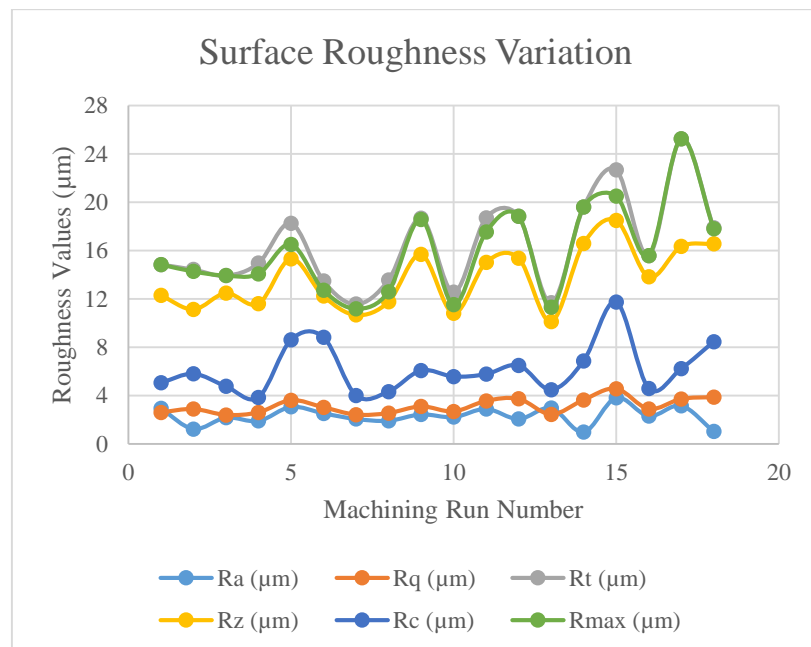


Figure 6.5: Graphical representation of the variation of Ra, Rq, Rt, Rz, Rc, and Rmax.

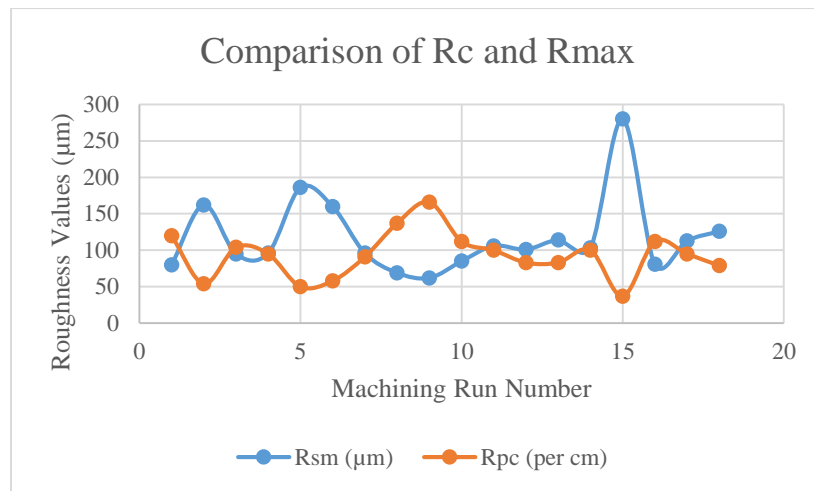


Figure 6.6: Graphical representation of the variation of R_{sm} and R_{pc}.

6.5.2 Tool Wear Analysis

To analyze the tool wear, the direction of the workpiece and cutting tool is very important. Figure 6.7 shows all these directions while machining on a lathe machine. The workpiece is rotating clockwise and the cutting insert movement is from right to left direction. The removed chip flow is along with the rake face of the cutting insert. Whereas flank wear which is abrasive wear occurs due to the interaction of the cutting insert with the workpiece. Figure 6.8 shows the areas where flank and crater wear occurs.

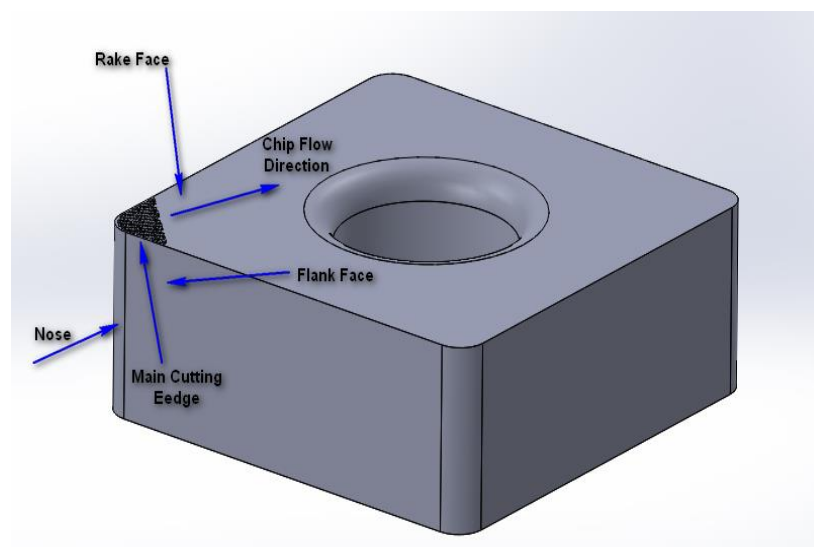


Figure 6.7: Different areas of wear in a cutting insert.

After performing the experiments, different types of deformations have been observed on the surface of the cutting inserts. Obtained shapes of built-up edges, flank wear,

crater wear, fracture, and nose radius wear are shown in Figures 6.8 (a) and 6.8 (b). Analysis of flank wear and crater wear has been done.

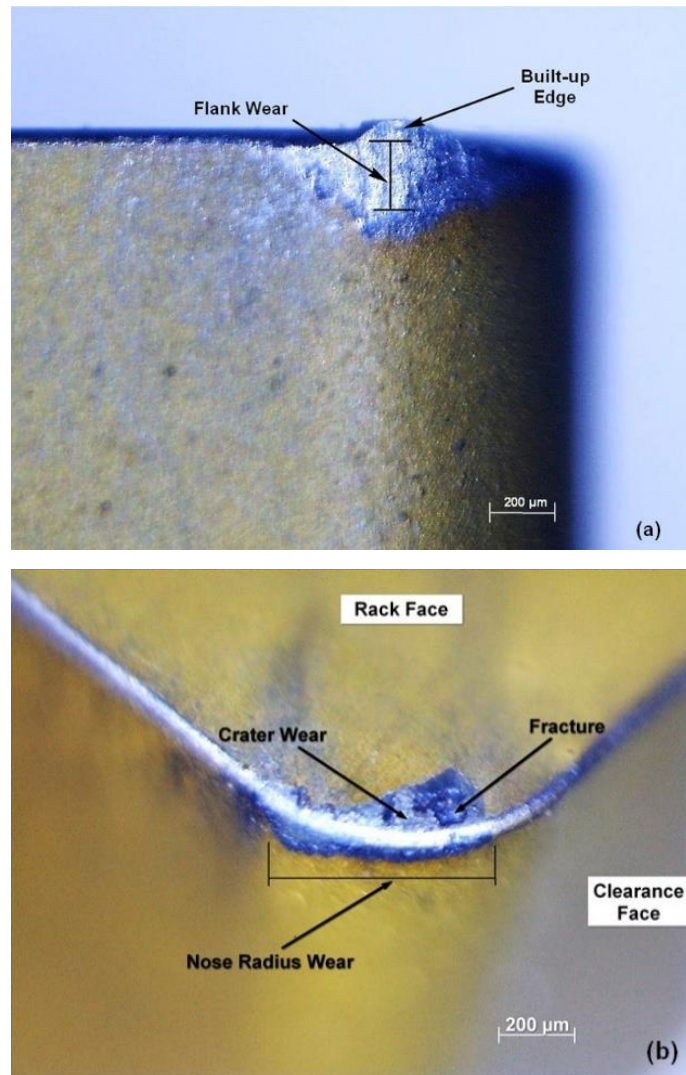


Figure 6.8: (a), (b) Deformations occurred on the surface of the cutting insert after machining.

6.5.3 Flank Wear

Flank wear is the abrasive wear that occurs due to the interaction of cutting insert with workpiece surface at high speed. It depends on the cutting temperature while machining. In turning operation on Titanium Gr2, two types of tungsten carbide with TiCN layer cutting inserts have been used. The measured temperature during machining with plain cutting insert is ranging from 230°C to 664°C and 0.293 mm to 0.431 mm of flank wear has occurred. Whereas with honeycomb micro-textured cutting inserts the observed temperature range is 210°C to 591°C and 0.159 mm to 0.274 mm of flank

wear has occurred. Table 6.3 shows the details of temperature and corresponding flank wear in all machining runs.

Table 6.3: Values of flank wear and cutting temperature for different types of cutting inserts.

Rotational Speed (rpm)	Feed (mm/rev)	Type of Insert	Temperature (°C)	Flank Wear ($V_{B \text{ Max}}$) (mm)
325	0.04	Plain Insert	230	0.293
325	0.04	Honeycomb	210	0.274
325	0.06	Plain Insert	264	0.296
325	0.06	Honeycomb	240	0.147
325	0.08	Plain Insert	327	0.305
325	0.08	Honeycomb	268	0.148
550	0.04	Plain Insert	378	0.35
550	0.04	Honeycomb	295	0.149
550	0.06	Plain Insert	404	0.367
550	0.06	Honeycomb	317	0.188
550	0.08	Plain Insert	363	0.321
550	0.08	Honeycomb	340	0.159
930	0.04	Plain Insert	475	0.409
930	0.04	Honeycomb	591	0.25
930	0.06	Plain Insert	625	0.431
930	0.06	Honeycomb	548	0.192
930	0.08	Plain Insert	604	0.425
930	0.08	Honeycomb	577	0.231

Higher cutting temperature and more flank wear have been observed when titanium grade 2 rod is machined with plain cutting insert whereas it is lower while machining with honeycomb micro-textured cutting insert. It is due to the reason that with honeycomb micro-texture heat dissipation rate has been increased and cutting temperature is reduced which was one of the reasons for the occurrence of flank wear. Figure 6.9 shows graphically the variation of flank wear concerning temperature for both types of cutting inserts.

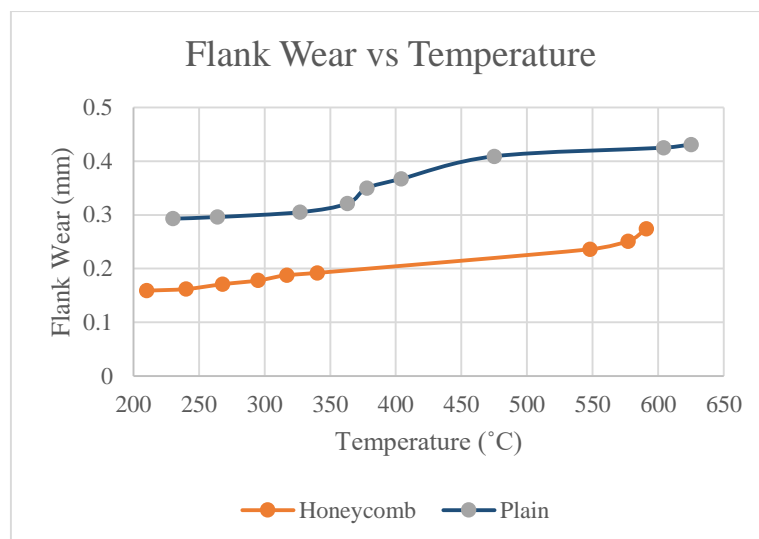


Figure 6.9: Variation of flank wear with temperature.

An increase in flank wear with the increase in feed has been observed. For the plain cutting insert, at the feed of 0.04 mm/rev the observed flank wear range is 0.293 mm to 0.409 mm. At a feed of 0.06 mm/rev, it has the range of 0.296 mm to 0.431 mm and 0.305 mm to 0.425 mm when the feed is 0.08 mm/rev. For honeycomb micro-textured cutting insert, at the feed of 0.04 mm/rev the flank wear range is 0.149 mm to 0.274 mm. At a feed of 0.06 mm/rev, it has the range of 0.147 mm to 0.192 mm and 0.148 mm to 0.231 mm when the feed is 0.08 mm/rev which is quite lower as compared to the flank wear in the plain insert.

The analysis has been carried out for the variation of flank wear with speed also. It has been observed that the effective flank wear has increased with an increase in rotational speed of titanium rod using plain cutting insert but decreased when machining has been done with honeycomb micro-textured cutting insert. For the plain cutting insert, at the speed of 325 rpm, the flank wear range is 0.293 mm to 0.305 mm. At speed of 550 rpm, it has a range of 0.321 mm to 0.350 mm and 0.409 mm to 0.431 mm when the speed is 930 rpm. Whereas for honeycomb micro-textured cutting insert, at the speed of 325 rpm the flank wear range is 0.147 mm to 0.274 mm. At speed of 550 rpm, it has a range of 0.149 mm to 0.188 mm and 0.192 mm to 0.250 mm when the speed is 930 rpm which is still lower as compared to the flank wear in the plain insert.

The standard cutting tool life has been considered up to 0.3 mm of the flank wear [141]. It has an average value of 0.193 mm while machining with honeycomb micro-textured cutting inserts. So the honeycomb micro-texture has increased the

cutting tool life for the same speed and feed range for machining of titanium grade 2 rod. Figure 6.10 shows the variation of flank wear concerning speed and feed for both the plain and honeycomb micro-textured cutting inserts.

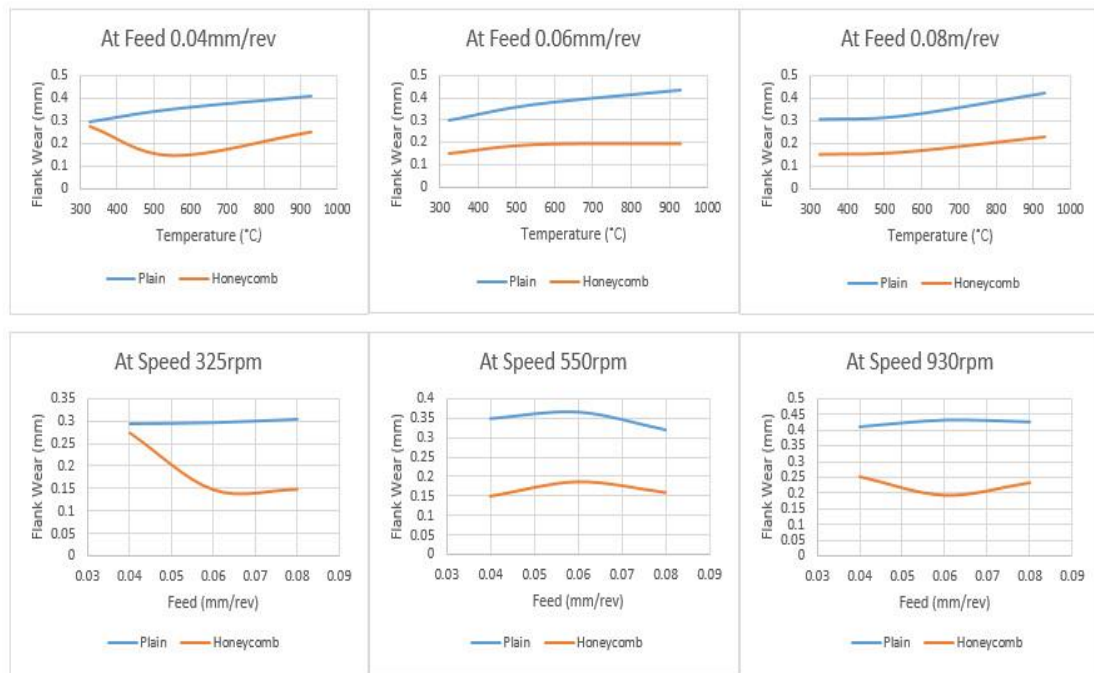
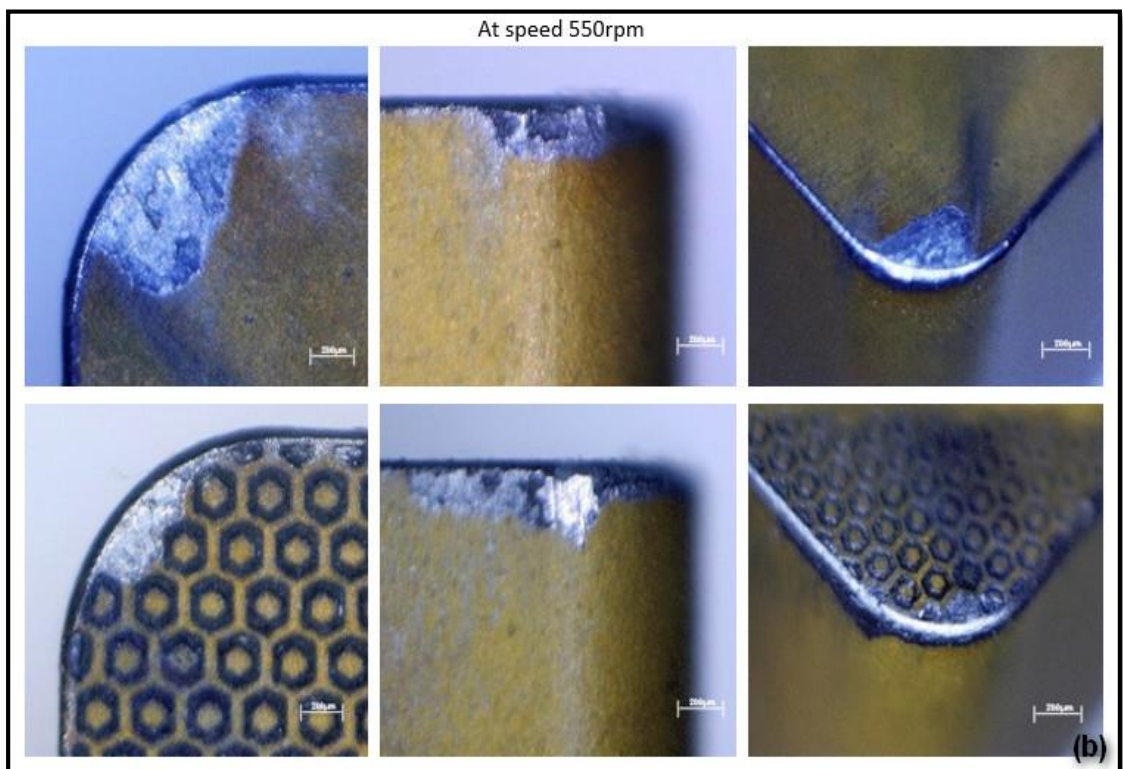
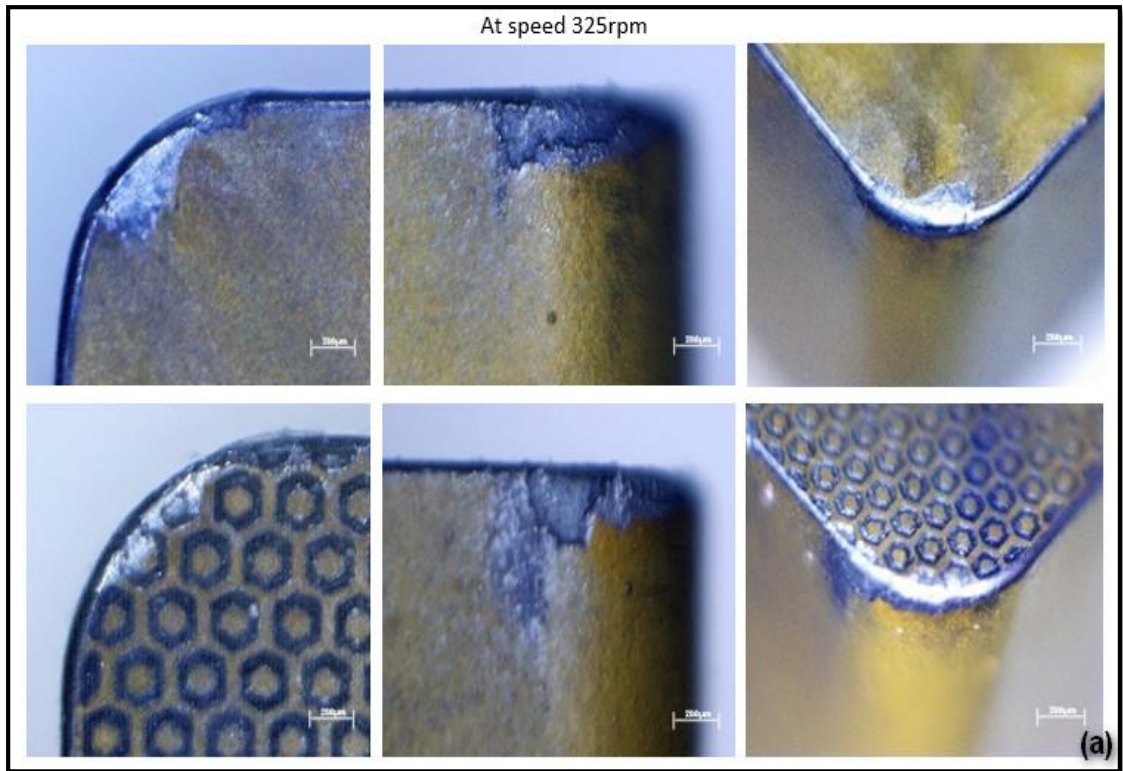


Figure 6.10: Variation of flank wear with speed and feed.

6.5.4 Crater Wear

Crater wear occurs due to the interaction of removed chips on the rake face of the cutting insert. The honeycomb micro-texture fabricated on the rake face of the cutting insert has reduced the contact surface area between high temperature removed chips and the rake face of the cutting insert. It also provides more area for heat dissipation as new and long walls have been created. Due to these reasons, the observed crater wear has reduced and cutting tool life has increased. Figure 6.11 (a), (b) & (c) shows the comparison of flank wear, crater wear, nose radius wear for normal and honeycomb micro-grooved cutting inserts after performing a machining operation on titanium grade 2 rod of diameter 50 mm at different speeds.



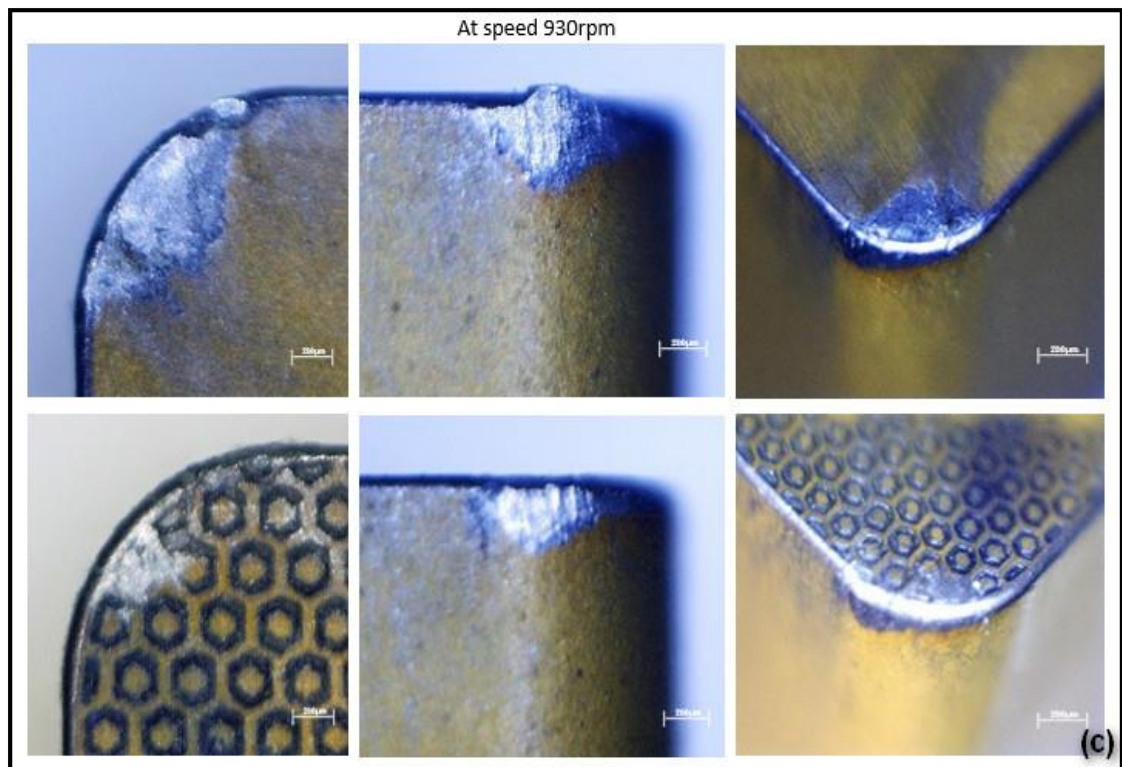


Figure 6.11: (a), (b) & (c) Comparison of flank, crater and nose radius wear at different speeds.

6.5.5 Chip Morphology

Variety of chips has been removed while machining of titanium grade 2 rod with tungsten carbide inserts such that snarled ribbon, snarled corkscrew, long corkscrew, snarled helical, long tubular, etc.[142]. Table 6.4 has the comparison of types of chips removed with plain and honeycomb micro-textured cutting insert at different parameters. Machining with a plain cutting insert has produced snarled ribbon-type chips at all speeds with 0.04 mm/rev of feed. After that when the feed has been increased then the corkscrew type of chips has been obtained which remains the same for all turning speed values. Whereas honeycomb micro-textured cutting insert has removed a variety of chips.

Both have produced the same type of chips at lower feed but when the feed has been increased then the honeycomb micro-texture has converted the chip type from a corkscrew to ribbon and long tubular. It is due to the reason that at a higher feed chips have got lesser time to make contact with the rake face of the cutting insert. Also because of the honeycomb micro-pattern, chips are stuck at the microgrooves and generate tubular or ribbon-type small diameter chips. This results in the reduction of

crater wear of the tool. Figure 6.12 shows the comparison of the type of removed chips with speed and feed for both plain and honeycomb micro-textured cutting insert. Figure 6.13 gives the details of the machining parameter, affected rake face of cutting insert, and type of removed chip obtained. Reduction in chip diameters with scale and their respective effect on the rock face have been shown.

Table 6.4: Comparison of types of chips removed at various parameters.

Parameters	Type of chip for Plain	Type of chip for Honeycomb micro-texture
	Insert	insert
325-0.04	Snarled Ribbon	Snarled Helical
325-0.06	Snarled Cork Screw	Long Tubular
325-0.08	Snarled Cork Screw	Long Tubular
550-0.04	Snarled Ribbon	Snarled Ribbon
550-0.06	Snarled Cork Screw	Snarled Cork Screw
550-0.08	Long Cork Screw	Snarled Ribbon
930-0.04	Snarled Ribbon	Snarled Ribbon
930-0.06	Snarled Cork Screw	Snarled Cork Screw
930-0.08	Snarled Cork Screw	Snarled Cork Screw

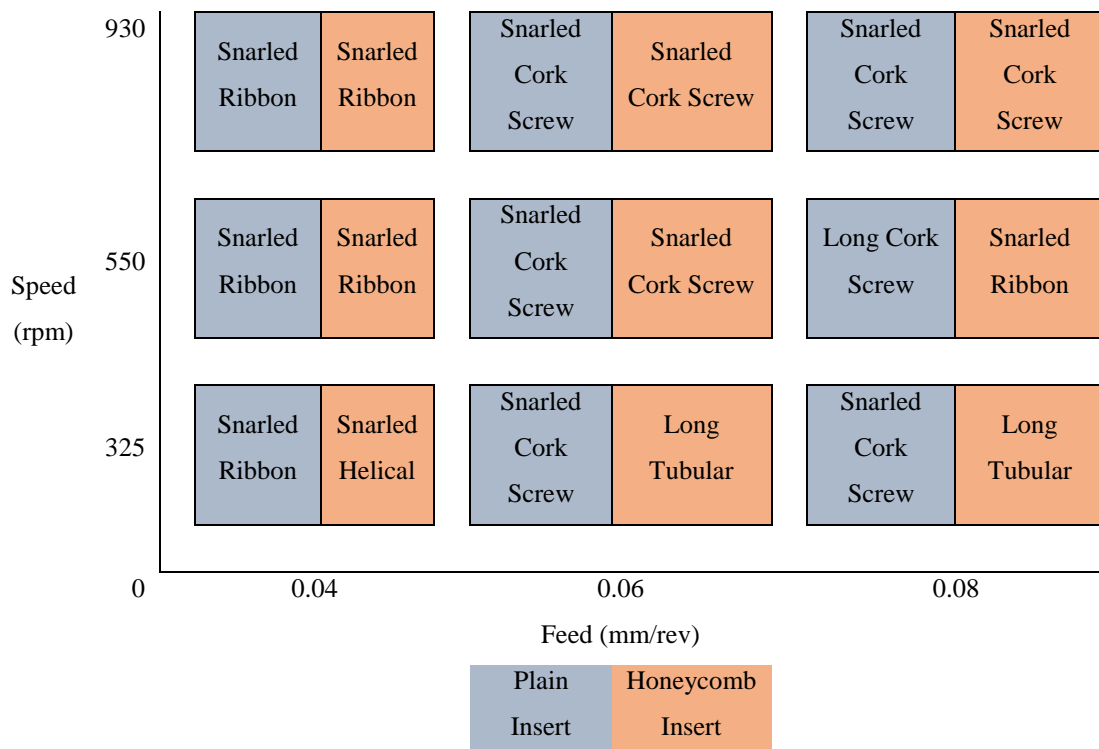
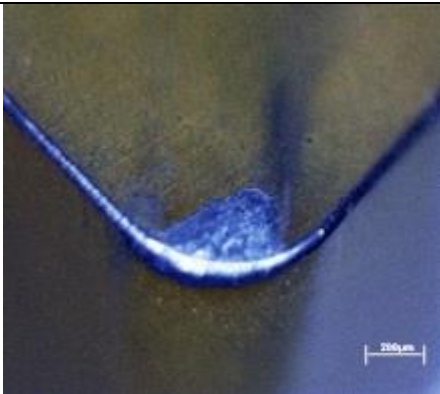
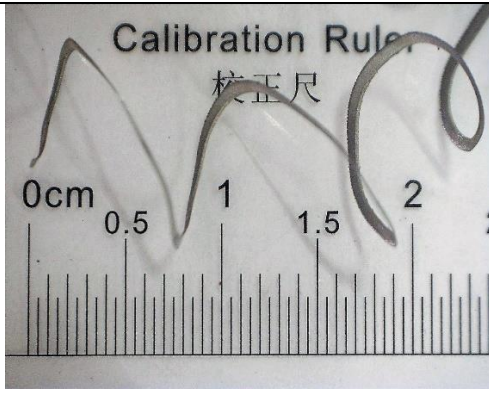
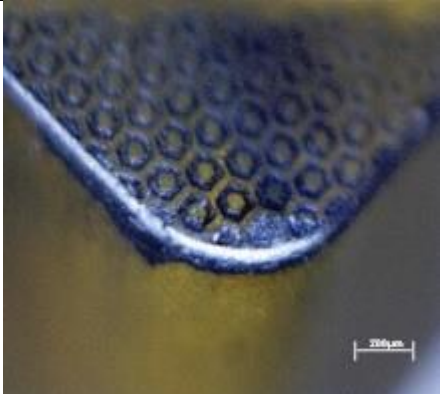
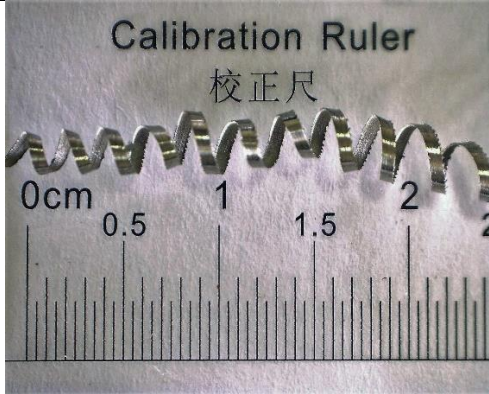
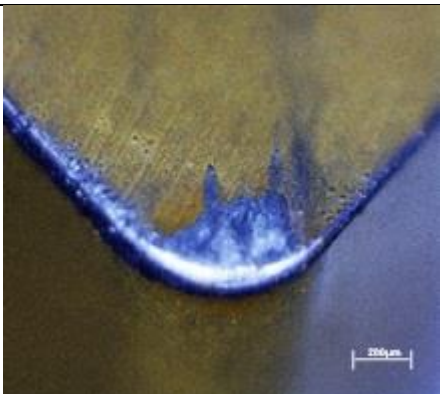
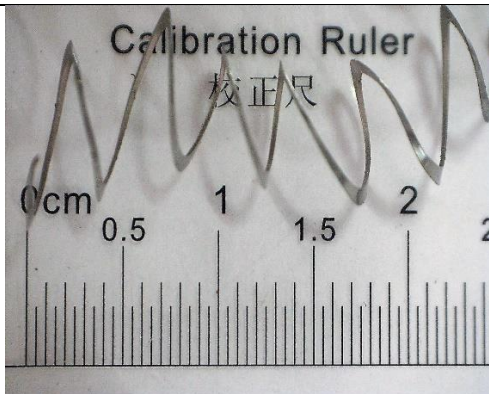
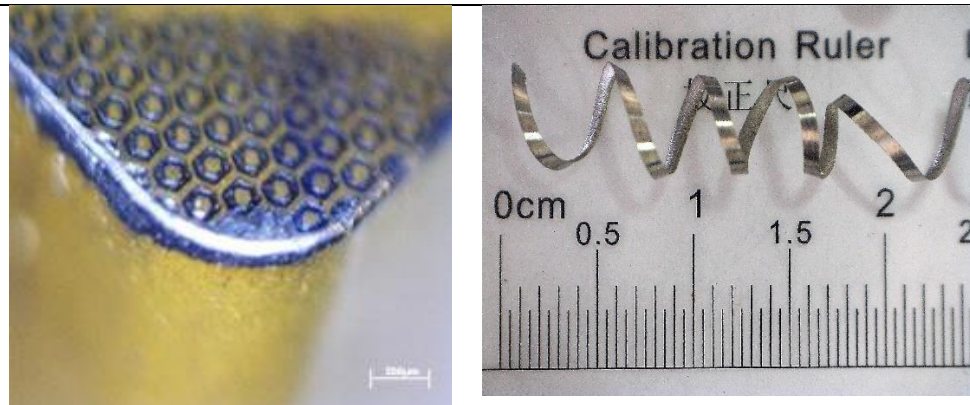
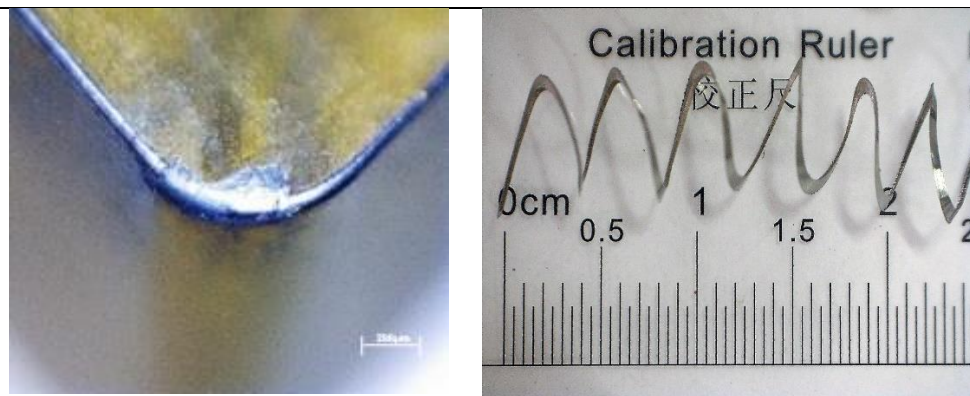


Figure 6.12: Variation of removed Chips type with speed and feed.

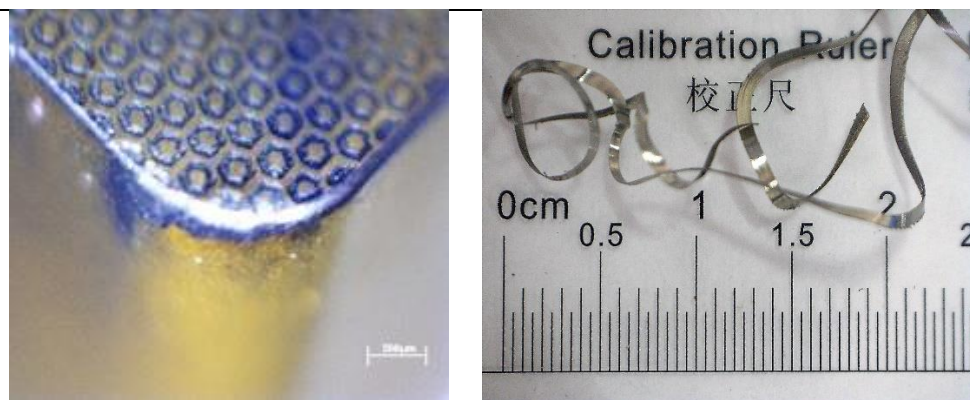
Rake Face of cutting Insert	Type of Removed Chip
	
<p>Run: 3; Speed 325 rpm; Feed: 0.06 mm/rev; Type of Insert: Plain; Type of Chip: Snarled cork Screw</p>	
	
<p>Run: 4; Speed: 325 rpm; Feed: 0.06 mm/rev; Type of Insert: Honey Comb; Type of Chip: Long Tubular</p>	
	
<p>Run: 5; Speed: 325 rpm; Feed: 0.08 mm/rev; Type of Insert: Plain; Type of Chip: Snarled Cork Screw.</p>	



Run: 6; Speed: 325 rpm; Feed: 0.08 mm/rev; Type of Insert: Honey Comb; Type of Chip: Long Tubular



Run: 11; Speed: 550 rpm; Feed: 0.08 mm/rev; Type of Insert: Plain; Type of Chip: Long Cork Screw



Run: 12; Speed: 550 rpm; Feed: 0.08 mm/rev; Type of Insert: Honey Comb; Type of Chip: Snarled Ribbon

Figure 6.13: Shape and size of removed chips.

Analysis has also been carried at micro levels for the shape of removed chips. It has been observed that in straight chips like snarled ribbon, various horizontal lines with more depth have been found on the convex side of chips. These straight groove fractures

are considered to be the reason for their straight shape. More and large-sized teeth have been found in long corkscrew chips in comparison to the long tubular chips. Due to these sharp edge teeth, there are more fluctuations in force components and hence more deformations occur at the rake face [13]. Vertical straight line fractures have been observed on the concave side of the corkscrew and long tubular chips. Figure 6.14 shows the micro-level details of various types of removed chips.

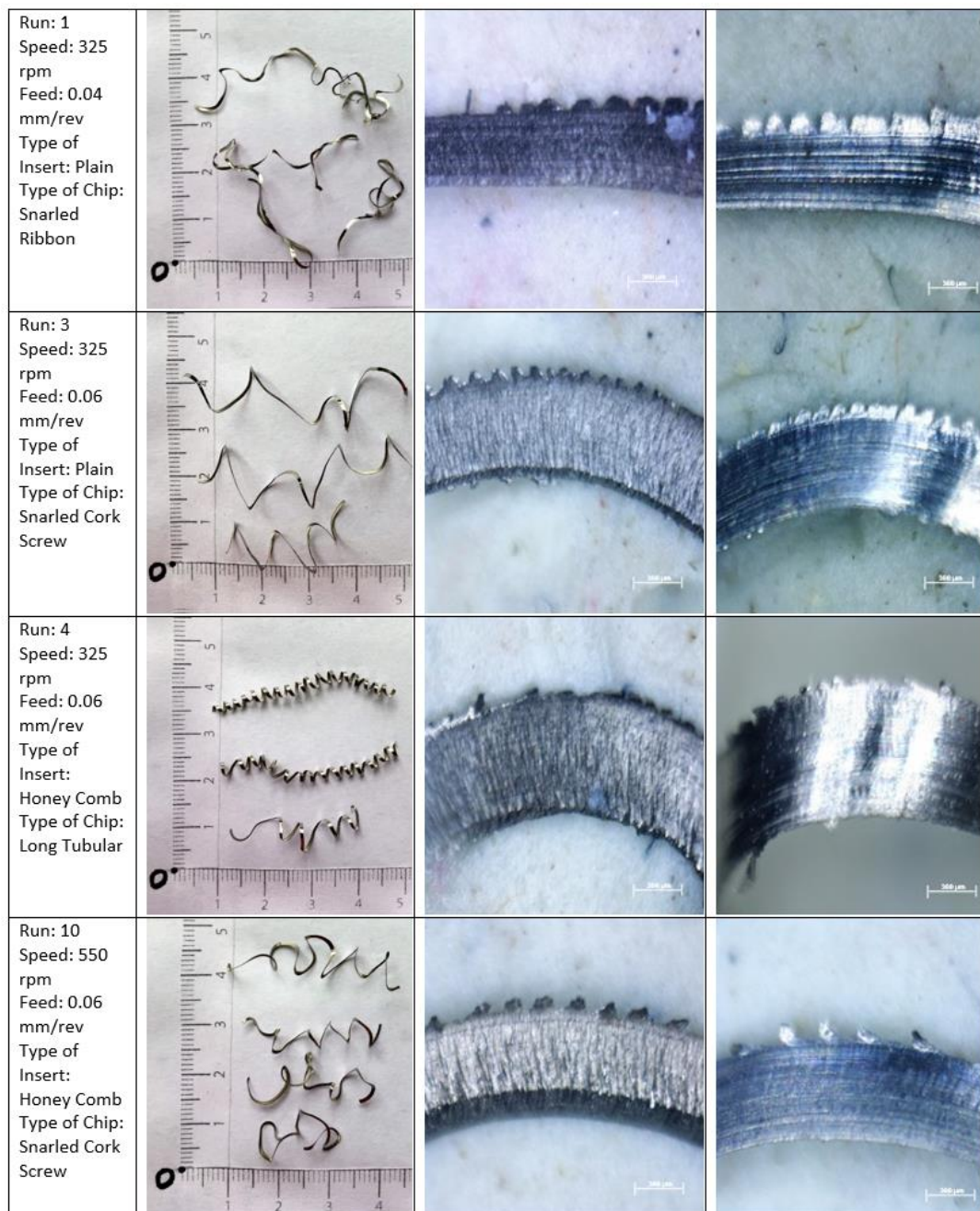


Figure 6.14: Micro-shape comparison of removed chips.

6.6 Deform 3D Simulation Analysis for Temperature Variation

The temperature variation analysis has been carried out for the turning operation of titanium grade 2 using DEFORM[®] 3D software and the results are compared with experimental results. FEA simulation has been conducted using the L9 orthogonal layout. Two variable parameters such that cutting speed and feed have been taken. The cutting depth, size of the workpiece, and cutting time have been taken as fixed parameters. The results are calculated in terms of temperature. All the simulation results have been verified with experimental outputs. After that effect of various machining parameters has been studied.

6.6.1 FEM Simulation

The simulation process has been carried out in DEFORM[®] 3D software. All process parameters are defined. After selecting turning as a machining operation and SI units the process set up has been done. The three cutting speeds 325 rpm, 550 rpm, and 930 rpm have been taken. The second variable parameter is feed and three levels of feed have been taken as 0.04 mm/rev, 0.06 mm/rev, and 0.08 mm/rev. The depth of cut has been selected as constant in all simulations and that is 0.5 mm. The complete simulation process mainly comprises three parts as shown in figure 6.15.

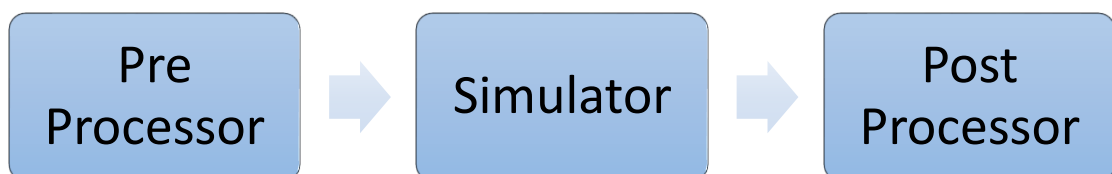


Figure 6.15: Main parts of simulation in DEFORM 3D.

In the pre-process, the selection of machining operation, problem ID, and machining type have been decided. After this, the process setup is given that requires the machining conditions like cutting speed in rpm, the diameter of the workpiece, depth of cut, and feed. Then it leads to the tool set up for which a 3D design of cutting tool SNMA 120408 HK1500 has been prepared in Solidworks[®] in (.STL) format taking the standard dimensions of 12.7 X 12.7 mm side, 4.76 mm of thickness, and 0.8 mm radius at cutting edge. The material of this rigid type of cutting insert is tungsten carbide which is taken directly from the library file provided by the DEFORM[®] 3D software. The direction of the movement of insert for cutting is given in +Y and the

linear direction of feed has been selected in $-X$ direction. Then the preprocessor section leads to the mesh generation of the cutting insert. After this, the plastic-type of workpiece shape and material is also selected from the library file of DEFORM[®] 3D software as Titanium Grade 2 (Ti6Al4V). The workpiece is fixed from all directions. The mesh count generated for both workpiece and cutting insert is 25000. After generating the mesh in the workpiece, simulation control has been given in terms of the number of simulation steps.

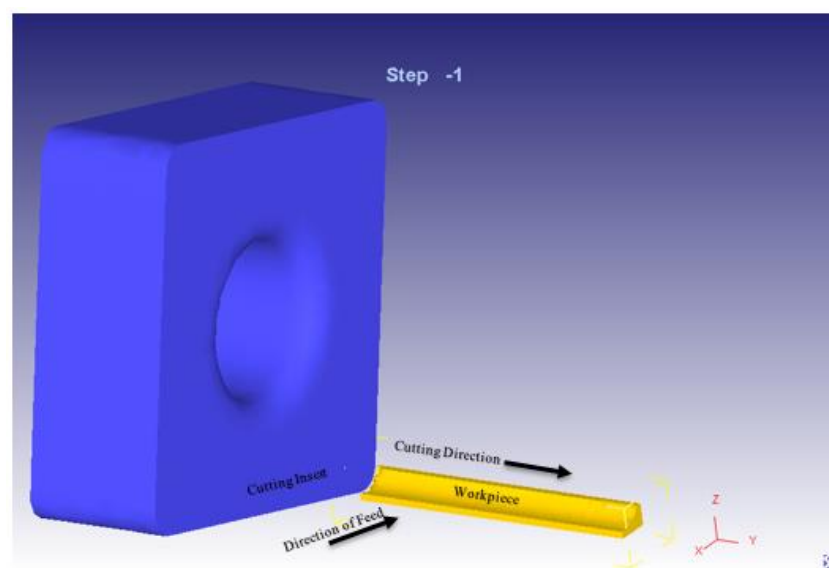


Figure 6.16: Selected workpiece and cutting insert for mesh generation.

The last phase of the pre-processor is to verify and generate the database file in a selected directory. Figure 6.16 shows the selected cutting tool and workpiece in DEFORM[®] 3D software along with the selected direction of cutting and feed. Figure 6.17 shows the mesh generation in both the cutting tool as well as in the workpiece. The simulator is the main part in which the machining operation occurs in the software. In this, all the calculations have been done for various outputs and at all the nodes and mesh generated in the cutting insert and workpiece. It gives the detail of the step number for which calculation is running in a summary form. It also provides the simulation graphics option to visualize the current and crossed steps details. The last part of DEFORM[®] 3D software is the post-processor in which all the values and results have been stored in database files which are then used for the simulation analysis purpose in the post-processor part of the software.

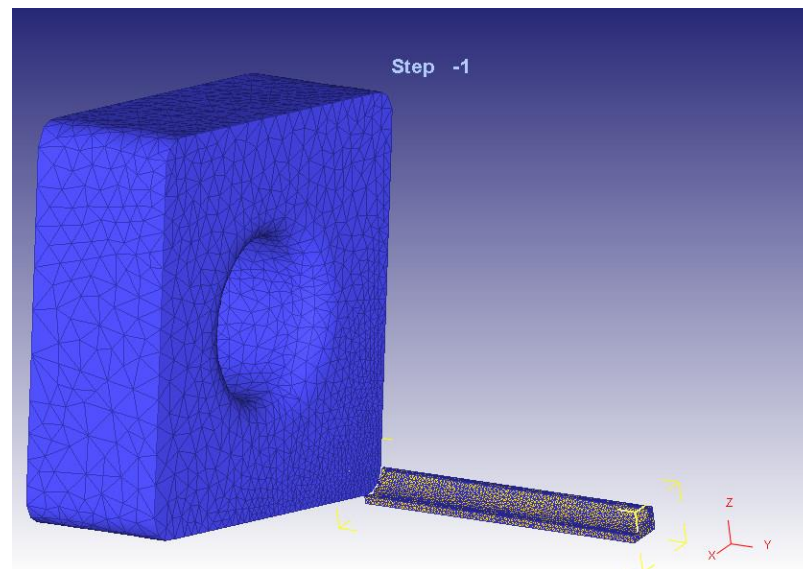


Figure 6.17: Generation of mesh in workpiece and cutting insert.

In DEFORM[®] 3D simulation, cutting speed and feed are two variable process factors. The three levels of cutting speed 325 rpm, 550 rpm, and 930 rpm have been taken. Similarly the given values of feed are 0.04 mm/rev, 0.06 mm/rev and 0.08 mm/rev. The depth of cut has been taken uniform in all simulations and that is 0.5. The diameter of a Titanium alloy rod is 50 mm and its length is 10 mm. All the experiments and simulations have conducted at room temperature of 20 °C. Figure 6.18 shows the observation of tool chip interface temperature as 426°C at step 925 for the simulation run number 7. In this way, all the tool chip interface temperature has been observed and tabulated. Table 6.5 shows all the values of considered process parameters and their levels with output results. It also gives the value of observed output temperature after simulation in DEFORM[®] 3D software. A turning operation has been performed on the titanium rod of diameter 50mm and 450mm long on NH22 lathe machine. All these simulation output values are compared with the experimental values taken from the published data with same input variables. A An error of 3% has been calculated using equation 6.1, which is in the range of acceptance [143]. Figure 6.19 shows the comparison graph between the observed temperature values of a simulation run in DEFORM[®] 3D software and the actual experimental measured temperature. All the runs have matched with an acceptable range of values.

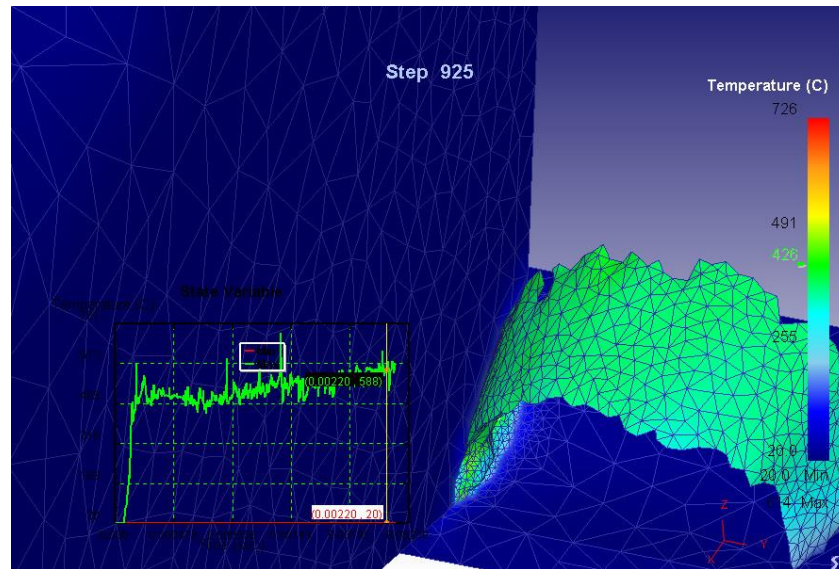


Figure 6.18: Measurement of tool chip interface temperature in DEFORM 3D software.

Table 6.5: Observed output temperature in simulation and experiments.

S. No.	Speed (rpm)	Feed (mm/rev)	Simulation output Temperature (°C)	Experimental output Temperature (°C)
1	325	0.04	270	268
2	325	0.06	182	125
3	325	0.08	271	273
4	550	0.04	151	136
5	550	0.06	435	447
6	550	0.08	191	163
7	930	0.04	426	421
8	930	0.06	350	334
9	930	0.08	512	519

$$\text{Percentage Error (\%)} = \frac{(\text{Simulation Temperature} - \text{Experimental Temperature})}{\text{Simulation Temperature}} \times 100 \quad (\text{Eq. 6.1})$$

When a comparison graph has been plotted between the speed and temperature to study its effect then an increase in temperature has been observed. When the cutting speed is less the cutting tool chip interface temperature is less as well. The maximum temperature has been observed at a speed of 930 rpm. Here the increased cutting speed will engender more friction between the tool and workpiece which ultimately intensifies the temperature.

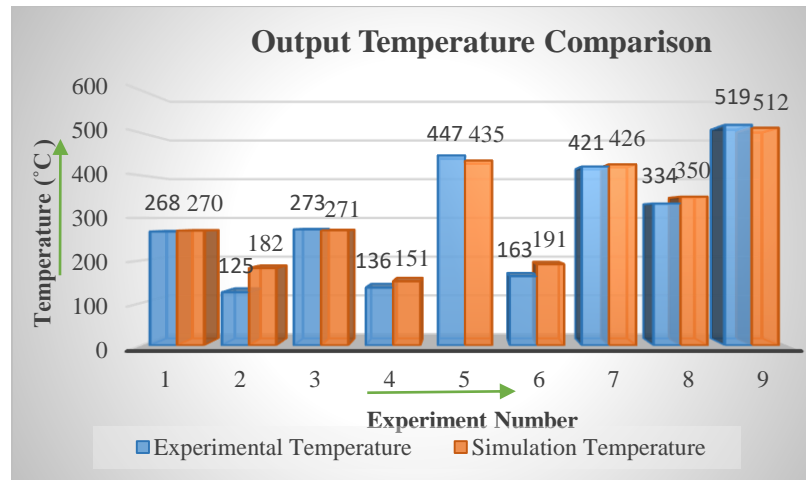


Figure 6.19: Temperature comparison graph for simulation and experimental data.

Figure 6.20 shows a change in temperature concerning speed. The value of the depth of the cut is constant. It shows that when the feed was 0.04 mm/sec and 0.08 mm/sec the value of temperature first decreased and then increased when the speed has been raised above 525 rpm. It might be due to the reason that with low and high feed, the heat dissipation rate is more. But at feed of 0.06 mm/sec it follow the same trend of sudden rise in temperature up to the speed limit of 525 rpm. After that when the speed has increased the temperature has been dropped down. It might be due to the softening effect because of the increase in temperature. Figure 6.21 shows the effect of feed on temperature. It is clearly shown that at a speed of 325 rpm and 930 rpm the temperature has decreased first and then increased when the feed given is above 0.06 mm/sec.

For the speed 550 rpm temperature has increased then decreased when given feed is above 0.06 mm/sec. The maximum temperature is obtained at a speed of 930 rpm in all sets of experiments. It is due to an increase in friction while increasing speed. From these two graphs, it can be perceived that the cutting tool-chip interface temperature has raised with the increase in cutting speed and feed.

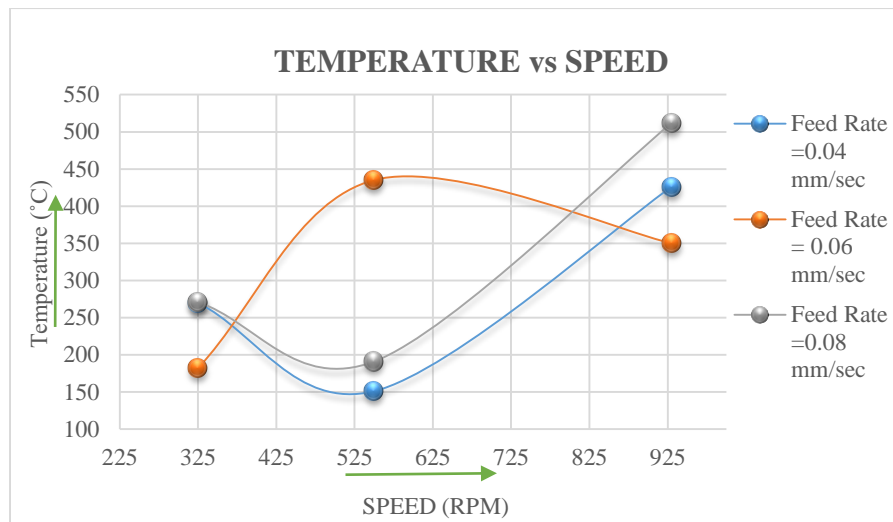


Figure 6.20: Variation in temperature with speed for three levels of feed.

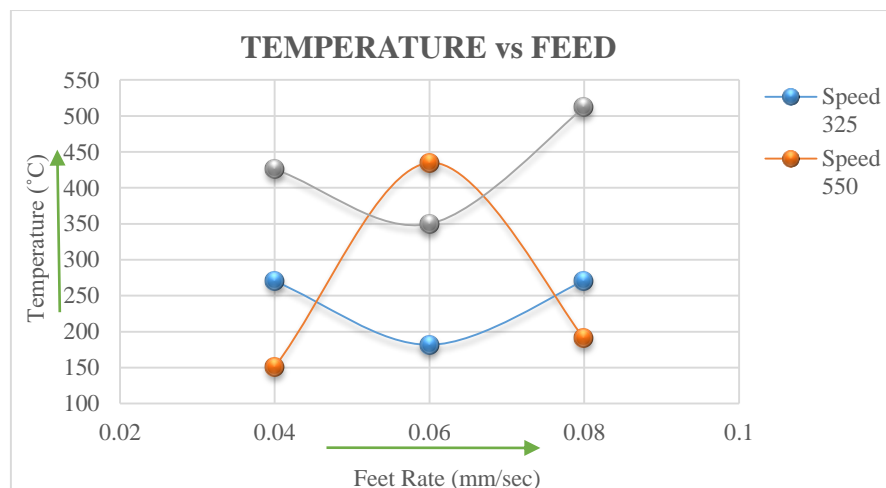


Figure 6.21: Variation in temperature with feed for three levels of speed.

All the observed values in the simulation match with the experimental values with an error percentage of 3% only. So simulation of turning operation on titanium grade 2 using DEFORM[®] 3D software is quite accurate. Now various conditional experimentations and precise results can be obtained. Moreover, it will save time and expenses to set up [144].

6.7 Comparison, Validation and Prediction of Machinability Aspects

Most of the research work has been conducted on various operations using plain cutting inserts under different conditions of machining. This paper has been focused on the use of DEFORM[®] 3D simulation tool to predict the effective stress and strain values after validating the data with the experimental results of cutting tool temperature and

tool wear. The turning operation has been performed using plain and micro-textured cutting inserts.

6.7.1 Comparison of Experimental Setup

A turning operation has been performed on Titanium Grade 2 rod of diameter 50 mm and length 510 mm. A lathe machine with a three-step speed and feed variation has been selected. The various machining parameters are rotational speed of workpiece, feed, and type of cutting inserts. The available speed values on the lathe machine have been measured with the help of a digital tachometer and these are 325 rpm, 550 rpm, and 930 rpm. The experiments have been conducted at room temperature and found to be 25°C. The lathe machine has three levels of feed and that is 0.04 mm/rev, 0.06 mm/rev, and 0.08 mm/rev.

For this experiment analysis, double square tungsten carbide cutting inserts have been used. These have thin TiCN coating up to 20 microns, zero relief angle, and a cylindrical hole to clamp on the tool holder without any chip breaker. Using these, further three types of cutting inserts have been prepared, and are Plain cutting insert (without any micro-texture), spiral triangular micro-textured, and honeycomb micro-textured cutting inserts. The micro-textures have been designed on Solidworks® 2015 and then CNC codes are generated using MasterCAM. Figure 6.22 demonstrates the dimensional comparison of Plain, Spiral Triangular, and Honeycomb micro-texture designs. The standard available square side of the cutting insert is 12.7 mm and the main affected zone of the cutting insert while machining is presented in figure 6.23. So the designs have been prepared to consider that. In spiral triangular micro-textured cutting insert the area covered for the fabrication of micro-texture is 1.12 mm X 1.12 mm on both sides of the cutting edge whereas in honeycomb micro-texture, it is 2.11 mm X 2.11 mm. The width of the groove taken in spiral triangular design has a value of 0.01 mm and 0.03 mm in honeycomb design. It merely depends on the structure of the design.

The spiral triangular design has been focused on increasing the count of continuous straight walls which act as fins to dissipate the heat whereas the honeycomb design has been focused on providing the micro pools along with the increase of continuous walls. These micro-pools act as a reservoir of coolant which will store the

coolant for a longer duration of time. The long removed chips are always a problem for machining operation and these micro-textures also act as a chip breaker to produce small-sized or discontinuous chips.

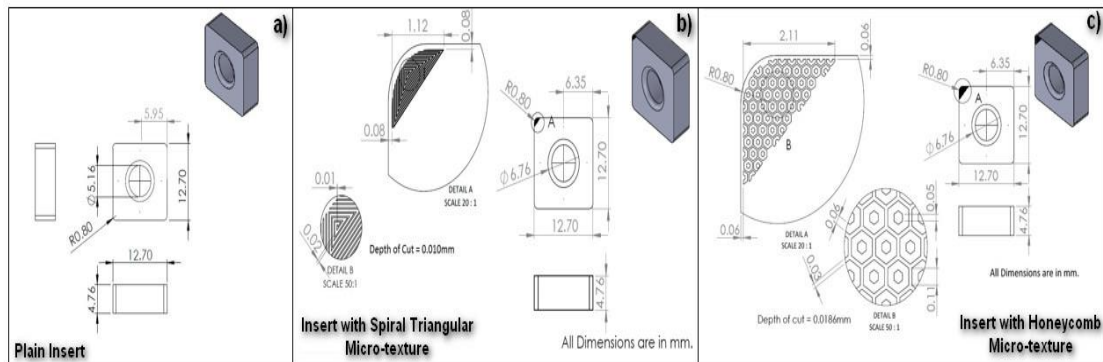


Figure 6.22: Dimensional comparison of Plain, Spiral Triangular, and Honeycomb micro-texture designs.

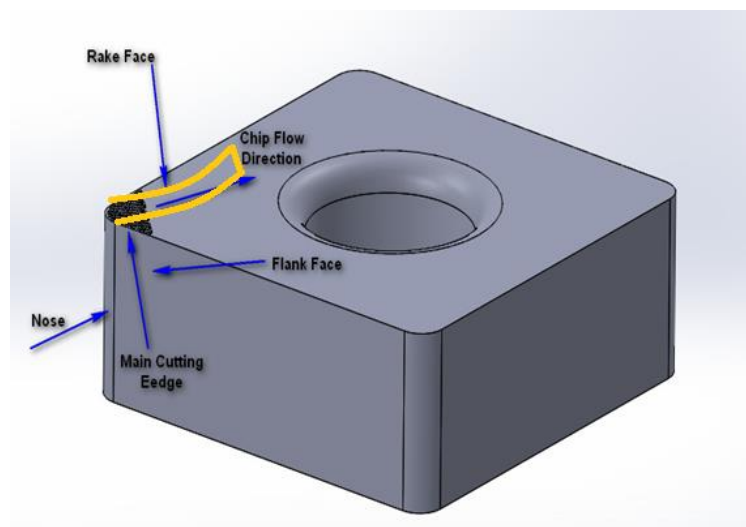


Figure 6.23: Effective elements on a cutting insert during machining.

Figure 6.24 gives a 3D outlook comparison of Plain, Spiral Triangular, and Honeycomb micro-texture designs. The created NC program having G and M Codes have been used in computer-controlled Femtosecond laser cutting machine. The micro-textures have been fabricated and analyzed using an Olympus topography machine which gives conclusive evidence of the presence of thin coating of TiCN. Figure 6.25 illustrates the comparison of actually fabricated cutting inserts. Taguchi L27 orthogonal array has been used for the design of experiments.

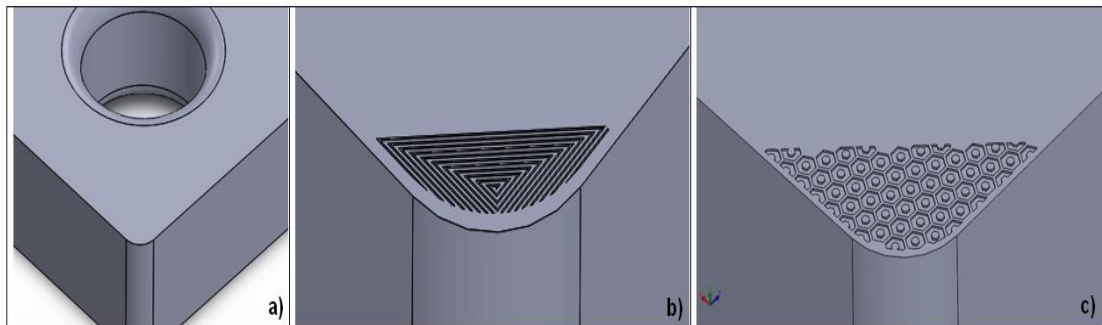


Figure 6.24: 3D Outlook comparison of a) Plain b) Spiral Triangular and c) Honeycomb micro-texture designs.

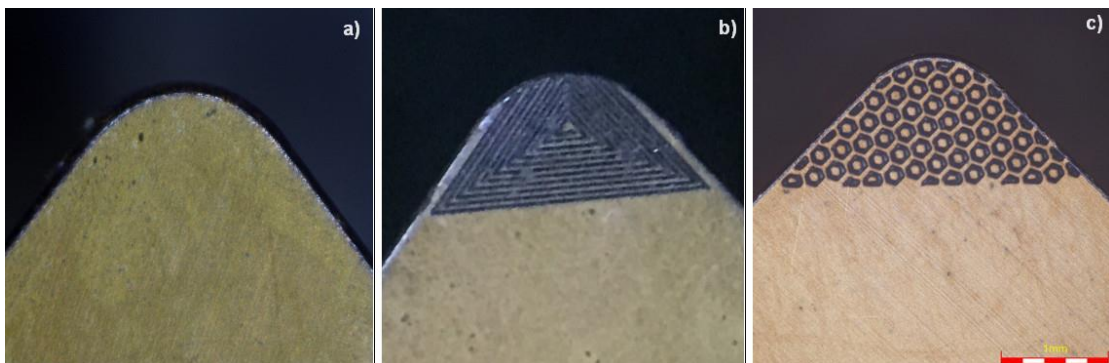


Figure 6.25: Actual cutting insert comparison of with and without micro-texture.

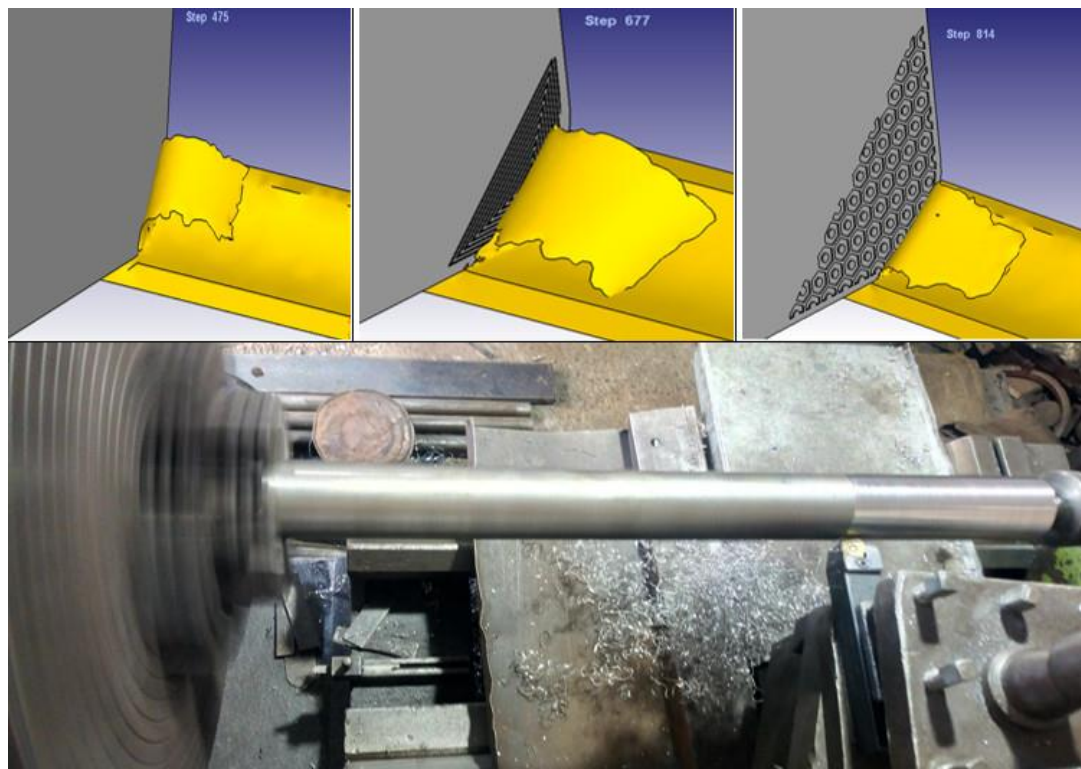


Figure 6.26: Actual Experimentation and simulation machining process.

DEFORM[®] 3D software has been used for the simulation process. The pre-processor stage started with the selection of operation and units for measurements. Process setup values of rotational speed, the diameter of the workpiece, depth of cut, and feed are chosen the same as that of actual experiments for all 27 runs. Simulation has been performed at the same room temperature of 25°C, with a convection coefficient value of 0.02 W/m²K. A total number of 50,000 meshes have been generated in the workpiece and cutting insert individually focusing on the areas of contact during the machining operation. Figure 6.26 shows the comparison of actual experimentation and simulation processes for all three types of cutting inserts.

6.7.2 Comparison of Cutting Tool Temperature

To analyze the simulation and experimental output results, cutting insert temperature and cutting tool wear are taken into observation. HTC IRX-65 contactless IR Thermometer has been used to measure the real-time cutting insert temperature during machining operation for all the runs. Table 6.6 has the experimental and simulation temperature values along with the speed, feed, and type of inserts. The value of maximum cutting tool temperature is observed with plain cutting insert at 930 rpm of speed and 0.06 m/rev of feed whereas the minimum values with honeycomb micro-textured cutting insert at 325 rpm of speed and 0.04 mm/rev of feed. The comparison of simulation and experimental temperature values for plain cutting insert is shown in figure 6.27, for Spiral triangular in figure 6.28, and Honeycomb micro-textured cutting insert is in figure 6.29.

In the actual experiment process, the temperature has been measured using the IR thermometer but in simulation, the graph of temperature variation has been plotted concerning time intervals. Figure 6.30 indicates the measurement of tool temperature for plain cutting insert, figure 6.31 for spiral triangular, and figure 6.32 for honeycomb micro-textured cutting insert. The tool temperature graph of the plain cutting insert is rising even after observing the 232 steps but for textured cutting inserts, it becomes a horizontal straight line even after 57 and 82 steps of simulations. It indicates that the control on cutting temperature has been attained using textured cutting inserts.

Table 6.6: Comparison of experimental and simulation temperatures with input parameters.

Run No.	Input Factors			Measured Temperature (°C)	
	Rotational Speed (rpm)	Feed (mm/rev)	Type of Insert	In Experiment	In Simulation
1	325	0.04	Plain	230	224
2	325	0.04	Spiral Triangular	227	232
3	325	0.04	Honeycomb	210	223
4	325	0.06	Plain	264	265
5	325	0.06	Spiral Triangular	254	262
6	325	0.06	Honeycomb	240	246
7	325	0.08	Plain	327	330
8	325	0.08	Spiral Triangular	295	290
9	325	0.08	Honeycomb	268	274
10	550	0.04	Plain	378	381
11	550	0.04	Spiral Triangular	336	342
12	550	0.04	Honeycomb	295	285
13	550	0.06	Plain	404	412
14	550	0.06	Spiral Triangular	372	376
15	550	0.06	Honeycomb	317	321
16	550	0.08	Plain	363	359
17	550	0.08	Spiral Triangular	313	321
18	550	0.08	Honeycomb	340	346
19	930	0.04	Plain	475	480
20	930	0.04	Spiral Triangular	404	413
21	930	0.04	Honeycomb	591	597
22	930	0.06	Plain	625	632
23	930	0.06	Spiral Triangular	476	482
24	930	0.06	Honeycomb	548	552
25	930	0.08	Plain	604	610
26	930	0.08	Spiral Triangular	502	512
27	930	0.08	Honeycomb	577	583

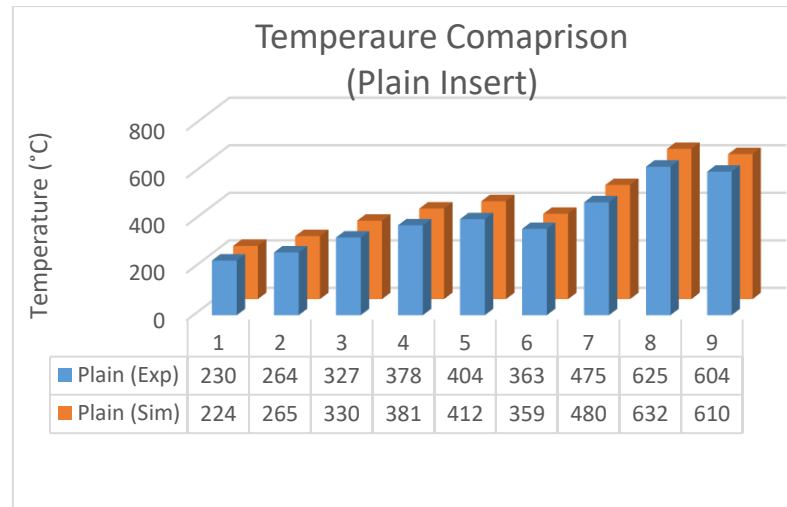


Figure 6.27: Temperature comparison for Plain cutting insert.

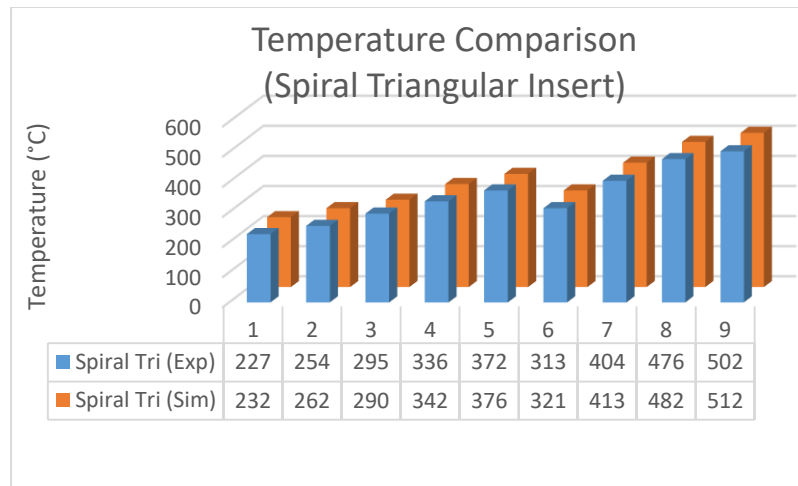


Figure 6.28: Temperature comparison for Spiral triangular micro-textured cutting insert.

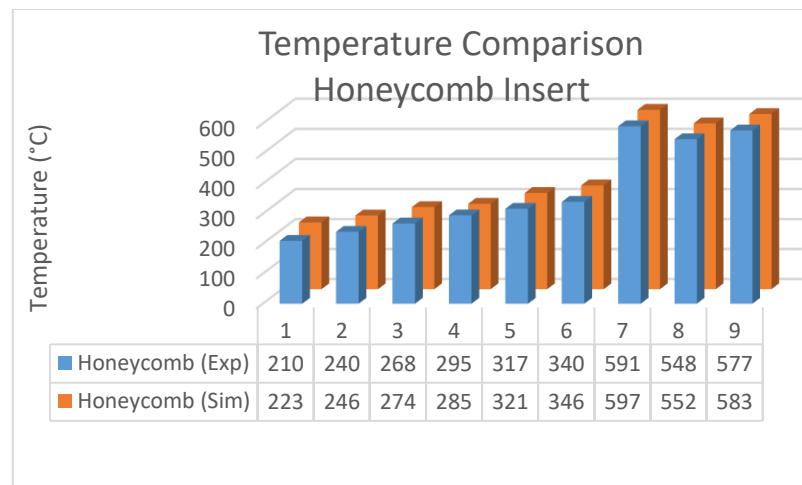


Figure 6.29: Temperature comparison for Honeycomb micro-textured cutting insert.

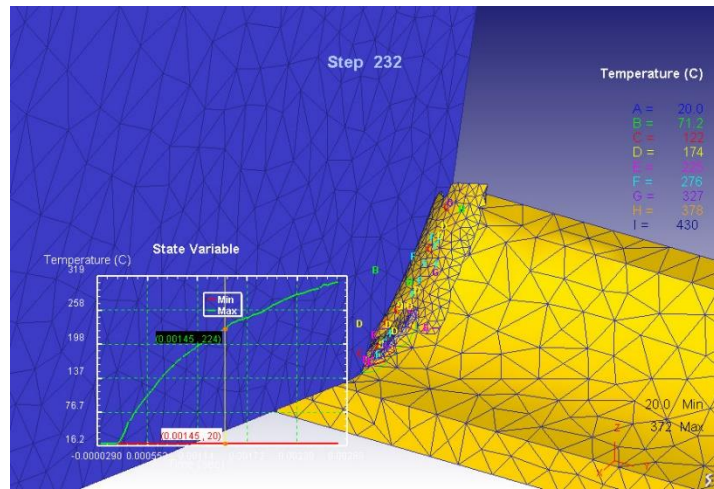


Figure 6.30: Temperature Measurements in simulation for Plain cutting insert.

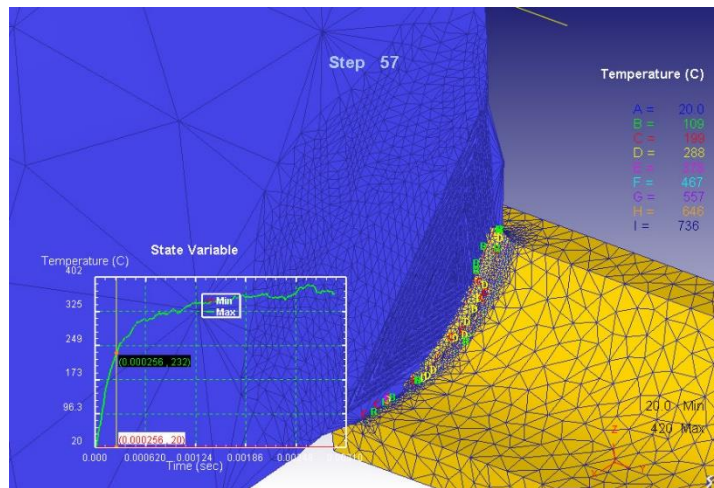


Figure 6.31: Temperature Measurements in for Spiral Triangular micro-textured cutting insert.

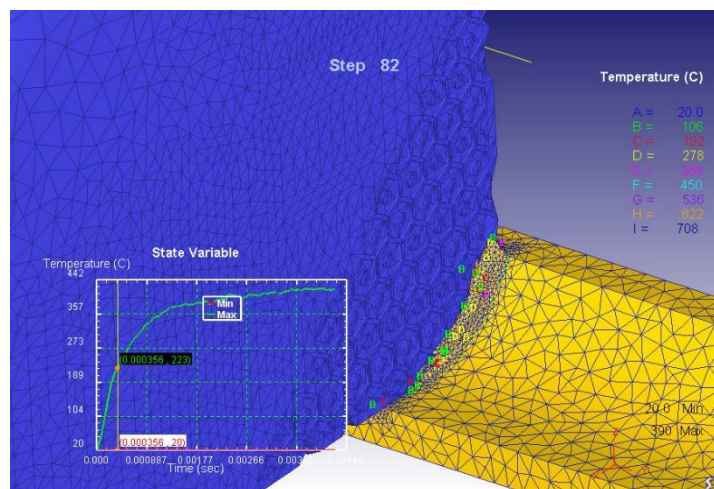


Figure 6.32: Temperature Measurements for Honeycomb micro-textured cutting insert.

Figure 6.33 demonstrates the heat-affected zones in the plain cutting insert after performing the turning operations on titanium grade 2 rod. Figure 6.34 shows the elemental distribution of temperature zones. It indicates that the rake face and flank both are having high-temperature zones which will cause wear of the cutting tool. Figure 6.34 and figure 6.36 have the temperature zones for the spiral triangular micro-textured cutting insert. The area of the high-temperature zone has been reduced. The effect of long walls fabricated as per design pattern has distributed and dissipated the heat which results in lowering the cutting tool temperature. Similarly the figure 6.37 and figure 6.38 have the temperature zones obtained in the honeycomb micro-textured cutting insert which is still smaller in size as compared to both of the others.

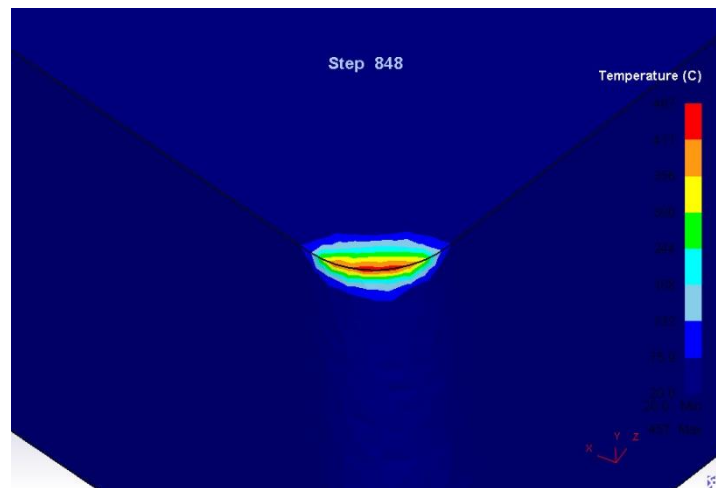


Figure 6.33: Heat effected zones in Plain cutting insert.

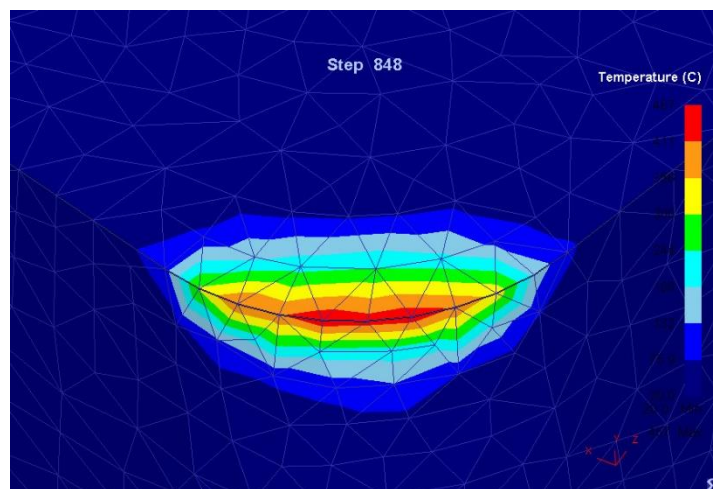


Figure 6.34: Elemental temperature distribution in Plain cutting insert.

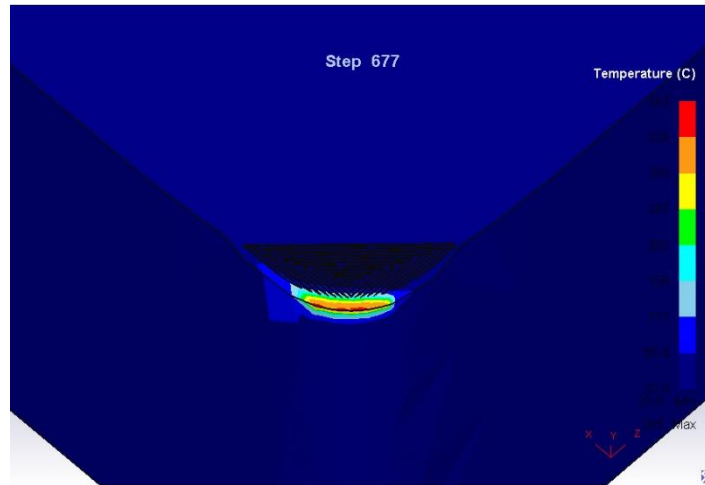


Figure 6.35: Heat effected zones in Spiral Triangular micro-textured cutting insert.

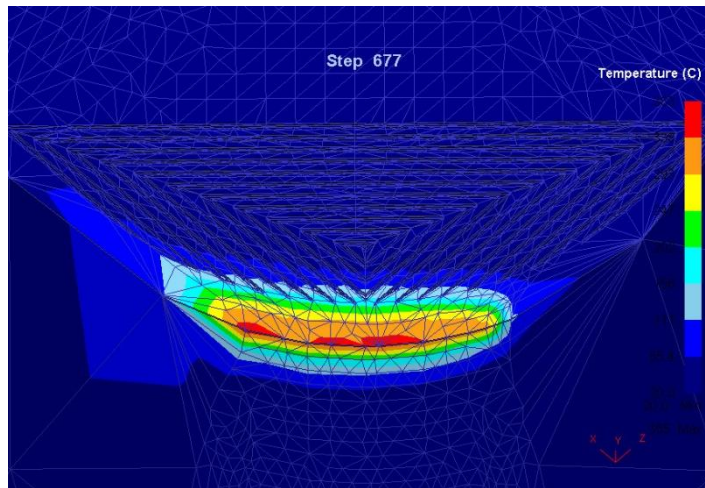


Figure 6.36: Elemental temperature distribution in Spiral Triangular micro-textured cutting insert.

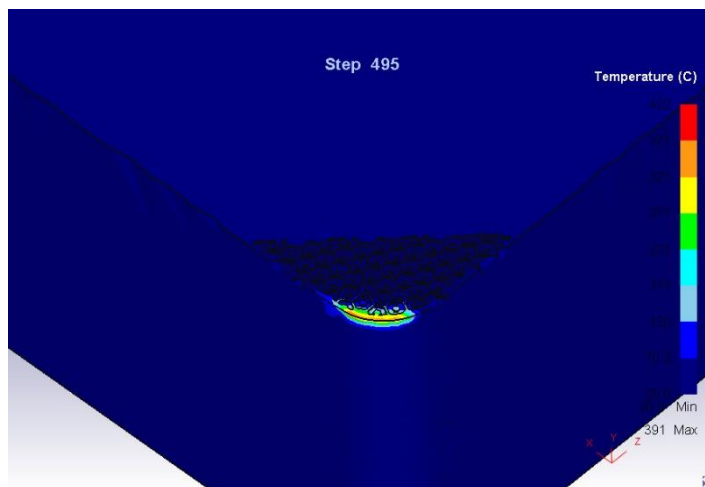


Figure 6.37: Heat effected zones in Honeycomb micro-textured cutting insert.

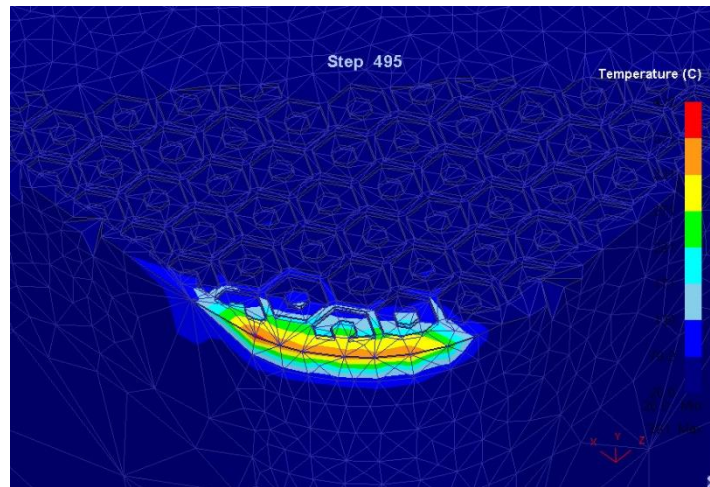


Figure 6.38: Elemental temperature distribution in Honeycomb micro-textured cutting insert. Temperature variation has been studied. Cutting tool temperature rise is observed with an increase in rotational speed of titanium rod and feed, for all types of cutting inserts. Obtained results in simulation analysis follow the same type of graph with small eccentricities of values. The compared results exhibit a maximum of 1.11% error of deviation which is in the suitable range. Therefore the simulation outcomes have been corroborated with the experimental values. Figure 6.39 have the comparison graph of experimental and simulation temperature values for all type of cutting inserts.

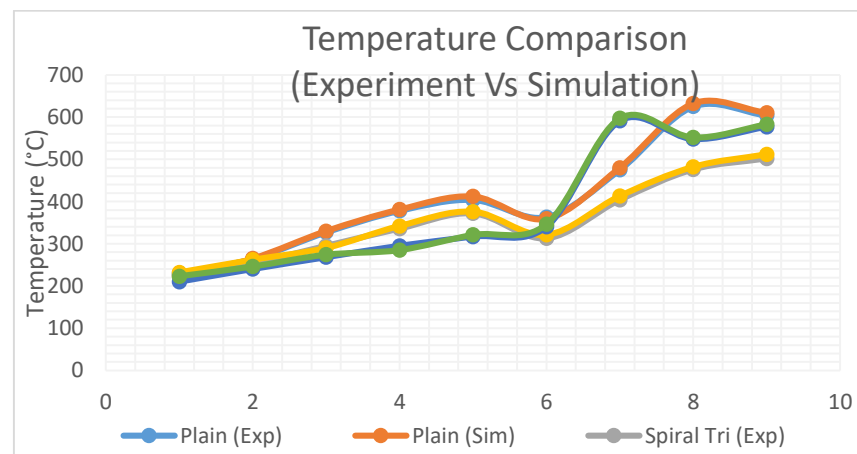


Figure 6.39: Variation in temperature for all types of cutting inserts.

6.7.3 Comparison of Tool Wear

To validate the simulation analysis with one more factor, analysis of tool wear has been accompanied. Flank wear in experiments has been measured with the help of a Celestron optical microscope. In the simulation, the tool wear segment has measured

the flank wear in mm units. Both the experimental and simulation flank wear values have been shown in table 6.7 with the percentage of error. The average percentage of error is 2.19% which is in the adequate range.

Table 6.7: Cutting tool wear in experiments and simulation with the percentage of error.

Experiment Run No.	Type of Insert	Tool Wear in Experiment (mm)	Tool Wear in Simulation (mm)	Percentage of Error (%)
1	Plain	0.293	0.289	1.37
2	Spiral Triangular	0.286	0.282	1.40
3	Honeycomb	0.274	0.278	1.46
4	Plain	0.296	0.293	1.01
5	Spiral Triangular	0.210	0.214	1.90
6	Honeycomb	0.147	0.152	3.40
7	Plain	0.305	0.312	2.30
8	Spiral Triangular	0.246	0.242	1.63
9	Honeycomb	0.148	0.156	5.41
10	Plain	0.35	0.358	2.29
11	Spiral Triangular	0.260	0.263	1.15
12	Honeycomb	0.149	0.158	6.04
13	Plain	0.367	0.360	1.91
14	Spiral Triangular	0.282	0.285	1.06
15	Honeycomb	0.188	0.192	2.13
16	Plain	0.321	0.325	1.25
17	Spiral Triangular	0.234	0.241	2.99
18	Honeycomb	0.159	0.164	3.14
19	Plain	0.409	0.402	1.71
20	Spiral Triangular	0.296	0.289	2.36
21	Honeycomb	0.25	0.257	2.80
22	Plain	0.431	0.428	0.70
23	Spiral Triangular	0.283	0.278	1.77
24	Honeycomb	0.192	0.199	3.65
25	Plain	0.425	0.422	0.71
26	Spiral Triangular	0.280	0.284	1.43
27	Honeycomb	0.231	0.236	2.16

The maximum tool wear of 0.425 mm has been perceived on the plain cutting insert and a minimum of 0.147 mm on the honeycomb micro-textured cutting insert. The variation in the values of tool wear has been compared with the measured cutting tool temperature and it can be concluded that the rise in temperature causes more tool wear but due to the micro-textures the tool wear has been reduced. Figure 6.40 contains the comparison of experimental and simulation cutting tool wear in the plain cutting insert. Figure 6.41 has the comparison for spiral triangular micro-textured cutting insert and figure 6.42 for honeycomb micro-textured cutting insert.

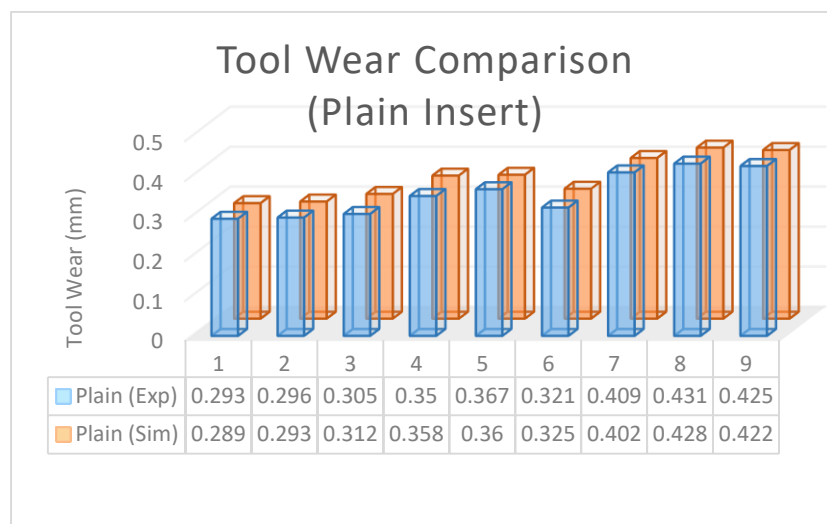


Figure 6.40: Comparison of tool wear for Plain cutting insert.

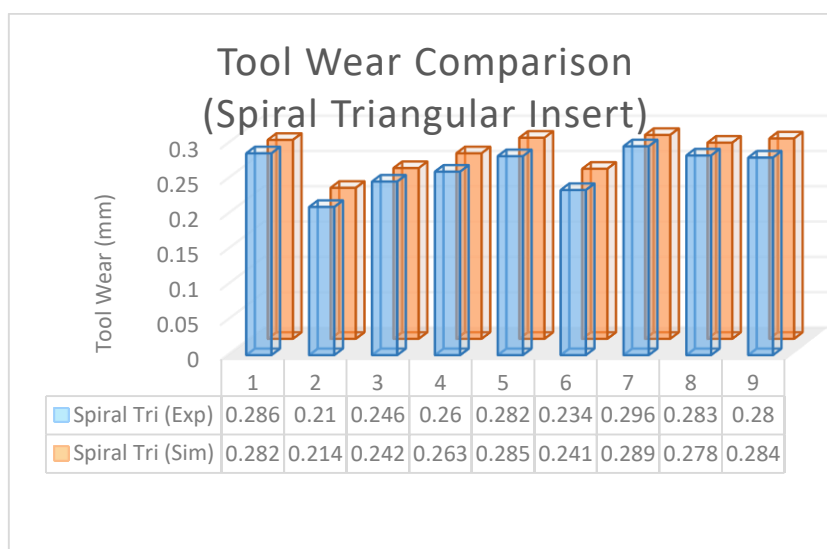


Figure 6.41: Comparison of tool wear for Spiral Triangular micro-textured cutting insert.

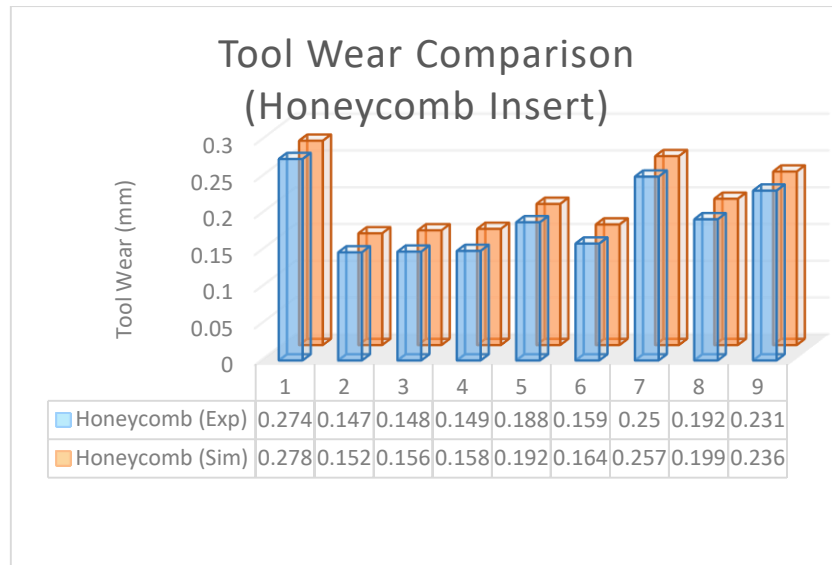


Figure 6.42: Comparison of tool wear for Honeycomb micro-textured cutting insert.

DEFORM[®] 3D has the graphical representation of tool wear geometry concerning time. In the simulation of the plain cutting insert, five concentric round shape forms have been obtained which represent the damage of cutting edge and reduction in tool life. After that, the quality of the surface finish has been reduced. Figure 6.43 illustrates the same tool wear geometry for the plain cutting insert whereas figure 6.44 has for the spiral triangular micro-textured cutting insert which is quite smaller in comparison.

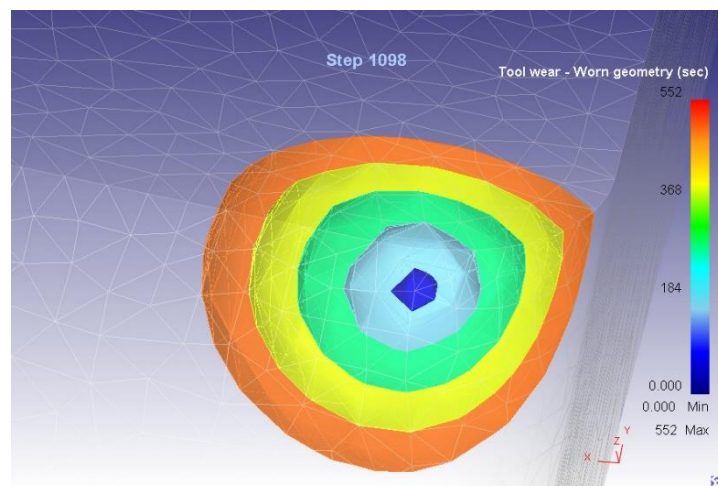


Figure 6.43: Tool wear geometry in Plain cutting insert.

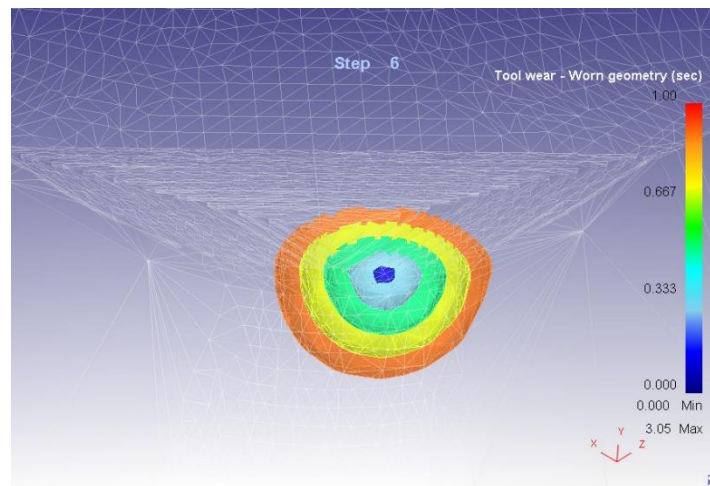


Figure 6.44: Tool wear geometry in Spiral Triangular micro-textured cutting insert.

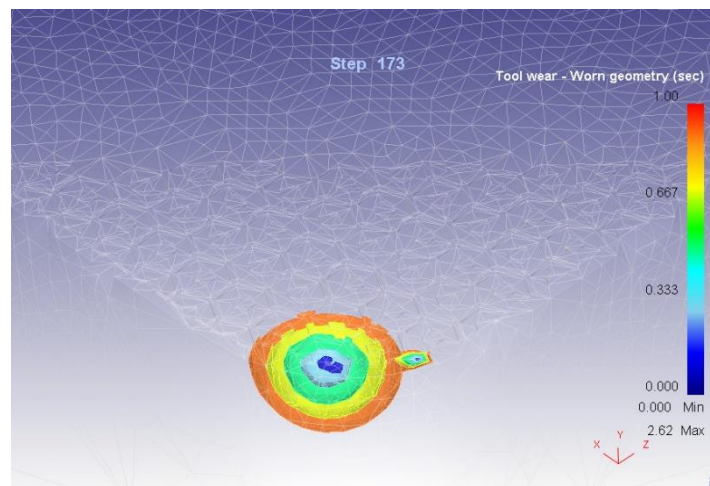


Figure 6.45: Tool wear geometry in Honeycomb micro-textured cutting insert.

In the tool wear geometry of honeycomb micro-textured cutting insert, it has been observed that the size and affected area are very less. The damage of pools and walls of few honeycomb patterns are found. Due to this, the size of fabricated micro pools has been increased which will accumulate the additional amount of coolant and that will also help to reduce the cutting tool temperature. Figure 6.45 demonstrates the tool wear geometry in the honeycomb micro-textured cutting insert.

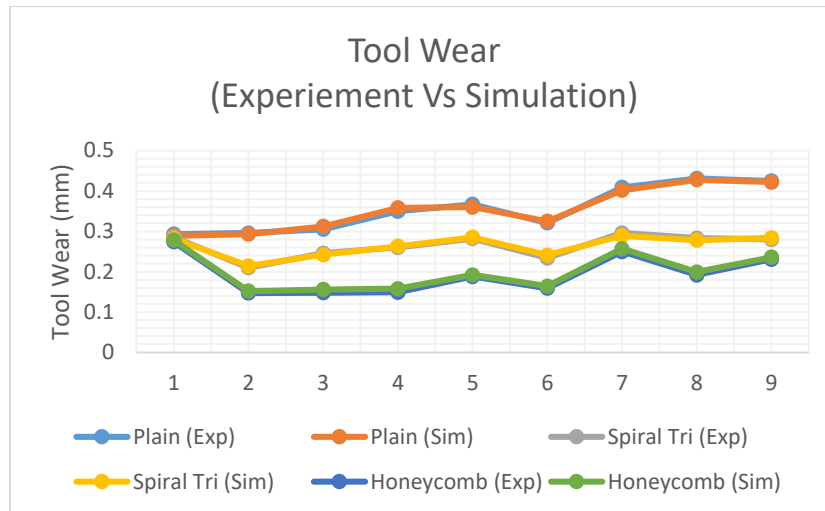


Figure 6.46: Tool wear comparison for experimental and simulation data.

The comparison of the tool wear data has been plotted in a graph and shown in figure 6.46 which epitomizes the same variation in experimental and simulation results for all the types of cutting inserts. Therefore the simulation results for cutting tool temperature and tool wear are manifestly authenticated with the experimental data. Based on this the effective principal stress and effective strain values for these sets of experiments have been predicted.

Predicted values obtained in DEFORM[®] 3D analysis for effective stress and effective strain for plain (without micro-texture), spiral triangular, and honeycomb micro-textured cutting inserts are included in table 6.8. It has been perceived that the effective stress increases with an increase in rotational speed as well as with feed. The maximum of 2.74Mpa e+03 effective principal stress has been measured with plain cutting insert at speed of 930 rpm and 0.08 mm/rev of feed. The tool life has deteriorated at this speed & feed combination. Therefore a large amount of force needs to be applied to the plain cutting tool to perform the machining which increases the value of effective stress in operation. Figure 6.47 explains the variation of the values of effective stress in plain, spiral triangular, and honeycomb micro-textured cutting inserts. Figure 6.48 shows the variation of effective strain for all the type of cutting inserts. Effective strain is also rising with an increase of rotational speed and feed values.

Table 6.8: Predicted effective stress and strain values of three types of cutting inserts.

Simulation Run No.	Type of Insert	Effective Stress (MPa) (e +03)	Effective Strain (mm/mm) (e -05)
1	Plain	1.22	4.11
2	Spiral Triangular	1.14	2.94
3	Honeycomb	1.12	3.17
4	Plain	1.53	4.24
5	Spiral Triangular	1.08	3.68
6	Honeycomb	1.25	3.27
7	Plain	1.88	4.21
8	Spiral Triangular	1.64	3.56
9	Honeycomb	1.39	3.32
10	Plain	1.92	4.64
11	Spiral Triangular	1.7	3.41
12	Honeycomb	1.38	3.37
13	Plain	2.07	4.92
14	Spiral Triangular	1.91	3.65
15	Honeycomb	1.44	3.44
16	Plain	2.38	4.82
17	Spiral Triangular	2.02	3.88
18	Honeycomb	1.62	3.55
19	Plain	1.91	5.07
20	Spiral Triangular	2.13	3.94
21	Honeycomb	1.77	3.86
22	Plain	2.56	5.25
23	Spiral Triangular	2.21	4.04
24	Honeycomb	1.81	3.91
25	Plain	2.74	5.37
26	Spiral Triangular	2.28	4.18
27	Honeycomb	1.84	3.94

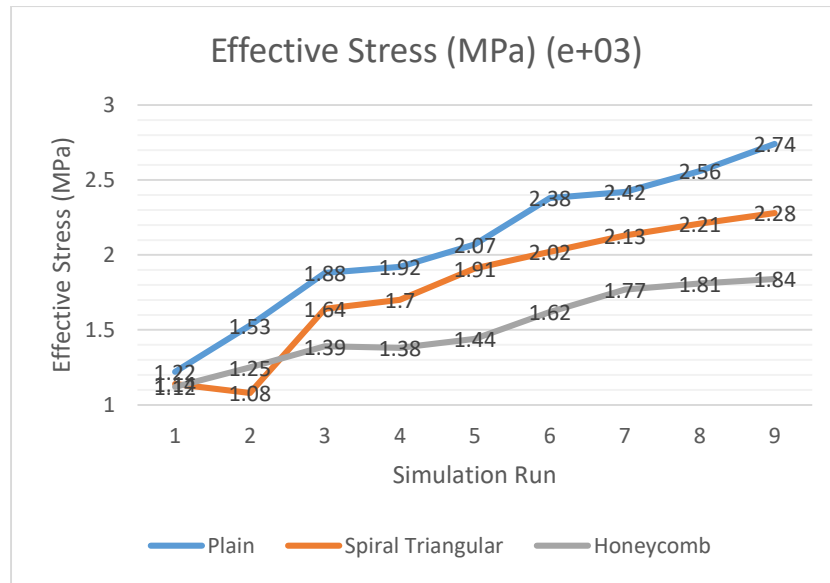


Figure 6.47: Variation of effective stress in three types of cutting inserts.

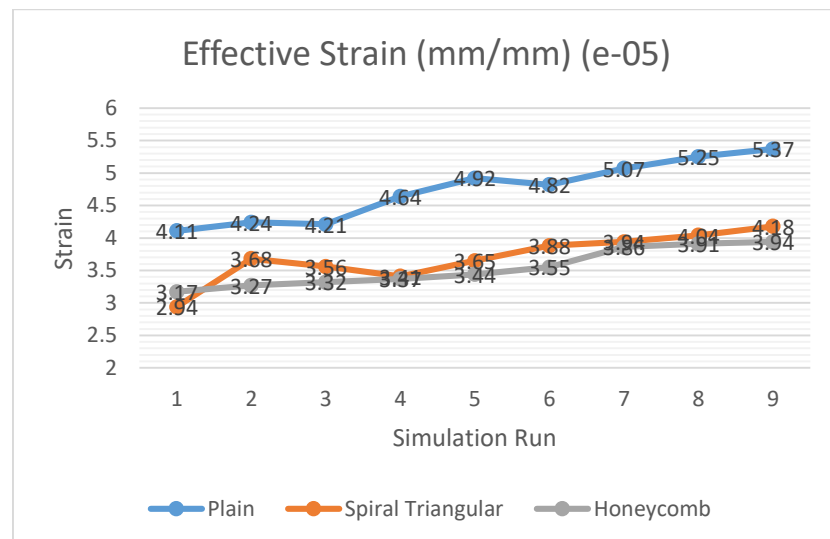


Figure 6.48: Variation of effective strain in three types of cutting inserts.

6.8 Finding the Optimal Parameters

The grey Taguchi method is the most commonly used method to find out the optimal parameters when a large number of parameters and their levels have been selected. The machining parameters and their levels have been finalized according to the available resources. The process parameters and their levels are shown in table 6.9. After this, the design of the experiment has been prepared using Taguchi L27 orthogonal array and shown in table 6.10.

Table 6.9: Process parameters and their levels

Machining Parameter	Levels
Rotational Speed	1. 325 rpm 2. 550 rpm 3. 930 rpm
Feed	1. 0.04 mm/rev 2. 0.06 mm/rev 3. 0.08 mm/rev
Type of Cutting Insert	1. Plain cutting insert without any micro-texture 2. Spiral Triangular micro-textured cutting insert 3. Spiral Triangular micro-textured cutting insert
Depth of Cut	0.5 mm

Table 6.10: Taguchi L27 Orthogonal array for the design of experiments

Design of Experiments			
Run	Parameters		
	Rotational Speed (rpm)	Feed (mm/rev)	Type of insert
1	1	1	1
2	1	1	2
3	1	1	3
4	1	2	1
5	1	2	2
6	1	2	3
7	1	3	1
8	1	3	2
9	1	3	3
10	2	1	1
11	2	1	2
12	2	1	3
13	2	2	1
14	2	2	2
15	2	2	3
16	2	3	1
17	2	3	2
18	2	3	3
19	3	1	1
20	3	1	2
21	3	1	3
22	3	2	1
23	3	2	2

24	3	2	3
25	3	3	1
26	3	3	2
27	3	3	3

Table 6.11: Measured values of output responses after machining operation.

Process Parameters				Obtained Results			
Experiment Run No.	Rotational Speed (rpm)	Feed (mm/rev)	Type of insert	Temperature (°C)	Surface Roughness Ra (µm)	PISF (%)	Material Removal Rate (mm ³ Per min)
1	325	0.04	1	230	2.942	27	6.799
2	325	0.04	2	227	1.687	58.14	6.916
3	325	0.04	3	210	1.228	69.53	6.786
4	325	0.06	1	264	2.17	46.15	9.633
5	325	0.06	2	254	2.093	48.06	9.496
6	325	0.06	3	240	1.892	53.05	9.672
7	325	0.08	1	327	3.062	24.02	13.884
8	325	0.08	2	295	2.886	28.39	13.26
9	325	0.08	3	268	2.522	37.42	13.286
10	550	0.04	1	378	2.062	48.83	10.978
11	550	0.04	2	336	1.654	58.96	10.67
12	550	0.04	3	295	1.911	52.58	10.788
13	550	0.06	1	404	2.439	39.48	16.566
14	550	0.06	2	372	1.38	65.76	16.203
15	550	0.06	3	317	2.209	45.19	16.104
16	550	0.08	1	363	2.895	28.16	22
17	550	0.08	2	313	2.203	45.33	21.56
18	550	0.08	3	340	2.054	49.03	21.648
19	930	0.04	1	475	2.964	26.45	19.344
20	930	0.04	2	404	2.034	49.53	18.972
21	930	0.04	3	591	0.967	76	18.451
22	930	0.06	1	625	3.822	5.16	28.625
23	930	0.06	2	476	1.54	61.79	27.955
24	930	0.06	3	548	2.297	43	27.676
25	930	0.08	1	604	3.158	21.64	37.423
26	930	0.08	2	502	2.946	26.9	38.985
27	930	0.08	3	577	1.02	74.69	39.58
Maximum Value in Column				625	3.822	76	39.58
Minimum Value in Column				210	0.967	5.16	6.786
(Max. Value) – (Min. Value)				415	2.855	70.84	32.794

After performing the experiments, the output results have been tabulated and shown in Table 6.11. Total four output responses have been obtained and these are cutting tool temperature, surface roughness, and MRR (material removal rate), and PISF (percentage improvement in the surface finish). After that GREY Taguchi method has been applied. This widely used analysis method has four steps of calculation.

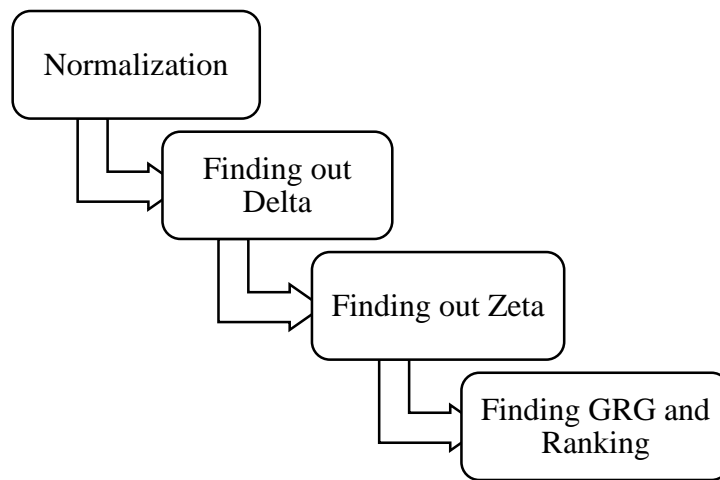


Figure 6.49: Steps of Grey Taguchi method of finding optimal parameters.

In step 1, all the obtained result values have been normalized. First, the difference between maximum and minimum values in a particular response column has been calculated. There is a total of four obtained responses out of which the cutting temperature and surface roughness are considered lower to be better and the other two i.e. percentage improvement in surface finish and material removal rate have taken bigger to be better. In normalizing the values two different formulas have been used. Equation 6.2 is being used for smaller to be better and equation 6.3 has been used for bigger to be a better response.

Smaller is better:

$$x_i^*(k) = \frac{\max y_i(k) - y_i(k)}{\max y_i(k) - \min y_i(k)} \quad (\text{Eq. 6.2})$$

Larger is better:

$$x_i^*(k) = \frac{y_i(k) - \max y_i(k)}{\max y_i(k) - \min y_i(k)} \quad (\text{Eq. 6.3})$$

Value of delta (absolute responses):

$$\Delta_{0i}(k) = |x_0^*(k) - x_i^*(k)| \quad (\text{Eq. 6.4})$$

Zeta (Grey relational coefficients):

$$\xi_i(k) = \frac{\Delta_{\min} + \zeta\Delta_{\max}}{\Delta_{0i}(k) + \zeta\Delta_{\max}} \quad (\text{Eq. 6.5})$$

GRG:

$$\gamma_i = \frac{1}{n} \sum_{i=1}^n \xi_i(k) \quad (\text{Eq. 6.6})$$

Table 6.12: Normalized value of the obtained results.

Experiment Run No.	Temperature (°C)	Surface Roughness Ra (μm)	PISF (%)	Material Removal Rate (mm ³ Per min)
1	0.951807	0.329247	0.3083	0.000396
2	0.959036	0.768827	0.747883	0.003964
3	1	0.929597	0.908667	0
4	0.86988	0.59965	0.578628	0.086815
5	0.893976	0.62662	0.60559	0.082637
6	0.927711	0.697023	0.67603	0.088004
7	0.718072	0.287215	0.266234	0.216442
8	0.795181	0.348862	0.327922	0.197414
9	0.860241	0.476357	0.455392	0.198207
10	0.595181	0.637478	0.61646	0.127828
11	0.696386	0.780385	0.759458	0.118436
12	0.795181	0.690368	0.669396	0.122035
13	0.53253	0.505429	0.484472	0.298225
14	0.609639	0.876357	0.855449	0.287156
15	0.742169	0.585989	0.565076	0.284137
16	0.631325	0.345709	0.324675	0.463926
17	0.751807	0.588091	0.567053	0.450509
18	0.686747	0.64028	0.619283	0.453193
19	0.361446	0.321541	0.300536	0.382936
20	0.53253	0.647285	0.626341	0.371592
21	0.081928	1.021016	1	0.355705
22	0	0.021016	0	0.665945
23	0.359036	0.820315	0.799407	0.645514

24	0.185542	0.555166	0.534161	0.637007
25	0.050602	0.25359	0.232637	0.934226
26	0.296386	0.327846	0.306889	0.981856
27	0.115663	1.002452	0.981508	1

Table 6.13: Difference of the absolute value (Δ_{oi})

Experiment Run No.	Temperature (°C)	Surface Roughness in Experiment Ra (μm)	PISF (%)	Material Removal Rate (mm^3 Per min)
1	0.048193	0.670753	0.6917	0.99S9604
2	0.040964	0.231173	0.252117	0.996036
3	0	0.070403	0.091333	1
4	0.13012	0.40035	0.421372	0.913185
5	0.106024	0.37338	0.39441	0.917363
6	0.072289	0.302977	0.32397	0.911996
7	0.281928	0.712785	0.733766	0.783558
8	0.204819	0.651138	0.672078	0.802586
9	0.139759	0.523643	0.544608	0.801793
10	0.404819	0.362522	0.38354	0.872172
11	0.303614	0.219615	0.240542	0.881564
12	0.204819	0.309632	0.330604	0.877965
13	0.46747	0.494571	0.515528	0.701775
14	0.390361	0.123643	0.144551	0.712844
15	0.257831	0.414011	0.434924	0.715863
16	0.368675	0.654291	0.675325	0.536074
17	0.248193	0.411909	0.432947	0.549491
18	0.313253	0.35972	0.380717	0.546807
19	0.638554	0.678459	0.699464	0.617064
20	0.46747	0.352715	0.373659	0.628408
21	0.918072	-0.02102	0	0.644295
22	1	0.978984	1	0.334055
23	0.640964	0.179685	0.200593	0.354486
24	0.814458	0.444834	0.465839	0.362993
25	0.949398	0.74641	0.767363	0.065774
26	0.703614	0.672154	0.693111	0.018144
27	0.884337	-0.00245	0.018492	0

Table 6.14: Grey relational coefficients (zeta) of the responses

Experiment Run No.	Temperature (°C)	Surface Roughness in Experiment Ra (µm)	PISF (%)	Material Removal Rate (mm ³ Per min)
1	0.838384	0.271517	0.265477	0.200063
2	0.859213	0.519563	0.497891	0.200636
3	1	0.780268	0.732423	0.2
4	0.657686	0.384408	0.372372	0.214927
5	0.7022	0.401039	0.387952	0.214158
6	0.775701	0.452098	0.435563	0.215147
7	0.469989	0.259663	0.254125	0.241883
8	0.549669	0.277427	0.271127	0.23751
9	0.641422	0.323147	0.314621	0.237689
10	0.381785	0.408149	0.394608	0.222782
11	0.451578	0.532351	0.50964	0.220933
12	0.549669	0.446722	0.430586	0.221638
13	0.348447	0.335764	0.326572	0.262667
14	0.390405	0.669088	0.633631	0.259648
15	0.492289	0.3765	0.365004	0.258836
16	0.40409	0.27646	0.270175	0.318036
17	0.501814	0.377695	0.36606	0.312699
18	0.44385	0.410024	0.396374	0.313752
19	0.281356	0.269263	0.263307	0.288329
20	0.348447	0.41479	0.40086	0.284606
21	0.214028	1.091778	1	0.27955
22	0.2	0.20342	0.2	0.428042
23	0.280595	0.581822	0.554825	0.413575
24	0.234861	0.359798	0.349241	0.407835
25	0.208438	0.250901	0.245733	0.791705
26	0.26216	0.271104	0.26508	0.932336
27	0.220393	1.009904	0.931125	1

After calculating, table 6.12 has been prepared with normalized values of all the responses. In the next step of the Grey Taguchi method, the values of delta (absolute responses) have been calculated and shown in table 6.13. The formula used for this calculation is given in equation 6.4. After this step, the value of zeta (Grey relational coefficients) has been found as per the formula given in equation 6.5 and the results have been recorded in table 6.14. To calculate GRG in the next step, equation 6.6 has

been used. Based on the value of GRG, the ranking has been given and shown in table 6.15.

Table 6.15: Values of GRG and the final ranking of parameters.

Experiment Run No.	Rotational Speed (rpm)	Feed (mm/rev)	Type of insert	GRG	Rank
1	325	0.04	1	0.39386	13
2	325	0.04	2	0.519326	4
3	325	0.04	3	0.678173	2
4	325	0.06	1	0.407348	12
5	325	0.06	2	0.426337	10
6	325	0.06	3	0.469627	6
7	325	0.08	1	0.306415	25
8	325	0.08	2	0.333933	22
9	325	0.08	3	0.37922	16
10	550	0.04	1	0.351831	20
11	550	0.04	2	0.428626	9
12	550	0.04	3	0.412154	11
13	550	0.06	1	0.318362	23
14	550	0.06	2	0.488193	5
15	550	0.06	3	0.373157	18
16	550	0.08	1	0.31719	24
17	550	0.08	2	0.389567	15
18	550	0.08	3	0.391	14
19	930	0.04	1	0.275564	26
20	930	0.04	2	0.362176	19
21	930	0.04	3	0.646339	3
22	930	0.06	1	0.257865	27
23	930	0.06	2	0.457704	7
24	930	0.06	3	0.337934	21
25	930	0.08	1	0.374194	17
26	930	0.08	2	0.43267	8
27	930	0.08	3	0.790356	1

Chapter 7

7. Conclusions

To analyze the machinability aspects of micro-textured cutting inserts, plain, spiral triangular, and honeycomb micro-pattern has been designed on Solidworks® and fabricated on the rake face of tungsten carbide inserts using a femtosecond laser machine. Topography, EDS, and XRD analysis of cutting inserts with micro-texture have been performed. As titanium is difficult to cut metal nevertheless having numerous applications in several fields, turning operation has been performed on Titanium Grade 2 rod. A lathe machine with a three-step speed and feed variation has been selected. The various machining parameters are rotational speed of workpiece, feed, and type of cutting inserts. For this experiment analysis, double square tungsten carbide cutting inserts have been used. These have thin TiCN coating up to 20 microns, zero relief angle, and a cylindrical hole to clamp on the tool holder without any chip breaker. Cutting tool temperature, surface roughness, MRR, PISF, tool wear, and chip morphology has been analyzed. Finite element analysis has been performed using DEFORM® 3D simulation tool. Simulation results have been validated and compared with the experimental results. Few other factors which are responsible for machinability, have been predicted. Grey Taguchi analysis has been conducted to find out optimal parameters. The various conclusions made after this research are:

- The spiral triangular design has been focused on increasing the count of continuous straight walls whereas the honeycomb design has been focused on providing the micro pools along with the increase of continuous walls. These micro-pools act as a reservoir of coolant which will store the coolant for a longer duration of time. The long removed chips are always a problem for machining operation and these micro-textures also act as a chip breaker to produce small-sized or discontinuous chips.
- In spiral triangular micro-textured cutting insert the area covered for the fabrication of micro-texture is 1.12 mm X 1.12 mm on both sides of the cutting edge whereas in honeycomb micro-texture, it is 2.11 mm X 2.11 mm. The width

of the groove taken in spiral triangular design has a value of 0.01 mm and 0.03 mm in honeycomb design. It merely depends on the structure of the design.

- There is the formation of varying depths of the groove due to the overlapping of pulses of the laser beam which is set to be completed in the shortest time. EDS shows the formation of new oxides and a 33.7% increase of carbon elements inside the groove. It will not affect the heat dissipation rate because the effect of an increase of surface area and fin length is more in comparison. XRD analysis endorses the existence of a thin coating retaining all of its properties.
- Reduction of cutting tool temperature has been observed while machining with micro-textured cutting inserts. A significant reduction in surface roughness has obtained while using micro-textured cutting inserts because of improved machinability characteristics.
- The standard cutting tool life has been considered up to 0.3 mm of the flank wear. It has an average value 0.193 mm of while machining with honeycomb micro-textured cutting inserts. So the honeycomb micro-texture has increased the cutting tool life.
- The honeycomb micro-texture has reduced the contact surface area between high-temperature removed chips and the rake face of the cutting insert. It also provides more area for heat dissipation as new and long walls have been created. Due to these reasons, the observed crater wear has reduced and cutting tool life has increased.
- Snarled ribbon, snarled corkscrew, long corkscrew, snarled helical, and long tubular type of chips has been obtained. Because of the honeycomb micro-pattern, chips get stuck at the microgrooves and generate tubular or ribbon-type small diameter chips. This results in the reduction of crater wear of the tool. In straight chips like snarled ribbon, various horizontal lines with more depth have been found on the convex side of chips. These straight groove fractures are considered to be the main reason for their straight shape.
- More and large-sized teeth have been found in long corkscrew chips in comparison to the long tubular chips. Due to these sharp edge teeth, more

deformations occur at the rake face. Vertical straight line fractures have been observed on the concave side of the corkscrew and long tubular chips.

- The slope of the graphs indicates the control on cutting temperature using textured cutting inserts. The area of the high-temperature zone is maximum in plain insert and minimum in honeycomb micro-textured cutting insert. The experimental and simulation temperature values exhibit a maximum of 1.11% error of deviation which is in the suitable range. Therefore the simulation outcomes have been corroborated with the experimental values.
- The predicted values of effective stress and strain increase with the increase in rotational speed as well as with feed. The maximum of 2.74Mpa e+03 effective principal stress has been measured with plain cutting insert at speed of 930 rpm and 0.08 mm/rev of feed. A minimum of 2.94 e-5 mm/mm effective strain has been observed with a spiral triangular micro-textured cutting insert.
- From this Grey Taguchi analysis, the optimal parameter has been observed at run 27. The best machining results are obtained with 930 rpm of rotational speed and 0.08 mm/rev of feed using a honeycomb micro-textured cutting insert.

7.1 Contribution to Research

- This research work has given novel micro-design patterns and professed their better enactment while machining with Titanium Grade 2 metal. The effect of various factors responsible for the machinability of cutting inserts has been declared.
- Feasible design ideas have been generated for double side square cutting inserts. Fabrication of micro-textures was a challenge. So the use of the femtosecond laser machine and its fabrication process parameters have been explained.
- The study of tool wear and chip morphology has given new ideas for better designs and cutting tool modifications. Variation of flank wear with the rotational speed of the workpiece and cutting feed has given a wide range of operative machining parameters.
- Variation of parameters like temperature, surface roughness, level of material removal, perfection in surface finish, flank wear, crater wear, removed chips

shape, size, and types, etc. have been expressed graphically concerning various machining factors.

- Use of DEFORM[®] 3D tool to the prediction of other results after validating with experimental data has been given. Grey Taguchi analysis has given the optimal parameter for this machining analysis.

7.2 Scope of Future Research

- Machining of other difficult-to-cut metals can also be done using these designed and fabricated micro-textured cutting inserts. Few other process parameters can also be taken into consideration while performing the experiments.
- Micro study of crater wear and removed chips can provide more conclusions regarding improvement in machinability aspects of cutting inserts.
- Finite element analysis of other machine process parameters can be conducted for the same or different metals of the same category.

Publications

Published

- **Research Paper** with the title "Design and Fabrication of Honeycomb Micro-Texture Using Femtosecond Laser Machine" has been **published in** the *Material and Manufacturing Processes, 2021. (SCIE, SJR – 1.077)*
- **Review Paper** with the title "Machinability Aspects of Difficult to Cut Materials Using Micro Texture Patterns" has been **published in** the esteem book title "Advanced Manufacturing and Processing Technology", CRC Press Taylor & Francis 2020, (3). (*Scopus*)
- **Research Paper** with the title "Design and Fabrication of Spiral Triangular Micro Texture on Chemical Vapor Deposition Coated Cutting Insert Using Femtosecond Laser Machine" has been **published in** *Materials Today: Proceedings, 2020. (Scopus, SJR – 0.304)*
- **Research Paper** with the title "Deform 3D Simulation Analysis for Temperature Variation in Turning Operation on Titanium Grade 2 Using CVD Coated Carbide Insert" has been **published in** *Lecture Notes in Mechanical Engineering, 2021. (Scopus, SJR - 0.165.*
- **Research Paper** with the title "Optimization of machinability criteria during dry machining of Ti-2 with micro-groove cutting tool using WASPAS approach" has been **published in** *Materials Today: Proceedings, 2020. (Scopus, SJR – 0.304)*

Conference Proceedings

- **Presented the paper** titled "Design and Fabrication of Spiral Triangular Micro Texture on Chemical Vapor Deposition Coated Cutting Insert Using Femtosecond Laser Machine" during "International Conference on Aspects of Materials Science and Engineering" **ICAMSE 2020** held on 29th – 30th May 2020 Organized by University Institute of Engineering and Technology (UIET),

Panjab University, Chandigarh, India in collaboration with Government College of Engineering and Technology (GCET), Jammu, India.

- **Presented the paper** titled “Deform 3D Simulation Analysis for Temperature Variation in Turning Operation on Titanium Grade 2 Using CVD Coated Carbide Insert” during “2nd International Conference on Future Learning Aspects of Mechanical Engineering” **FLAME 2020** held on 5th – 7th August 2020 Organized by Amity University, Uttar Pradesh, India.

Communicated

- Rahul Sharma, Swastik Pradhan, and Ravi Nathuram Bathe "*Machinability Aspects of Non-Textured and Micro Textured Cutting Inserts in Turning of Titanium Gr 2*" in *International Journal of Refractory Metals and Hard Materials (SCIE) Under Review.*
- Rahul Sharma, Swastik Pradhan, and Ravi Nathuram Bathe "*Analysis of Surface Roughness, Tool Wear and Chip Morphology in Machining of Titanium Gr2 Using Plain and Micro-Textured Cutting Inserts*" in *Journal of the Brazilian Society of Mechanical Sciences and Engineering (SCIE) Under Review.*
- Rahul Sharma, Swastik Pradhan "*Comparison, Validation and Prediction of machinability aspects of textured and non-textured cutting inserts*" in *International Journal of Mechanical Sciences (SCIE) Under Review.*

Bibliography

1. Habrat W, Markopoulos AP, Motyka M, Sieniawski J (2019) Machinability. In: Nanocrystalline Titanium. Elsevier, pp 209-236
2. Trent EM, Wright PK (2000) Metal cutting. Butterworth-Heinemann
3. Youssef HA (2015) Machining of stainless steels and super alloys: traditional and nontraditional techniques. John Wiley & Sons
4. Kus A, Isik Y, Cakir MC, Coskun S, Ozdemir KJ (2015) Thermocouple and infrared sensor-based measurement of temperature distribution in metal cutting. *Sensor* 15 (1):1274-1291
5. Cherukuri R, Molian P (2003) Lathe turning of titanium using pulsed laser deposited, ultra-hard boride coatings of carbide inserts. *Machining science and technology* 7 (1):119-135
6. Sharma R, Pradhan S (2020) Investigation of machinability criteria during micro-abrasive finishing of SUS-304L steel using fuzzy combined with WASPAS approach. *Journal of the Brazilian Society of Mechanical Sciences and Engineering* 42 (3):116. doi:10.1007/s40430-020-2198-5
7. Boubekri N, Shaikh V, Foster PR (2010) A technology enabler for green machining: minimum quantity lubrication (MQL) *Journal of Manufacturing Technology Management* 21(5).
8. Tai BL, Stephenson DA, Furness RJ, Shih AJ (2014) Minimum quantity lubrication (MQL) in automotive powertrain machining. *Procedia Cirp* 14:523-528
9. Elshwain A, Redzuan N, Yusof NM (2013) Machinability of Nickel and Titanium alloys under of gas-based coolant-lubricants (cls)—A Review. *International Journal of Research in Engineering and Technology* 2 (11):690-702
10. Vasumathy D, Meena A, Duraiselvam M (2017) Experimental study on evaluating the effect of micro textured tools in turning aisi 316 austenitic stainless steel. *Procedia Engineering* 184:50-57
11. Biermann D, Steiner M (2012) Analysis of micro burr formation in austenitic stainless steel X5CrNi18-10. *Procedia Cirp* 3:97-102

12. Enomoto T, Sugihara T (2011) Improvement of anti-adhesive properties of cutting tool by nano/micro textures and its mechanism. *Procedia Engineering* 19:100-105
13. Zhang S, Li J, Zhu X, Lv H (2013) Saw-tooth chip formation and its effect on cutting force fluctuation in turning of Inconel 718. *International Journal of Precision Engineering and Manufacturing* 14 (6):957-963
14. Sahoo A, Pradhan S, Rout AK (2013) Development and machinability assessment in turning Al/SiCp-metal matrix composite with multilayer coated carbide insert using Taguchi and statistical techniques. *Archives of Civil and Mechanical Engineering* 13:27-35
15. Sahoo AK, Pradhan S (2013) Modeling and optimization of Al/SiCp MMC machining using Taguchi approach. *Measurement* 46 (9):3064-3072
16. Zetek M, Cesakova I, Svarc V (2014) Increasing cutting tool life when machining Inconel 718. *Procedia Engineering* 69 (0):1115-1124
17. Parida AK, Maity K (2017) Effect of nose radius on forces, and process parameters in hot machining of Inconel 718 using finite element analysis. *Engineering Science and Technology* 20 (2):687-693
18. Maity K, Pradhan S (2017) Study of chip morphology, flank wear on different machinability conditions of titanium Alloy (Ti-6Al-4V) using response surface methodology approach. *International Journal of Material Forming and Machining Processes* 4 (1):19-37
19. Maity K, Pradhan S Investigation of tool wear and surface roughness on machining of titanium alloy with MT-CVD cutting tool. In: *IOP Conference Series: Materials Science and Engineering*, 2018. vol 1. IOP Publishing, p 012053
20. Maity K, Pradhan S Study of process parameter on mist lubrication of Titanium (Grade 5) alloy. In: *IOP conference series: materials science and engineering*, 2017. vol 1. IOP Publishing, p 012030
21. Ribeiro M, Moreira M, Ferreira JR (2003) Optimization of titanium alloy (6Al-4V) machining. *Journal of material Processing Technology* 143:458-463
22. Haron CC, Jawaid A (2005) The effect of machining on surface integrity of titanium alloy Ti-6Al-4V. *Journal of material processing technology* 166 (2):188-192
23. Da Silva R, Vieira J, Cardoso R, Carvalho H, Costa E, Machado A, De Avila (2011) Tool wear analysis in milling of medium carbon steel with coated cemented carbide

- inserts using different machining lubrication/cooling systems. *Wear* 271 (9-10):2459-2465
24. Gente A, Hoffmeister H-W, Evans CJ (2001) Chip formation in machining Ti6Al4V at extremely high cutting speeds. *CIRP Annals* 50 (1):49-52
25. Hua J, Shivpuri R (2004) Prediction of chip morphology and segmentation during the machining of titanium alloys. *Journal of material processing technology* 150 (1-2):124-133
26. Sun S, Brandt M, Dargusch MS (2009) Characteristics of cutting forces and chip formation in machining of titanium alloys. *International Journal of Machine Tools and Manufacture* 49 (7-8):561-568
27. Rao CM, Rao SS, Herbert MA (2018) Development of novel cutting tool with a micro-hole pattern on PCD insert in machining of titanium alloy. *Journal of Manufacturing Processes* 36:93-103
28. Zanger F, Schulze V (2013) Investigations on mechanisms of tool wear in machining of Ti-6Al-4V using FEM simulation. *Procedia Cirp* 8:158-163
29. Pradhan S, Maity K (2017) Investigation of surface roughness, tool wear and chip reduction coefficient during machining of titanium alloy with PVD Al-Ti-N coating carbide insert *Analysis* 2:4
30. Obikawa T, Asano Y, Kamata Y (2009) Computer fluid dynamics analysis for efficient spraying of oil mist in finish-turning of Inconel 718. *International Journal of Machine Tools and Manufacturing* 49 (12-13):971-978
31. Umbrello D (2008) Finite element simulation of conventional and high speed machining of Ti6Al4V alloy. *Journal of material processing technology* 196 (1-3):79-87
32. Tsao C, Chiu Y (2011) Evaluation of drilling parameters on thrust force in drilling carbon fiber reinforced plastic (CFRP) composite laminates using compound core-special drills. *International Journal of Machine Tools and Manufacture* 51 (9):740-744
33. Schulze V, Zanger F (2011) Numerical Analysis of the influence of Johnson-Cook-Material parameters on the surface integrity of Ti-6Al-4 V. *Procedia Engineering* 19:306-311
34. Stovall M, Smith SA, Langholz BM, Boice Jr JD, Shore RE, Andersson M, Buchholz TA, Capanu M, Bernstein L, Lynch CF (2008) Dose to the contralateral

- breast from radiotherapy and risk of second primary breast cancer in the WECARE study. *International Journal of Radiation Oncology Biology Physics* 72 (4):1021-1030
35. Jiang H, He L, Yang X, Zou Z, Zhan G (2017) Prediction and experimental research on cutting energy of a new cemented carbide coating micro groove turning tool. *International Journal of Advance Manufacturing Technology* 89 (5-8):2335-2343
36. Zhang K, Deng J, Meng R, Gao P, Yue H (2015) Effect of nano-scale textures on cutting performance of WC/Co-based Ti55Al45N coated tools in dry cutting. *Internatinal Journal of Refractory Metals and Hard Materials* 51:35-49
37. Ma J, Duong NH, Chang S, Lian Y, Deng J, Lei S (2015) Assessment of microgrooved cutting tool in dry machining of AISI 1045 steel. *Jjournal of Manufacturing Science and Engineering* 137 (3)
38. Yu Z, Zhang C, Wang W, Zhou Y, Yu H Design of micro grove texture tool and experimental study on high speed micro-turning. In: 2015 IEEE International Conference on Mechatronics and Automation (ICMA), 2015. IEEE, pp 1088-1093
39. Qiu C, Ma J, Lei S Assessment of the Effects of Microgrooved Cutting Tool on the Machining Induced Residual Stress in Machining of Ti-6Al-4V. In: *International Manufacturing Science and Engineering Conference*, 2016. American Society of Mechanical Engineers, p V001T002A042
40. Darshan C, Singh P, Saini S, Goswami R Comparative evaluation of untextured and textured wc inserts under dry and near dry machining of C45 steel. *International Journal of General Engineering*.
41. Orra K, Choudhury SK (2018) Tribological aspects of various geometrically shaped micro-textures on cutting insert to improve tool life in hard turning process. *Journal of Manufacturing Processes* 31:502-513
42. Maity K, Pradhan S (2018) Investigation of FEM Simulation of Machining of Titanium Alloy Using Microgroove Cutting Insert. *Silicon* 10 (5):1949-1959
43. Patel K, Kaftanoglu B, Ozel T (2019) Micro textured cutting tool effects on cutting forces, volumetric wear and adhesion in dry turning of titanium alloy. *International Jjournal of Mechatronics and Manufacturing Systems* 12 (3-4):180-195
44. Alagan NT, Zeman P, Hoier P, Beno T, Klement U(2019) Investigation of micro-textured cutting tools used for face turning of alloy 718 with high-pressure cooling. *Journal of Manufacturing Processes* 37:606-616

45. Arrazola P, Ugarte D, Dominguez X (2008) A new approach for the friction identification during machining through the use of finite element modeling. *International Journal of Machine Tools and Manufacture* 48 (2):173-183
46. Yen Y-C, Jain A, Altan T (2004) A finite element analysis of orthogonal machining using different tool edge geometries. *Journal of materials processing technology* 146 (1):72-81
47. Zouhar J, Piska M (2008) Modelling the orthogonal machining process using cutting tools with different geometry. *MM Science Journal* 3:48-51
48. Ee K, Dillon Jr O, Jawahir (2005) Finite element modeling of residual stresses in machining induced by cutting using a tool with finite edge radius. *International Journal of Mechanical Sciences* 47 (10):1611-1628
49. Tounsi N, Otho A (2000) Identification of machine–tool–workpiece system dynamics. *International Journal of Machine tools and Manufacture* 40 (9):1367-1384
50. Enomoto T, Sugihara T (2010) Improving anti-adhesive properties of cutting tool surfaces by nano-/micro-textures. *CIRP annals* 59 (1):597-600
51. Caliskan H, Kucukkose M (2015) The effect of aCN/TiAlN coating on tool wear, cutting force, surface finish and chip morphology in face milling of Ti6Al4V superalloy. *International Journal of Refractory Metals and Hard Materials* 50:304-312
52. Sima M, Ozel T (2010) Modified material constitutive models for serrated chip formation simulations and experimental validation in machining of titanium alloy Ti–6Al–4V. *International Journal of Machine tools and Manufacture* 50 (11):943-960
53. Sivaiah P, Guru Prasad M, Singh M M, Uma B (2020) Machinability evaluation during machining of AISI 52100 steel with textured tools under Minimum Quantity Lubrication–A comparative study. *Material and Manufacturing Processes* 35 (15):1761-1768
54. Caliskan H, Kucukkose M (2015) The effect of aCN/TiAlN coating on tool wear, cutting force, surface finish and chip morphology in face milling of Ti6Al4V superalloy. *International Journal of Refractory Metals* 50:304-312
55. Kannan K, Radhika D, Sadasivuni KK, Reddy KR, Raghu AV (2020) Nanostructured metal oxides and its hybrids for biomedical applications. *Advances in Colloid and Interface Science* 102178
56. Wenlong S, Jianxin D, Ze W, Hui Z, Pei Y, Jun Z, Xing A (2011) Cutting

- performance of cemented-carbides-based self-lubricated tool embedded with different solid lubricants. *International Journal of Advanced Manufacturing Technology* 52 (5-8):477-485
57. Deng J, Song W, Zhang H, Yan P, Liu A (2011) Friction and wear behaviors of the carbide tools embedded with solid lubricants in sliding wear tests and in dry cutting processes. *Wear* 270 (9-10):666-674
58. Zhang N, Yang F, Jiang F, Liu G (2020) Study of the effect of surface laser texture on tribological properties of cemented carbide materials. *Journal of Engineering Manufacture* 234 (6-7):993-1006
59. Zhang J, Yang H, Chen S, Tang H (2020) Study on the influence of micro-textures on wear mechanism of cemented carbide tools. *International Journal of Advance Manufacturing Technology* 108:1701-1712
60. Krolczyk G, Legutko S, Raos P (2014) Microhardness and surface integrity in turning process of duplex stainless steel (DSS) for different cutting conditions. *Journal of Materials Engineering and Performance* 23 (3):859-866
61. Khan MA, Gupta K (2020) A study on machinability of nickel based superalloy using micro-textured tungsten carbide cutting tools. *Material Research Express* 7 (1):016537
62. Jianxin D, Wenlong S, Hui ZJIJoMT, *Manufacture* (2009) Design, fabrication and properties of a self-lubricated tool in dry cutting. 49 (1):66-72
63. Parida A, Rao P, Ghosh S (2020) Performance of textured tool in turning of Ti-6Al-4V alloy: numerical analysis and experimental validation. *Journal of Brazilian Society of Mmechanical Science and Engineering* 42 (5):1-14
64. Patel K, Liu G, Shah SR, Özel T (2020) Effect of micro-textured tool parameters on forces, stresses, wear rate, and variable friction in titanium alloy machining. *Journal of Manufacturing science and Engineering* 142 (2)
65. Qiu C, Ma J, Lei S Assessment of the Effects of Microgrooved Cutting Tool on the Machining Induced Residual Stress in Machining of Ti-6Al-4V. In: *ASME 2016 11th International Manufacturing Science and Engineering Conference*, 2016. V001T02A042. doi:10.1115/msec2016-8656
66. Sharma V, Pandey P (2017) Geometrical design optimization of hybrid textured self-lubricating cutting inserts for turning 4340 hardened steel. *The International*

Journal of Advanced Manufacturing Technology 89 (5):1575-1589

67. Shivakoti I, Kibria G, Das S, Sharma A, Pradhan BB, Chatterjee S (2021) Laser surface texturing on Ti-6Al-4V. *Materials and Manufacturing Processes* 36 (7):858-867
68. Koizumi H, Takeuchi Y, Imai H, Kawai T, Yoneyama T (2019) Application of titanium and titanium alloys to fixed dental prostheses. *Journal of Prosthodontic Research* 63 (3):266-270
69. Thakur A, Gangopadhyay S (2016) State-of-the-art in surface integrity in machining of nickel-based super alloys. *International Journal of Machine tools and Manufacture* 100:25-54
70. Mouritz AP (2012) *Introduction to aerospace materials*. Elsevier
71. Hallab N (2004) Orthopedic applications. *Journal of Saitmim* 526-554
72. Pramanik A (2014) Problems and solutions in machining of titanium alloys. *The Internatinal journal of Advanced Manufacturing* 70 (5-8):919-928
73. M'Saoubi R, Axinte D, Soo SL, Nobel C, Attia H, Kappmeyer G, Engin S, Sim W-M (2015) High performance cutting of advanced aerospace alloys and composite materials. *CIRP Annals* 64 (2):557-580
74. Guo Y, Li W, Jawahir I (2009) Surface integrity characterization and prediction in machining of hardened and difficult-to-machine alloys: a state-of-art research review and analysis. *Machining Science and Technology* 13 (4):437-470
75. Nishanth B, Kulkarni VN, Gaitonde V A review on conventional and non-conventional machining of titanium and nickel based alloys. In: *AIP Conference Proceedings*, 2019. vol 1. AIP Publishing LLC, p 020091
76. Masood I (2019) Sustainable Machining for Titanium Alloy Ti-6Al-4V. *Proceedings of Iinternational Conference* 1-15
77. Devaraj S, Malkapuram R, Singaravel B (2021) Performance analysis of micro textured cutting insert design parameters on machining of Al-MMC in turning process. *International Journal of Lightweight Materials and Manufacture* 4 (2):210-217
78. Arulkirubakaran D, Senthilkumar V, Kumawat VJIJoRM, Materials H (2016) Effect of micro-textured tools on machining of Ti-6Al-4V alloy: an experimental and numerical approach. *International Journal of Refractory Metals and Hard Materials* 54:165-177
79. Wu Z, Bao H, Liu L, Xing Y, Huang P, Zhao G (2020) Numerical investigation of

- the performance of micro-textured cutting tools in cutting of ti-6al-4v alloys. *Journal of Advance manufacturing Technology* 108:463-474
80. Niketh S, Samuel GJJOMP (2018) Drilling performance of micro textured tools under dry, wet and MQL condition. *Journal of Manufacturing Processes* 32:254-268
81. Olleak A, Ozel T (2017) 3D finite element modeling based investigations of micro-textured tool designs in machining titanium alloy Ti-6Al-4V. *Procedia Manufacturing* 10:536-545
82. Sugihara T, Enomoto T (2012) Improving anti-adhesion in aluminum alloy cutting by micro stripe texture. *Precision Engineering* 36 (2):229-237
83. Sivaiah P, Revantha Kumar M, Bala Subramanyam S, Prasad K (2020) A comparative study on different textured and untextured tools performance in turning process. *Materials and Manufacturing Processes* 1-10
84. Chamkha AJ, Rufuss DDW, Kabeel A, Sathyamurthy R, Abdelgaid M, Manokar AM, Madhu B (2020) Augmenting the potable water produced from single slope solar still using CNT-doped paraffin wax as energy storage: an experimental approach. *Journal of the Brazilian Society of Mechanical Sciences and Engineering* 42 (12):1-10
85. Sahithya K, Balasundar I, Pant P, Raghu T, Nandi HK, Singh V, Ghosal P, Ramakrishna M (2019) Deformation behaviour of an as-cast nickel base superalloy during primary hot working above and below the gamma prime solvus. *Materials Science and Engineering* 754:521-534
86. Rosa SdN, Diniz AE, Andrade CLF, Guesser W (2010) Analysis of tool wear, surface roughness and cutting power in the turning process of compact graphite irons with different titanium content. *Journal of Brazilian Society of Mechanical Engineering* 32 (3):234-240
87. Arrazola P-J, Garay A, Iriarte L-M, Armendia M, Marya S, Le Maitre F (2009) Machinability of titanium alloys (Ti6Al4V and Ti555. 3). *Journal of Material Processing Technology* 209 (5):2223-2230
88. Kene AP, Orra K, Choudhury S (2016) Experimental Investigation of Tool Wear Behavior of Multi-Layered Coated Carbide Inserts Using Various Sensors in Hard Turning Process. *IFAC Paers Online* 49 (12):180-184
89. Lalbondre R, Krishna P, Mohankumar G (2014) An experimental investigation on machinability studies of steels by face turning. *Procedia Materials Science* 6:1386-1395

90. Maruda RW, Krolczyk GM, Nieslony P, Wojciechowski S, Michalski M, Legutko S (2016) The influence of the cooling conditions on the cutting tool wear and the chip formation mechanism. *Journal of Manufacturing Processes* 24:107-115
91. Hoyne AC, Nath C, Kapoor SGJJOMS, Engineering (2015) On cutting temperature measurement during titanium machining with an atomization-based cutting fluid spray system. *Journal of Manufacturing Science and Engineering* 137 (2)
92. Nguyen T, Kwon P, Kang D, Bieler T (2016) The origin of flank wear in turning Ti-6Al-4V. *Journal of Manufacturing Science and Engineering* 138 (12)
93. Kumar A, Sehrawat G Investigation of Surface Roughness and Tool wear during turning of Titanium Alloy Grade 5 (Ti-6Al-4V) by using coated carbide tool and optimization of process parameters. In: *IOP Conference Series: Materials Science and Engineering*, 2021. vol 1. IOP Publishing, p 012067
94. Agrawal C, Wadhwa J, Pitroda A, Pruncu CI, Sarikaya M, Khanna N (2021) Comprehensive analysis of tool wear, tool life, surface roughness, costing and carbon emissions in turning Ti-6Al-4V titanium alloy: cryogenic versus wet machining. *Tribology* 153:106597
95. Biermann D, Abrahams H, Metzger M (2015) Experimental investigation of tool wear and chip formation in cryogenic machining of titanium alloys. *Advances in Manufacturing* 3 (4):292-299. doi:10.1007/s40436-015-0122-5
96. Lotfi M, Jahanbakhsh M, Farid A (2016) Wear estimation of ceramic and coated carbide tools in turning of Inconel 625: 3D FE analysis. *Tribology International* 99:107-116
97. Amin AN, Ismail AF, Khairusshima M (2007) Effectiveness of uncoated WC-Co and PCD inserts in end milling of titanium alloy—Ti-6Al-4V. *Journal of Materials Processing Technology* 192:147-158
98. Uddin MS, Pham B, Sarhan A, Basak A, Pramanik A (2017) Comparative study between wear of uncoated and TiAlN-coated carbide tools in milling of Ti6Al4V. *Advances in Manufacturing* 5 (1):83-91. doi:10.1007/s40436-016-0166-1
99. Barry J, Byrne G, Lennon D (2001) Observations on chip formation and acoustic emission in machining Ti-6Al-4V alloy. *International Journal of Machine tools and Manufacturing* 41 (7):1055-1070
100. Sun J, Guo Y (2008) A new multi-view approach to characterize 3D chip

- morphology and properties in end milling titanium Ti–6Al–4V. *International Journal of machine tools and manufacturing* 48 (12-13):1486-1494
101. Joshi S, Tewari A, Joshi S (2015) Microstructural characterization of chip segmentation under different machining environments in orthogonal machining of Ti6Al4V. *Journal of Engineering Materials and Technology* 137 (1)
102. Maruda RW, Krolczyk GM, Feldshtein E, Nieslony P, Tyliczszak B, Pusavec F (2017) Tool wear characterizations in finish turning of AISI 1045 carbon steel for MQCL conditions. *Wear* 372:54-67
103. Li T, Shi T, Tang Z, Liao G, Duan J, Han J, He Z (2021) Real-time tool wear monitoring using thin-film thermocouple. *Journal of Materials Processing Technology* 288:116901
104. Sun S, Brandt M, Dargusch MSJPotIoME, Part B: *Journal of Engineering Manufacture* (2017) Effect of tool wear on chip formation during dry machining of Ti-6Al-4V alloy, part 1: effect of gradual tool wear evolution. 231 (9):1559-1574
105. Liang X, Liu Z, Wang B, Song Q, Cai Y, Wan Y (2021) Prediction of residual stress with multi-physics model for orthogonal cutting Ti-6Al-4V under various tool wear morphologies. *Journal of Materials Processing Technology* 288:116908
106. Lin H, Wang C, Yuan Y, Chen Z, Wang Q, Xiong W (2015) Tool wear in Ti-6Al-4V alloy turning under oils on water cooling comparing with cryogenic air mixed with minimal quantity lubrication. *Journal of Material Processing Technology* 81 (1):87-101
107. Antic A, Kozak D, Kosec B, Simunovic G, Saric T, Kovacevic D, Cep R (2013) Influence of tool wear on the mechanism of chips segmentation and tool vibration. 20 (1):105-112
108. Kumar CS, Patel SK, Das A Experimental and numerical investigations on the temperature distribution in PVD AlTiN coated and uncoated Al₂O₃/TiCN mixed ceramic cutting tools in hard turning of AISI 52100 steel. In: *IOP Conference Series: Materials Science and Engineering*, 2018. vol 1. IOP Publishing, p 012021
109. Parida AK, Maity K (2019) Analysis of some critical aspects in hot machining of Ti-5553 superalloy: experimental and FE analysis. *Defence Technology* 15 (3):344-352
110. Parida AK, Maity K (2018) Numerical analysis of chip geometry on hot machining of nickel base alloy. *Jjournal of the Brazilian society of mechanical science and Engineering* 40 (10):1-9

111. Arisoy YM, Ozel T (2015) Prediction of machining induced microstructure in Ti–6Al–4V alloy using 3-D FE-based simulations: Effects of tool micro-geometry, coating and cutting conditions. *Journal of Materials processing Technology* 220:1-26
112. Thepsonthi T, Özel T (2015) 3-D finite element process simulation of micro-end milling Ti-6Al-4V titanium alloy: experimental validations on chip flow and tool wear. *Journal of Materials processing Technology* 221:128-145
113. Parida A, Rao P, Ghosh S (2020) Numerical analysis and experimental investigation in the machining of AISI 316 steel. *Sadhana* 45 (1):1
114. Parida A, Maity K Finite element method and experimental investigation of hot turning of Inconel 718. In: *Advanced Engineering Forum*, 2016. Trans Tech Publ, pp 24-32
115. Parida A, Rao P, Ghosh S (2020) Influence of cutting speed and nose radius in the machining of Al-6061: FEM and experimental validation. *Materials Today: Proceedings* 27:2569-2573
116. Parida AK, Maity K (2019) FEM analysis and experimental investigation of force and chip formation on hot turning of Inconel 625. *Defence Technology* 15 (6):853-860
117. Parida AK, Maity K (2019) Numerical and experimental analysis of specific cutting energy in hot turning of Inconel 718. *Measurement* 133:361-369
118. Prasad BS, Babu MP, Reddy Y, Part B: *Journal of Engineering Manufacture* (2016) Evaluation of correlation between vibration signal features and three-dimensional finite element simulations to predict cutting tool wear in turning operation. 230 (2):203-214
119. Shunhua L Finite Element Simulation of Whirling Temperature of Titanium Alloy Based on DEFORM.
120. Obiko J, Mwema F, Akinlabi E (2020) Strain rate-strain/stress relationship during isothermal forging: A Deform-3D FEM. *Engineering Solid Mechanics* 8 (1):1-6
121. Kumar U, Mishra AK, Ohdar R (2014) Simulation Study of Stub Axle Forging using DEFORM. *International Journal of Mechanical Engineering and Robotics Research* 3 (4):206
122. Obiko JO, Mwema FM, Bodunrin M (2021) Validation and optimization of cutting parameters for Ti-6Al-4V turning operation using DEFORM 3D simulations and Taguchi method. *Manufacturing* 8:5

123. Satyanarayana K, Venu Gopal A, Bangaru Babu P Finite Element Simulation of Cutting Forces in Turning Ti6Al4V Using DEFORM 3D. In: ASME 2013 International Mechanical Engineering Congress and Exposition, 2013. American Society of Mechanical Engineers Digital Collection,
124. Mwema FM, Obiko J (2020) Finite Element Modeling Of Non-Constrained Closed Die Forging (Modified Upsetting) Using Deform 3dtm.
125. Prasad KK, Tamang SK, Chandrasekaran M Comparative Study on Cutting Force Simulation Using DEFORM 3D Software during High Speed Machining of Ti-6Al-4V. In: Key Engineering Materials, 2020. Trans Tech Publ, pp 50-56
126. Gardner JD, Dornfeld D (2006) Finite element modeling of drilling using DEFORM.
127. Khanawapee U, Butdee S (2020) A study of barreling and DEFORM 3D simulation in cold upsetting of bi-material. *Materials Today: Proceedings* 26:1262-1270
128. Sharma R, Pradhan S, Bathe R (2020) Design and fabrication of spiral triangular micro texture on chemical vapor deposition coated cutting insert using femtosecond laser machine. *Materials Today: Proceedings* 28(3) 1439-1444
129. Krolczyk G, Legutko S, Raos P (2013) Cutting wedge wear examination during turning of duplex stainless steel. *20 (3):413-418*
130. Vasumathy D, Meena A (2017) Influence of micro scale textured tools on tribological properties at tool-chip interface in turning AISI 316 austenitic stainless steel. *Wear* 376:1747-1758
131. Gulevskiy V, Adamova A, Kidalov N, Yu BE, Blednova Z, Batalov D, Mukhametshin V, Dubinskiy G, Andreev V, Bolobov V Iop conference series: Earth and environmental science. In, 2018. Institute of physics publishing: International conference,
132. Lince J (2020) Effective application of solid lubricants in spacecraft mechanisms. *Lubricants* 8 (7):74
133. Sharma R, Pradhan S, Bathe RN (2020) Design and fabrication of spiral triangular micro texture on chemical vapor deposition coated cutting insert using femtosecond laser machine. *Materials Today: Proceedings* 28:1439-1444
134. Pradhan S, Indraneel S, Sharma R, Bagal DK, Bathe RN (2020) Optimization of

- machinability criteria during dry machining of Ti-2 with micro-groove cutting tool using WASPAS approach. *Materials Today: Proceedings* 33:5306-5312
135. Sharma R, Pradhan S, Bathe RN (2021) Design and fabrication of honeycomb micro-texture using femtosecond laser machine. *Materials and Manufacturing Processes* 1-9
136. Sharma R, Pradhan S, Bathe R (2020) Design and fabrication of spiral triangular micro texture on chemical vapor deposition coated cutting insert using femtosecond laser machine. *Materials Today: Proceedings*. doi:10.1016/j.matpr.2020.04.817
137. Li Q, Pan C, Jiao Y, Hu (2019) Investigation on cutting performance of micro-textured cutting tools. *Micromachines* 10 (6):352
138. Ratnam M (2017) 1.1 factors affecting surface roughness in finish turning. *Materials and Manufacturing Processes*. 3(4)
139. Hu L, Zhan J, Zheng DJ (2015) Study on the influence of the rotational speed of polishing disk on material removal in aspheric surface compliant polishing. *Advances in Mechanical Engineering* 7 (3):1687814015578359
140. Rowe WB (2014) 2 - Basic Material Removal. In: Rowe WB (ed) *Principles of Modern Grinding Technology (Second Edition)*. William Andrew Publishing, Oxford, pp 15-33
141. Salak A, Vasilko K, Selecka M, Danninger H (2006) New short time face turning method for testing the machinability of PM steels. *Journal of Materials Processing Technology* 176 (1-3):62-69
142. Knight WA, Boothroyd G (2019) *Fundamentals of metal machining and machine tools*. CRC Press,
143. Pradhan S, Indraneel S, Sharma R, Bagal DK, Bathe RN (2020) Optimization of machinability criteria during dry machining of Ti-2 with micro-groove cutting tool using WASPAS approach. *Materials Today Proceedings* 33(8), 5306-5312
144. Sharma R, Pradhan S Deform 3D Simulation Analysis for Temperature Variation in Turning Operation on Titanium Grade 2 Using CCD-Coated Carbide Insert. In: Phanden RK, Mathiyazhagan K, Kumar R, Paulo Davim J (eds) *Advances in Industrial and Production Engineering*, Singapore, 2021// 2021. Springer Singapore, pp 937-945

Annexures

Calculation of PISF

Three values of surface roughness, at different positions on titanium rod before and after machining has been measured for each experimental run. After that the percentage improvement in surface finish has been calculated using Equation 5.2 and tabulated in table 5.3. For example: For run 1 the average surface roughness after machining is 2.942 μm . Before machining it was 4.03 μm . Hence the improvement in surface finish is $(4.03 - 2.942) \mu\text{m} = 1.088 \mu\text{m}$. So putting these values in equation 5.2 we are getting the PISF equals to 27%. In this way all the values have been calculated.